Study of the influence of nanoparticles on the performance and the properties of polyamide 6

Von der Fakultät Chemie der Universität Stuttgart
zur Erlangung der Würde eines
Doktors der Naturwissenschaften (Dr. rer. nat.)
genehmigte Abhandlung

Vorgelegt von
Mohammad Reza Sarbandi
aus Teheran – Iran

Hauptberichter: Prof. Dr. Dr. h.c. Franz Effenberger

Mitberichter: Prof. Dr. rer. nat. Karl Bredereck

Tag der mündlichen Prüfung: 25. Oktober 2011

Universität Stuttgart
Institut für Polymerchemie

Lehrstuhl für Makromolekulare Stoffe und Faserchemie

2011

Acknowledgment

I would like to express my sincere appreciation to Prof. Dr. Dr. h.c. Franz Effenberger my supervisor who gave me the direction of this research and chance to study at the Polymer Institute.

I would like to thanks Prof. Dr. rer. nat. Karl Bredereck who has been always there to listen and give advice, also i thank Prof. Dr. rer. nat. Thomas Schleid as a chairperson of my doctoral exam.

My deepest gratitude to Dr. Rainer Gutmann for his support, guidance, inspiration, correction and all that he did to make this work possible.

I would like also thanks to Dr. Gabriele Hardtmann for her support and cooperation and all colleagues at polymer institute of university of Stuttgart.

Many thanks go to my colleagues at ITCF because of all of their help, very good cooperation, friendly and pleasant working atmosphere:
Dr. Michael Schweizer, Ms. Margit Böhl, Mrs Anne-Katrin Denninger, Mrs. Sabine Gneiting, Mr. Winfried Schuler, Mr. Rolf Neupert, Mr. Wölfl and all of my colleagues at ITCF Denkendorf.

Abstract:

The number of efforts in order to modify the properties of polymeric fibers by organic or inorganic particles has increased in recent times because of increasing interest of fiber research in high-tech fiber applications. In addition to these attempts, the innovation of nanotechnology also leads to the development of nanoparticles for various end uses such as nanocomposite fibers. In this study spherical silica nanoparticles were introduced into polyamide 6 and drawn into filaments through a melt extrusion process. With two different particle diameters, different particle concentrations and types of surface modified silica as variables, preparation of polyamide 6/ SiO_2 nanocomposites were investigated for three different nanocomposite preparation methods (i) melt intercalation, (ii) solution intercalation and (iii) in-situ polymerization, while pure polyamide 6 was spun under the same condition as a reference. The study was carried out for multifilament nanocomposite fibers consisting of nano-silica fillers embedded in a fiber grade polyamide 6 matrix. Thus the effect of SiO_2 nanoparticles on the thermal, structural, morphological and tensile properties of polyamide-silica nanocomposites fibers were investigated by using thermal gravimetric analysis (TGA), differential scanning calorimetry (DSC), X-ray diffraction (XRD), Fourier transform infrared spectroscopy (FTIR), scanning electron microscopy (SEM) and standard tensile testing methods, respectively. TGA results showed that thermal stability of nanocomposites was notably improved compared to pure polyamide 6. According to DSC and XRD results the introduction of different silica nanoparticles into the polymer matrix as well as the cooling rate in the preparation method caused a phase transformation of the crystals of the polymer matrix from α- to γ-form crystals. SEM observations show that *In-situ* polymerization and solution intercalation are suitable methods for the preparation of inorganic/organic nanocomposites which can avoid the agglomeration of inorganic particles in polymer matrices, moreover modified silica particle disperse more homogeneously in the PA 6 matrix in comparison with the unmodified silica particle. GPC and relative viscosity measurement indicate that by increasing the silica content the molecular weight of nanocomposites decreased in comparison to pure polyamide 6 which suggests that there is an interaction between silica and polyamide 6. This is supported by a change of the proportion of the amino and carboxylic acid end groups which not only prove a molecular weight reduction but also explains the observed decrease of tenacity of nanocomposite fibers. In contrast to these findings the modulus of PA 6/silica nanocomposite fibers show a tendency to increase with increasing silica content.

Key words: nanocomposites, PA6/SiO_2, in-situ polymerization, melt intercalation, solution intercalation, melt spinning

Table of Contents

Abbreviation

PA	Polyamide
PA6	Polyamide 6
PA66	Polyamide 66
PSX05	Polyamide 6 / Aerosil OX50, 0.05 wt. %
PSX2	Polyamide 6 / Aerosil OX50, 0.2 wt. %
PSX5	Polyamide 6 / Aerosil OX50, 0.5 wt. %
PSA	Polyamide 6 / Aerosil 150
PAL	Polyamide 6 / Alu
PCe	Polyamide 6 / Ceria
PSX-W	PA6/Silica(Aerosil OX50 dispersed in water)
PSX-E	PA6/Silica(Aerosil OX50 dispersed in Ethanol)
PET	Polyethyleneterphthalate
PEN	Polyethylenenaphthalate
PP	Polypropylene
PE	Polyethylene
HDPE	High density polyethylene
EVA	Ethylene vinyl acetate
EPDM	ethylene propylene diene Monomer
PS	Polystyrene
PU	Polyurethane
PDMS	Polydimethylsiloxane
PCL	polycaprolactone
PEO	POLYETHYLENE OXIDE
SiO_2	Silica
Al_2O_3	Alumina
CeO_2	Ceria
TEOS	Tetraethoxysilane
DP	Degree of polymerization
DSC	Differential scanning calorimetry
DMA	Dynamic Mechanical Analysis
TGA	Thermogravimetry analysis
FTIR	Fourier transfer infrared
XRD	X-ray diddraction
WAXS	Wide angle x ray scattering

SAXS	Small angle x ray scattering
TEM	Transmission electron microscopy
SEM	Scanning electron microscopy
AFM	Atomic force microscopy
RV	Relative viscosity
GPC	Gel permeation chromatography
SEC	size exclusion chromatography
EAB	Elongation at break
UV	Ultraviolet

List of Figures

List of Tables

Chapter 1

General introduction and objectives

1.1. Introduction

In recent years, nanotechnology has become one of the most important and exciting forefront fields in Physics, Chemistry, Engineering and Biology. It shows great promise for providing us in the near future with many breakthroughs that will change the direction of technological advances in a wide range of applications.

The current widespread interest in nanotechnology dates back to the years 1996 to 1998 when a panel under the auspices of the World Technology Evaluation Center (WTEC), funded by the National Science Foundation and other federal agencies, undertook a worldwide study of research and development in the area of nanotechnology, with the purpose of assessing its potential for technological innovation [1].

However, it is during the past decade that nanotechnology went through a variety of disciplines. From chemistry to biology, from materials science to electrical engineering, scientists are creating the tools and developing the expertise to bring nanotechnology out of the research labs and into the market place. Nanocomposite materials, when using organic polymer and inorganic fillers, represent a merger between traditional organic and inorganic materials, resulting in compositions that are truly hybrid. Nature has created many (composite) materials, such as diatoms, radiolarian and bone [2], from which scientists can learn. Organic-inorganic composites with nanoscale dimensions are of growing interest because of their unique properties, and numerous potential applications such as enhancement of conductivity, toughness , optical activity [3], catalytic activity [4], chemical selectivity [5,6] etc. In these materials, inorganic and organic components are mixed or hybridized at nanometer scale with virtually any composition leading to the formation of hybrid/nanocomposite materials. Ceramics are generally known for their hardness and brittleness, along with their resistance to high temperatures and severe physical/chemical environments. In addition, many inorganic materials such as silica glass have excellent optical properties such as transparency [7]. For most applications, the brittleness (lack of impact strength) is the major, sometimes fatal, deficiency of ceramics. On the other hand, organic polymers are usually noted for their low density and high toughness. (i.e. high impact

strength), However, lack of hardness is one of the most significant flaws of polymers in many applications. Associated with the lack of hardness are the problems of low wear and scratch resistance as well as dimensional stability. The developments of conventional composite materials with ceramics as fillers and polymers as matrices are being researched extensively. Important examples of these composite materials are the semi-crystalline polymers mixed with inorganic particles. They consist of an amorphous-crystalline matrix (with a lamella thickness of typical size of 10 to 100 nm) and dispersed nanoparticles. They can be tailor-made to exhibit excellent elasticity (e.g., synthetic rubber) or optical transparency (e.g., polymethacrylates or Plexiglas).

1.2. Nanotechnology

Nanotechnology is the engineering of functional systems at the molecular scale. It is a field of applied science whose theme is the control of matter on an atomic and molecular scale. Nanotechnology has created a key revolution in the 21th century exploiting the new properties, phenomena and functionalities exhibited by matters when dealt at the level of few nanometers as opposed to hundred nanometers and above [8]. Nanoscale materials are already recognized as unique because they produce qualitatively new behavior when compared with their macroscopic counterpart. It is understood that when the domain size within the materials becomes comparable with the physical length scale, such as segments of a polymer macromolecule, the expected physical phenomena and the response to any external disturbance do not follow the established principles. The field of nanotechnology is one of the most popular areas for current research and development in all technical disciplines. This obviously includes polymer science and technology and even in this field, the investigations cover a broad range of topics. This would include microelectronics (which could now be referred to as nanoelectronics) as the critical dimension scale for modern devices is now below 100 nm. Other areas include polymer-based biomaterials, nanoparticle drug delivery, mini emulsion particles, fuel cell electrode polymer bound catalysts, layer-by-layer self-assembled polymer films, electrospun nanofibers, imprint lithography, polymer blends and nanocomposites. Even in the field of nanocomposites, many diverse topics exist including composite reinforcement, barrier properties, flame resistance, electro-optical properties, cosmetic applications, bactericidal properties. Nanotechnology is not new to polymer science as prior studies before the age of nanotechnology involved nanoscale dimensions but were not specifically referred to as nanotechnology until recently. Phase separated polymer blends often achieve nanoscale phase dimensions; block copolymer domain morphology is usually at the nanoscale level; asymmetric

membranes often have nanoscale void structure, mini emulsion particles are below 100 nm; and interfacial phenomena in blends and composites involve nanoscale dimensions. Even with nanocomposites, carbon black reinforcement of elastomers, colloidal silica modification and even naturally occurring fiber (e.g., asbestos-nanoscale fiber diameter) reinforcement are subjects that have been investigated for decades [9].

Almost lost in the present nanocomposite discussions are the organic–inorganic nanocomposites based on sol–gel chemistry which have been investigated for several decades [10]. In essence, the nanoscale of dimensions is the transition zone between the macro level and the molecular level. Recent interest in polymer matrix based nanocomposites has emerged initially with interesting observations involving exfoliated clay and more recent studies with carbon nanotubes, carbon nanofibers, exfoliated graphite (graphene), nanocrystalline metals and a host of additional nanoscale inorganic filler or fiber modifications.

Why Nanotechnology?

In the last two decades, new terms with the prefix `nano' have rushed into the scientific vocabulary, nanoparticle, nanostructure, nanotechnology, nanomaterial, nanocluster, nanochemistry, nanocolloids, nanoreactor and so on. The enhanced interest of the researchers in nanoobjects is due to the discovery of unusual physical and chemical properties of these objects, which is related to manifestation of so-called `quantum size effects.'  A key reason for the change in the physical and chemical properties of small particles as their size decreases is the increased fraction of the `surface' atoms, which occur under conditions (coordination number, symmetry of the local environment, etc.) differing from those of the bulk atoms. From the energy standpoint, a decrease in the particle size results in an increase in the fraction of the surface energy in its chemical potential [11].

‘What are the potential uses of nanotechnology?’ In the limited number of years that nanotechnology has been investigated, a plethora of answers to this question have been presented. It seems that nanotechnology could potentially solve almost any problem; thus, a more interesting question is, 'what real problems will nanotechnology solve?' Nanocomposite technology has been described as the next great frontier of material science. For example, polymer resins containing well-dispersed layered silicate nanoclays are emerging as a new class of nanocomposites. The reason is that by employing minimal addition levels of filler (< 10 wt %) nanoclays enhance mechanical, thermal, dimensional and barrier performance properties

significantly. It has been said that for every 1 wt% addition, a property increase on the order of 10% (or more) is realized. This loading-to-performance ratio is known as the “nano-effect”.

1.3. Polymer Nanocomposite

Nanocomposite technology is a new developing field, in which nanofiller are added to a polymer to reinforce and provide novel characteristics. Nanocomposite technology is applicable to a wide range of polymers from thermoplastics and thermosets to elastomers. Two decades ago, researchers from Toyota Central Research and Development produced a new group of polymer-clay complexes or composites, which was aptly called polymer-layered silicate nanocomposite. Today, there is a variety of nanofillers used in nanocomposites. The most common types of fillers are natural clays, synthetic clays, nanostructured silicas, nanoceramics and carbon nanotubes. The property enhancements have allowed these materials to commercially compete with traditional materials [8].

In the field of nanotechnology, the synthesis and applications of polymer nanocomposites is an important and strategic field of nanomaterial science.
Polymer nanocomposites represent a new class of material alternative to conventional filled polymers. In this new class of material, a nanosized inorganic-filler (at least one dimension $\leq$ 100 nm) is dispersed in a polymer matrix offering a tremendous improvement in performance properties of the polymer.

1.4. Application of nanocomposites in fibers and textiles

The trend to use ever-smaller sized particles of the materials is apparently growing in many markets and applications. There are challenging issues involved in fiber spinning during incorporation of a whole range of additives including the nano particles, which have been developed for textile applications with specific properties. In fiber spinning the main issue is to develop fibers with low content of additive [12]. Textile fibers are commonly used as apparel, upholstery, and carpets. Flame retardancy is an important and necessary property for some applications in some special areas of these textile products such as curtains, floor coverings, etc. Furthermore, since the late 1970s, in accordance with the rapid developments in science and technology the applications of textile fibers have also expanded to and increased, especially, in technical fields. Fibers are now widely used in the field of technical textiles such as military applications, safety and protective garments, automotive and aerospace applications, electronic and optical devices, geotechnical applications, and so on. These application areas require

additional fiber properties and functions such as high mechanical performance, flame retardancy, chemical resistance, UV resistance, electrical conductivity, soil resistance, water repellency, magnetic field resistance, radar absorbing, etc. Therefore, the number of studies on modifying the properties of polymeric fibers by various ways has increased recently [13, 14]. Using organic and inorganic particles as fillers in polymeric materials such as composites, films, and fibers is one of the methods of modifying these materials for high-technology applications. In addition to these attempts nanotechnology leads to developing the nanoscale systems and particles for various end uses such as nanocomposite fibers. As the size of particles decreases, their effects increase because of their larger total surface area per unit volume. Furthermore conventional methods used to modify fibers and fabrics, more often, do not lead to permanent effects and lose their functions after laundering or wearing; however because of their high surface energy nanoparticles present better affinity to fibers and fabrics and increase the durability of their function. Consequently, the number of studies about modifying the properties of polymeric textile fibers and fabrics by nanoparticles has increased recently.

1.5. Concept of the project

Making good samples of polymer matrix nanocomposites is a challenging area that draws considerable effort. Researchers have tried a variety of processing techniques to make polymer matrix nanocomposites, but creating one universal technique for making polymer nanocomposites is difficult due to the physical and chemical differences between each system and various types of available equipments. Each polymer system requires a special set of processing conditions to be maintained, based on the processing efficiency and desired product properties. Also different processing techniques in general do not yield equivalent results. During the preparation, spinning, and drawing of fibers two main problems exist: These are, firstly the difficulty of obtaining homogenous distribution of particles (particle aggregation) in the polymer and, secondly, chemical compatibility (adhesion) of particles and polymers. Thus, an appropriate way of mixing nanoparticles into the polymer is generally preferred. The three main ways of mixing nanoparticles into fiber-forming polymers are melt intercalation, solution intercalation, and in-situ polymerization. There are also some other methods such as in situ sol-gel processing of particles inside the polymer and in situ formation of metal particles from suitable precursors for metal/polymer nanocomposites. In this work nanocomposites and nanocomposite fibers have been prepared and the effect of preparation method on structural properties of the nanocomposite fibers is studied.

In addition, silicas are functional due to their high thermal stability, strength, and high modules, but are usually very brittle. Polymers on the other hand are much easier to process and are very tough, but are thermally less stable. A suitable combination of organic–inorganic nanocomposites provides a way of exploiting the advantages of these rather disparate materials. Spherical silica nanoparticles were introduced into polyamide 6 and drawn into filaments through a melt-extrusion process. The idea was to improve the strength and modulus of the resulting filaments by utilizing the interactions between the nanoparticles and the polymer.

1.6. Objective of the project

The properties of a polymer-reinforced composite are mostly influenced by the size, weight percentage, preparation method and nanoparticle modification. One of the main problems in the synthesis of nanocomposites which involve the application of nanoparticles, is the aggregation of the nanoparticles in the polymeric matrix as well as in the fiber and that severely limits the filler loading level. In addition specific characteristics of the nanocomposites can only be effective provided that the nanoparticles are well dispersed in the matrix.

The objective of this thesis is the synthesis of polyamide 6/SiO_2 nanocomposites and nanocomposite fibers according to different preparation techniques as well as the investigation of thermal, structural, morphological and tensile properties of nanocomposite fibers.

The scientific challenges encountered in this thesis can be summarized as follows:

1- Seek a general and facile synthesis technique by which nanoscale inorganic particles can be well dispersed in polyamide 6 matrices in order to minimize agglomeration.

2- The investigation of nanocomposites spinnability via melt spinning process.

3- Study the effect of particle size and content on crystallization as well as thermal and tensile properties of nanocomposites fibers for three different nanocomposite preparation methods.

4- Study the effect of nanoparticle as well as preparation method on structure and crystal phase transformation. (α→γ- crystal form)

5- Study the effect of particle surface modification on the dispersion quality of nanoparticle in polymeric matrix.

6- Compare the thermal, structural and tensile properties of modified particle based nanocomposites with unmodified particle based nanocomposites for In-situ polymerization technique.

1.7. Outline of the thesis

In the present thesis, the synthesis of nanocomposites and nanocomposite fibers is described. The influence of the addition of spherical silica nanoparticles as well as alumina and ceria particles on the properties of semi-crystalline polyamide-6 (PA6) in both granule and fiber form is investigated. A general introduction as well as objective of the thesis is given in chapter 1. Overview of hybrid organic-inorganic nanocomposites as well as nanocomposite preparation methods is described in chapter 2. Structures and properties of nanoparticles are given in chapter 3. Physical structure and polymorphism of polyamide 6 nanocomposites in addition to literature review is discussed in chapter 4. Characterization techniques which are used in this thesis are described in chapter 5.

The practical part of this thesis is divided into three parts. Part I deals with SiO_2- polyamide 6 nanocomposites production as well as polyamid 6 fiber nanocomposites by melt intercalation method, Part II deals with incorporationg SiO_2 in polyamide 6 polymeric matrix by solution intercalation method and part III deals with nanocomposite production by in-situ polymerization. The thesis thus consists of the following chapters:

Part I. Synthesis of Polyamide 6 / SiO_2 nanocomposite by melt intercalation

In chapter 6 the developed route to homogenously dispersed silica as well as alumina and ceria nanoparticles into polyamide 6 by melt intercalation method is given. The chapter consists of two parts. While in the first part master batches of polyamide 6 with silica nanoparticle likewise alumina and ceria in three different particle weight percentages were prepared, in the second part the nanocomposites fibers were produced based on fiber melt spinning by diluting the master batches with polyamide 6.

Part II. Synthesis of Polyamide 6 / SiO_2 nanocomposite by solution intercalation

In chapter 7 the nanocomposites were prepared via solution intercalation technique. After dissolving polyamide 6 granules in formic acid, SiO_2 nanoparticle in three different concentrations (wt. %) were added to solution under temperature and stirring, then at 80℃ an ultrasonic device is used for better dispersing and de-agglomeration of the solid in the solvent.

After that the solvent is removed by heating and after several washings with water, the obtained nanocomposites were dried in vacuum oven. Nanocomposite fibers were also prepared by melt spinning process using mini HAAKE twin-screw extruder by diluting nanocomposites with polyamide 6.

Part III. Synthesis of Polyamide 6 / SiO_2 nanocomposite by In-Situ polymerization

In chapter 8, first PA6/SiO_2 nanocomposites were prepared by polymerization process in three weight percent, and after extraction of granules in hot water and drying the nanocomposites fiber were prepared by extrusion process.

For all products resulting from application of those three nanocomposite preparation methods the thermal, structural and morphologic as well as tensile properties were studied. Thermal stability of nanocomposites is determined by thermal gravimetry analysis (TGA). Thermal transitions of polymer were determined by means of differential scanning calorimetry (DSC) and the morphology was studied by means of XRD, FTIR and SEM. Furthermore, tensile properties of the nanocomposite fiber were measured.

And finally in chapter 9 general conclusions is given.

Chapter 2

Hybrid organic - inorganic nanocomposites

2.1. Introduction

Organic-inorganic hybrid materials represent the natural interface between two worlds of chemistry (organic and inorganic) each with very significant contributions to the field of material science, and each with characteristic properties that result in diverse advantages and limitation. Hybrid organic-inorganic materials will play a major role in the development of advanced functional nano-materials. Hybrid organic–inorganic materials are not simply physical mixtures. They can be broadly defined as molecular or nano-composites with organic and inorganic components, intimately mixed where at least one of the component domains has a dimension ranging within nanometers. In recent years, polymer-based organic–inorganic hybrid materials, considered as innovative advanced materials, have gained increasing attention in the field of material science [15–24]. These new materials, so-called nanocomposites or organic–inorganic hybrids, can be considered as composites of which at least one phase is nano-sized [23]. Because of the nano-scale structure, nanocomposites possess unique properties typically not shared by conventional microcomposites. Consequently the main idea when developing hybrid materials is to take advantage of the best properties of each component that forms the hybrid, trying to decrease or eliminate their drawbacks getting in an ideal way a synergic effect; which results in the development of new materials with new properties.

In this study polyamide was used as polymeric matrix of the organic part and spherical silica as inorganic part.

2.2. Polymer matrices

Polymer/inorganic particle-based nanocomposites have shown significant improvement in mechanical, thermal and electrical properties. The large variety of polymer systems used in nanocomposite preparation can be classified as follow:

1. Thermoplastics
2. Thermosets
3. Elastomers
4. Natural and biodegradable polymers

2.2.1. Thermoplastic

Thermoplastics, such as polypropylene (PP), polyethylene (PE), copolymers such as poly (ethylene-co vinyl acetate) (EVA), poly (ethylene propylene diene) rubber (EPDM), polyamides (PA), poly – ethylene terephthalate (PET) and polystyrene (PS) have been used as polymer matrices for the preparation of nanocomposites.

2.2.1.1. PA66/ SiO_2 nanocomposite

In spite of extensive studies made about polyamide-layered silicate nanocomposite, there is not much research about polymer/SiO_2 nanocomposite. HUIMIN LU et al. [25] prepared successfully PA66/nano- SiO_2 composites by melt compounding technique. They studied the effect of nano-SiO_2 on the morphology, crystallization and dynamic mechanical properties of polyamide 66. The influence of nano- SiO_2 on the tensile fracture morphology of the nanocomposites was studied by scanning electron microscopy (SEM), which suggested that the nanocomposites revealed an extensive plastic elongation of the matrix polymer. The crystallization behavior of polyamide 66 and its nanocomposites were studied by differential scanning calorimetry (DSC). DSC non-isothermal curves showed an increase in the crystallization temperature along with increasing degree of crystallinity. Dynamic mechanical properties (DMA) indicated significant improvement in the storage modulus and loss modulus compared with neat polyamide 66. In another study [26] the organic–inorganic hybrid nanocomposites comprising of polyamide-66 and SiO_2 were synthesized through sol–gel technique at ambient temperature. The inorganic phase was generated in-situ by hydrolysis–condensation of tetraethoxysilane (TEOS) in different concentrations, under acid catalysis, in presence of the organic phase, PA66, dissolved in formic acid. Infrared (IR) spectroscopy was used to monitor the microstructural evolution of the silica phase in the PA66 matrix. Wide angle X-ray scattering (WAXS) studies showed that the

crystallinity in PA66 phase decreased with increasing silica content. Atomic force microscopy (AFM) of the nanocomposite films revealed the dispersion of SiO_2 particle with dimensions of less than100 nm in the form of network as well as in the form of a linear structure. X-ray silicon mapping further confirmed the homogeneous dispersion of the silica phase in the bulk of the organic phase. The melting peak temperatures slightly decreased compared to neat PA66, while an improvement in thermal stability by about 20℃ w as achieved with hybrid nanocomposite films, as indicated by thermogravimetric analysis (TGA).

2.2.1.2. PET/SiO_2 nanocomposite

PET is a thermoplastic material that has contributed to applications in a wide array of fields, both in fiber and non-fiber application. PET/Silica nanocomposites were investigated by Wan-Gyu Hahm [56]. Two kinds of fumed silicas, hydrophilic/hydrophobic inorganic nano-particles of 7 nm, were used as filler, and PET-fumed silica nanocomposites were prepared by *in-situ* polycondensation. The various effects of fumed silicas in the PET matrix as functions of filler type and filler content were studied and compared with the results of former study by direct melt compounding [27]. The degree of particle-particle interaction and dispersion of each fumed silica on PET nonpolar matrix were investigated, and the crystallization behaviors and dynamic rheological properties of nanocomposites due to the improvement of dispersibility for nano-particles were discussed in detail. Mechanical analysis were also performed to explain the relationship between the structure and properties of these nanocomposites.

2.2.1.3. PEN/SiO_2 nanocomposite

High performance poly (ethylene 2, 6-naphthalate) (PEN), with its superior physical and mechanical properties, has been used in specialty films, fibers, and in blow moldings. However, the applications of PEN are limited, because PEN exhibits a relatively high melt viscosity, which makes fiber spinning and injection molding difficult. The effect of stearic acid modification on the dispersion quality of silica nanoparticles and the adhesion between the filler and polymer matrix with stearic acid concentration were investigated by Seon Hoon Ahn and co-workers [59]. Thus, the wettability of silica nanoparticles was improved by the addition of stearic acid. The presence of adsorbed stearic acid on the surface of the silica nanoparticles reduced the interaction between silica nanoparticles, and reduced as well the size of agglomerates with increasing concentration. Silica nanoparticle–reinforced poly (ethylene 2, 6-naphthalate) (PEN) composites were melt-blended to investigate their mechanical properties and the processability of the composites. The torque and total torque values of the composites decreased with increasing

silica nanoparticle content. The tensile modulus of the composites reinforced with unmodified silica nanoparticles increased with increasing silica content, whereas the tensile strength and elongation decreased.

2.2.1.4. PE/ SiO_2 nanocomposite

Polyethylene (PE) and silica are perhaps the simplest and most common organic and inorganic polymers, respectively. Sertchook et al. [27] describe, for the first time, a physically interpenetrating nanocomposite between these two elementary polymers. While polymer-silica composites are well known, the nanometric physical blending of PE and silica has remained a challenge. A method for the preparation of such materials, which is based on the entrapment of dissolved PE in a polymerizing tetraethoxysilane (TEOS) system, has been developed. Specifically, the preparation of submicron particles of low-density PE at silica and high-density PE at silica is detailed, which is based on carrying out a silica sol-gel polycondensation process within emulsion droplets of TEOS dissolved PE, at elevated temperatures. The key to the successful preparation of this new composite has been the identification of a surfactant, PE-b-PEG, that is capable of stabilizing the emulsion and promoting the dissolution of the PE. A mechanism for the formation of the particles as well as their inner structure are proposed, based on a large battery of analyses, including transmission electron microscopy (TEM) and scanning electron microscopies (SEM), surface area and porosity analyses, various thermal analyses including thermal gravimetric analysis (TGA/DTA) and differential scanning calorimetry (DSC) measurements, small-angle X-ray scattering (SAXS) measurements and solid-state NMR spectroscopy.

2.2.1.5. PP/ SiO_2 nanocomposite

Polypropylene (PP) has also been widely used for the preparation of nanocomposites. Since it does not include any polar group on its backbone, it is not possible to disperse the hydrophilic particle without using suitable compatibilizers. M. Garcia et al. [55] have reported preparation of Polypropylene-SiO_2 nanocomposites using twin-screw extruders. The properties of the nanocomposites were studied using two different inorganic fillers: colloidal (sol) and powdered silica nanoparticles. Reinforcing and toughening effects of the nanoparticles on the polymer matrix were found at a loading of 4.5 wt. %, which is lower than for most particulate filled composites. The use of silica nanoparticles led to different microstructure when compared with that of the pure polymer. Addition of colloidal silica to the polymer matrix produced good filler dispersion while the use of powdered silica resulted in aggregated silica particles in the polymer

matrix. There was no noticeable improvement of the mechanical properties when powder silica was added to the pure polymer. On the contrary, the presence of silica-sol nano-particles in the polymer matrix led to an increase of both Young modulus and impact strength, from 1.2 GPa to 1.6 GPa and from 3.4 kJ/m^2 to 5.7 kJ/m^2, respectively.

2.2.1.6. PTT/ SiO_2 nanocomposite

Poly (trimethylene terephthalate) (PTT) is a relatively new type of linear aromatic polyester. During recent decades, it has attracted attention not only because of its excellent mechanical and electrical properties, but also because one of its raw materials, 1,3-propanediol, is a renewable resource, which can be derived from renewable materials such as corn and starch. The sol–gel technique has provided promising opportunities for the preparation of polymer/inorganic hybrid materials at the molecular level, which ensures the inorganic particles, are well dispersed in the organic matrix. In this study [38], poly (trimethylene terephthalate) (PTT)/silica nanocomposites were fabricated via the sol–gel technique and *in-situ* polycondensation. Fourier transform infrared and nuclear magnetic resonance analyses confirmed that some PTT molecular chains were grafted to the surface of silica. Unlike pure PTT, the grafted PTT was insoluble in a mixed solvent of chloroform and hexafluoro-2-propanol. Both transmission electron microscopy and scanning electron microscopy showed that the silica particles, with a size of 40–50 nm, were homogeneously dispersed in the PTT matrix with no preferential accumulation in any region. Differential scanning calorimetry revealed that the glass transition temperature and cold-crystallization peak of the composites gradually increased with increasing silica loading. A simultaneous increase of stiffness and toughness was observed for the concentration of nanocomposites.

2.2.2. Thermosets

Epoxy and polyurethane have been used as polymer matrices for the preparation of nanocomposites, too. Polyurethane (PU) is becoming increasingly important as an engineering material because it has excellent abrasion resistance and displays properties of both elastomers and plastics. Wang and Pinnavaia [29] have synthesized intercalated nanocomposites based on elastomeric polyurethane. Khudyakov and Zopf [49] also studied the effect of colloidal silica and organoclays on properties of PU. The studies on epoxy systems considered the ring opening polymerization of epoxides to form polyether nanocomposites. Studies [30, 31] of both rubbery and glassy epoxy/clay nanocomposites using different type of amine curing agents were

conducted and the mechanisms leading to the mono-layer exfoliation of clay layers in thermoset epoxy systems were elucidated.

2.2.3. Elastomers

Burnside and Giannelis [32] have described the two-step preparation of silicon rubber-based nanocomposites. First, silanol-terminated poly (dimethyl siloxane) (PDMS) was blended at room temperature with dimethyl-ditallow ammonium-exchanged montmorillonite, followed by cross-linking of the silanol end groups with tetra ethyl- orthosilicate (TEOS) in the presence of bis(2-ethylhexanoate) as catalyst at room temperature. Also Okada and co-worker [33] obtained a nitrile rubber (NBR) – based nanocomposite in a dual-step synthesis.

2.2.4. Natural and biodegradable polymers

Natural and biodegradable polymers are a new generation of polymers that are relatively friendly to the environment with little or no impact when disposed. Such polymers include polylactide (PLA), starch, and cellulose among others. Although these polymers are considered to be environmentally-friendly, they have relatively weak mechanical properties, such as brittleness, low heat distortion, low tensile strength. And their use in packaging is limited due to high gas permeability [34]. Addition of nano-scale fillers has been shown to improve these properties significantly, allowing these polymers to be used in applications such as disposable food service items, food packaging, health care product, packing foams and agricultural mulch film. PLA polymers are linear aliphatic polyester, generally produced by ring-opening polymerization of lactide dimer. Sinha Ray and Okamoto [35] have shown that the addition of nanoscale modified montmorillonite increased both solid and melt state properties, such as flexural properties, rheological properties, reduced gas permeability and increased rate of biodegradability. Ogata et al. [36] also reported similar enhancement of properties. Another biodegradable polymer is polycaprolactone (PCL), linear polyester manufactured by ring-opening polymerization of ε-caprolactone. The PCL chain is flexible and exhibits high elongation at break and low modulus. Its physical properties make it very attractive, not only as a substitute material for non-degradable polymer but also as a plastic material for medical and agricultural applications. The main drawback of PCL is its low melting point (65℃), which can be overcome by blending it with other polymers. Many attempts to prepare PCL nanocomposites with much improved mechanical and materials properties than that of neat PCL have been reported [34].

2.3. Polyamide

Polyamides are considered to be one of the most important super-engineering materials because of their superior mechanical properties at elevated temperature due to their thermal stability. The two major types of polyamides are polyamide 6 and polyamide 66. PA 6 is prepared by the polymerization of caprolactam. PA 66 is derived from the polycondensation of hexamethyelene diamine with adipic acid. Polyamides are crystalline polymers. The key features include a high degree of solvent resistance, thoughness, and fatigue resistance. Polyamides do exhibit a tendency to creep under applied load. Glass fibers and mineral fillers are often used to enhance the properties of polyamides. In addition, the properties of polyamides are greatly affected by moisture. The largest area of application for polyamide is in fiber and engineering plastic. Molded applications include automotive component, related machine parts (gear, cams, pulleys, rollers, etc.), and electrical insulation.

Earlier studies [79] have illustrated that the addition of clay to PA has improved the strength, stiffness, barrier, and heat resistance properties of polyamide 6. The barrier resins exhibit reduced moisture absorption and increased melt stability. Toyota researchers (1989) have shown that, similar to other nanocomposites, PA nanocomposites are able to achieve a lot of improved characteristics compared to pure PA. Thus, it has been reported that PA6 nanocomposites show higher tensile strength, higher tensile modulus, higher heat distortion temperature, increased solvent resistance, decreased thermal expansion coefficient, reduced gas permeability and increased flame retardancy. With these enhanced properties, PA nanocomposites have found increased application in the automobile and textile industries, where stronger yarn could be produced, with better extensional characteristics [88-90].

2.3.1. Introduction and definition of polyamide [37-39]

Polyamides are polymers with amide groups –NH-CO- in the main chain. They are usually subdivided in either aliphatic and aromatic types or in polymers of the type -[-NH-R-CO-]-$_n$ and polymers of the type -[-NH-R_1-NH-CO-R_2-CO-]-$_n$ where the bi-functional units R,R_1, and R_2 can be aliphatic, cycloaliphatic, or aromatic. Branched polyamides are presently niche products. In accordance with DIN 60 001, part 3, 10.88 edition, PA fibers are classified as synthetic man-made fibers. The aliphatic chains by which up to at least 85% of molecular mass is bonded into the linear macromolecules are linked by amide groups. That means, one characteristic of the chain forming polymers is the continuously repeating functional acid amide groupings [CO-NH] in the main chain. Also in the international ISO 2076 standard, 12.89 edition “Generic name for

man-made fibers" polyamides or *nylon* are described as chemical fibers, where the polymers consist of linear (aliphatic) macromolecules with the repeating [CO-NH] functional group in the chain. These so-called homo-polyamides can be subdivided into two groups on the basis their chemical structure:

- amino carboxylic acid types (AB) and

- diamino dicarboxylic acid type (AA-BB),

Where *A* indicates the amino groups and B the carboxyl groups. The number of carbon atoms in the individual linear monomer serves as a code number. In the case of the AA-BB type, the number of carbon atoms of the diamine is indicated first of all, and then those of the dicarboxcylic acid. In English linguistic usage, the word nylon is also used synonymously as a generic term for polyamide. In the USA, other polyamides, e.g. PA11, may also be described as nylon in accordance with the concept definition valid there. It was originally the brand name selected by DuPont for PA66. Perlon on the other hand is a protected brand name for some PA6 fiber producers, and may not be used for the general description of caprolactam based PA fibers. Polyamide fibers are produced either by the polycondensation of diamines with dicarboxylic acids or by the polycondensation of ω-aminocarboxylic acid containing at least 6 carbon atoms, or by the hydrolytic polymerization of at least 7-link ring systems containing a carbonamide group, e.g. caprolactam. The aramids also belong to the polyamides. They consist of aromatic chain links which are directly bonded to at least 85% of their mass by amid groups into linear macromolecules, and in which up 50% of the amide bonds can be replaced by imide bonds. The aramides have their own published fiber table [49], and the aramides are therefore not treated here in further detail.

2.3.2. Invention and developments of PA 6 and PA66 [61-83]

The history of PA fibers begins at the turn of the century. In 1902 and 1904, S.GABRIEL, TH.M.MAASS, A.MANASSE and J. VON BRAUN [37, 40-42] became involved with the ring formation of Ɛ-aminocaproic acid, which was found capable of being 20-30% converted into caprolactam. The importance of this in industrial use was not however recognized at that time.

In 1929, W.H.CAROTHERS started to work at the DuPont de Nemours & Co. chemical group in the field of polycondensation and ring formation of bifunctional compounds. He knew about the work of H.STAUDINGER on macromolecule theory in the 2nd half of the 20s, and wanted to prove the concept by synthesizing very large molecules. The results of W.H.CAROTHERS's

work are documented in numerous publications [40- 42]. He established the fact that the polycondensation of a large number of bifunctional compounds led to undecomposed meltable fiber forming polymers, which were unknown until that time (1930). In 1932, W.H. CAROTHERS and J.W.HILL discovered that so-called superpolyester was produced from molten polyesters by molecular distillation, from which threads can be drawn, which solidify in air. The principle of producing synthetic fiber material was discovered in this way. In 1934, W.H CAROTHERS produced in a trial polyamide from 9-aminononanoic acid a starting material which was of interest from the technical standpoint. On 28 February 1935, he succeeded in synthesizing polyamide from hexamethylen diamine and adipic acid. Due to the practically unlimited raw material base (benzene and phenol), this polyamide was selected for further large scale development, and a patent was applied for on 9 April 1937. In the initial development stage of the subsequently so-called nylon process, trial production of the yarns was carried out under the name of Fiber 66. In 1938 DuPont published the results of research for the first time, and small scale production began in the same year. 1939 was the start of the industrial production of nylon, as the fiber was then called. Production was at first concentrated predominantly on military end-uses such as parachutes and aircraft tire cord yarn, but was extended to civil and industrial applications after the war. Unaware of CAROTHERS's work- as he himself said- P.SCHLACK was engaged from 1928 in the scientific laboratory of the I.G. Farben AG "Aceta" plant in producing a synthetic fiber, and also, among other projects, with the polymerization of caprolactam. Although, in his paper published in 1930, W.H.CAROTHERS disputed the polymerization of ε-caprolactam with or without catalyst, and trials conducted by him and G.J.BERCHET on polycondensation 6-aminocaproic acid led only to a polymer with a low degree of polymerization from which no fibers could be spun, P.SCHLACK worked on in this field unaware of the publication. On 29 January 1938 he succeeded in splitting up the lactam ring with aminocaproic acid hydrochloride as catalyst, and turns it into linear polymer. That was the hour of birth of PA6. A year later, independently of P.SCHLACK's discovery, O.WICHTERLE also successfully polymerized caprolactam. A patent on the caprolactam process was applied for on 11 June 1938 [43]. Polyamide 6 production started in 1939, at the end of this year the first monofils came on to the market under the name of Perluran, subsequently designated Perlon L. Large scale production of Perlon filament yarn began in 1943 in the plant located in Landsberg a.d. Warthe; the plant under construction in Premnitz (Westhavelland) was unable to start up its planned large scale production of Perlon filament yarns because of the war. The production of PA6 filament yarn was re-established in the Thüringian VEB "Wilhelm Pieck" artificial fiber plant in Schwarza near Rudolstadt in 1946 after small quantities had already been produced there

since 1945. Kunstseidenfabrik Bobingen near Augsburg started production in 1949, and production of Perlon filament yarns began in Glanzstoffwerk Oberbruch in 1950.

2.3.3. Polyamide 6 production

A polyamide that is derived from a diacid and a diamine is categorized as AABB type (e.g. polyamide 66). On the other hand, a polyamide synthesized from an amino acid or a lactam is termed as AB type (i.e. polyamide 6). Straight chain aliphatic polyamides are identified either as polyamide XY or polyamide Z, where X,Y and Z represent the number of carbon atoms present in respective structural units in the monomer. In an AABB type, the number X refers to the number of carbon atoms in the diamine and Y to that in the diacid. In the case of AB type, Z represents the number of carbon atoms in the monomer. Examples are given below [44].

Example 1

Raw material:	$H_2N—(CH_2)_6—NH_2$	+	$HOOC\text{-}(CH_2)_8\text{-}COOH$
Name:	Hexamethylene diamine (HMDA)		Sebacic acid(SA)
Type:	AA		BB

Polymer repeat unit:	$\text{-[-NH-}(CH_2)_6\text{-NH-CO-}(CH_2)_8\text{-CO-]-}$
Name:	Polyamide 610
Type:	AABB
	X = 6 , Y = 10

Example 2

Monomer: $OC\text{-}(CH_2)_5\text{-}NH$ (lactam ring)

Name:	Caprolactam
Type:	AB

Polymer repeat unit:	$\text{-[-OC-}(CH_2)_5\text{-NH-]-}$
Name:	Polyamide 6
Type:	AB
	Z = 6

2.3.3.1. Raw materials

Polyamide 6 is a polyamide Z type of polymer, where the Z represents the number of carbon atoms in the monomer. Polyamide 6 is typically produced from caprolactam in the following manner [45].

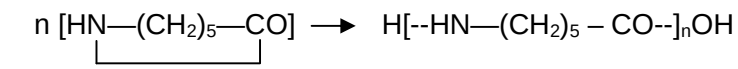

The purity of caprolactam is critically assessed for the production of polyamide 6 polymer. Caprolactam can be synthesized via a number of methods. All procedures start from raw materials like phenol, benzene, toluene or cyclohexane. The crude caprolactam must be carefully purified to have the specifications as given in Table 2.1 [46]

Table 2.1 Caprolactam specifications

Property	**Value**
Freezing point (dry basis) ˚C	69.0 (minimum)
Percentage transmission at 410 nm (65 wt. % aqueous solution)	92.0 (minimum)
Permanganate number	7 (maximum)
Moisture (%)	0.10 (maximum)
Iron as Fe (ppm)	0.5 (maximum)
Volatile bases (as NH_3) (ppm)	5 (maximum)
Ignition residue (ppm)	10 (maximum)
Water insoluble	Passes test
Cyclohexanone oxime (ppm)	10 (maximum)
Free alkalinity (meq kg^{-1})	0.04(maximum)

Detailed analytical methods for purity analysis are reported in the literature [41, 47, 48] .

2.3.3.2. Types of catalyst

Caprolactam does not polymerize in a completely dry condition [47- 49]. It requires a catalyst which converts a small amount of caprolactam(CL) to aminocaproic acid(ACA) which helps in polymerization process. The catalyst could be an acid, a base, or simply water which in this case makes the control of reaction easy [44, 45]. The conditions required and the effect of each type of catalyst system is given in Table 2.2 [44].

Table 2.2 Some characteristics of catalyst system for polymerization of caprolactam

	Catalyst systems		
Parameter	Acid	Base	Water
Type	Strong, like Hydrochloric acid or their salts	Carbonate, hydride, alcoholate, and hydroxide of alkali and alkaline earth metals	---
Rate	Fast	Very fast	slow
Special condition	Anhydrous	Anhydrous	---
Yield	Low	High	High
Use	Not used commercially	Slow promise	Commercially used

Although acid or base catalyst system may also be used, in contrast to these the base-catalysed system has the advantage of high production rate, high molecular weight and narrow molecular weight distribution, although the control of reaction in the system is rather critical. Hence, generally, the water-catalysed system is used in industry.

2.3.3.3. Parameters in the water-catalyzed system

In a water catalyst system the polymerization is controlled by temperature in the range of 225˚C-280˚C, amount of water present in the dissolved phase (5-10%), stabilizer content of 1% and time of polymerization [45]. The effect of various parameters on the polymerization of

caprolcatam catalysed by water is summarized in Table 2.3 [50]. Figures 2.1-2.2 show the effect of changes in these parameters.

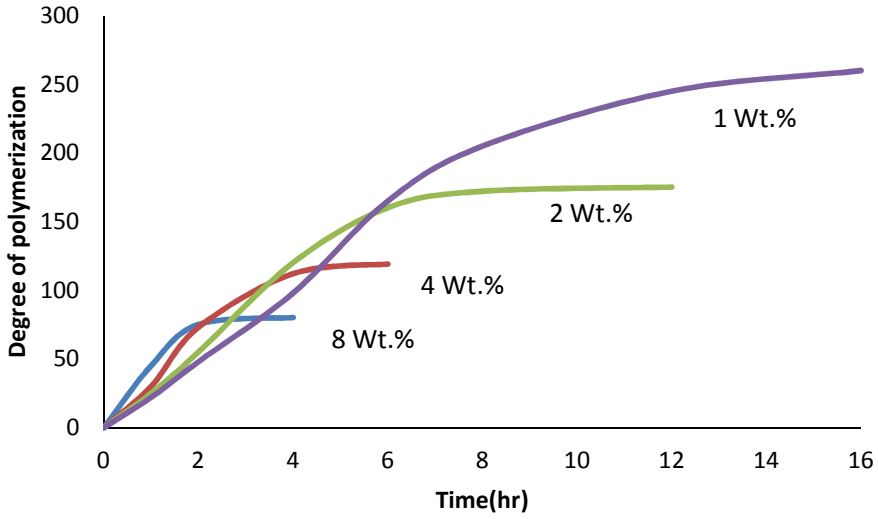

Figure 2.1 Effect of initial water concentration (W_0) on degree of polymerization

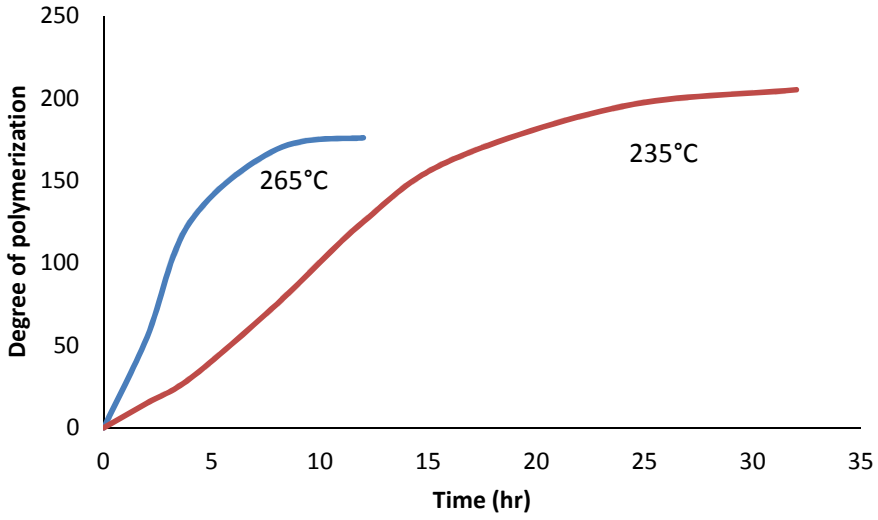

Figure 1.2 effect of temperature on degree of polymerization (W_0 = 2%)

Table 2.3 Effect of various parameters on caprolactam polymerization

Increase in Parameter	Molecular weight	Time of polymerization	End groups	Relevant figure number
Water concentration	Decrease	Decrease	Increase	2.1
Temperature	Decrease	Decrease	Decrease	2.2
Stabilizer content	Decrease	—	—	—
Time of polymerization	increase	—	Decrease	—

2.3.3.4. Control of molecular weight

The principal factors which control molecular weight are: (1) temperature, (2) amount of water, (3) time of polymerization and (4) stabilizer content (up to 1%). The stabilizer can be either an acid (e.g. acetic acid, benzoic acid) or a base (e.g. benzylamine). An acidic stabilizer leaves the carboxyl end group in the polymer free, thus making it reactive to basic dyes. On the other hand, use of a basic stabilizer yields an acid-dyeable polyamide. In the case of tire cord production, a thermal stabilizer has also to be incorporated. The following relationship [51, 52] provides a useful mean to industry to control the degree of polymerization (DP) of polyamide 6:

$$DP = \frac{p + r + q}{(1 + r)(1 - p)}$$

Where

$$p = 1 - \frac{[COOH] + [NH_2]}{[\mathrm{COOH}]_0 + [NH_2]_0}$$

$$r = \frac{[NH_2]_0}{[COOH]_0}$$

And

$$q = \frac{[COOH]_0^{'}}{[COOH]_0}$$

Here $[COOH]_0$ and $[COOH]$ represent the carboxyl group concentration at the start of polymerization and after time, t, respectively; $[NH_2]_0$ and $[NH_2]$ represent the amino group concentrations at the initial(start) and final(end) stage, respectively; and $[COOH]_0^{'}$ represents the

initial concentration of carboxyl group of a mono-functional acid acting as a stabilizer(e.g. acetic acid).

2.3.3.5. Polymerization mechanism

The preparation of PA6 proceeds from a ring-opening polymerization of caprolactam which can be divided into three types:

- hydrolytic polymerization
- anionic polymerization
- cationic polymerization

But the polymerization according to an anionic or cationic route plays only a minor role. Industrially caprolactam polymerization is preceded by a hydrolysis step,

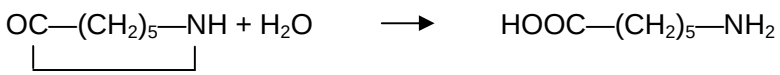

CL + Water ⟶ ACA (Ɛ-aminocaproic acid)

ACA, thus produced, adds to further monomer units, initiating polymerization. This is known as step addition,

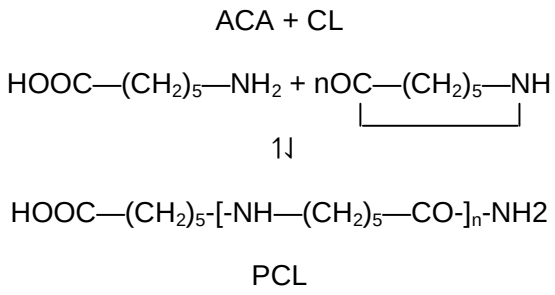

$$CL \rightleftharpoons PCL$$

$$10\% \quad 90\%$$

Once the equilibrium is reached, which usually takes about 4-6h in a polymerization reactor, a step growth polymerization occurs involving the PCL molecules formed. This reaction leads to an increase in molecular weight.

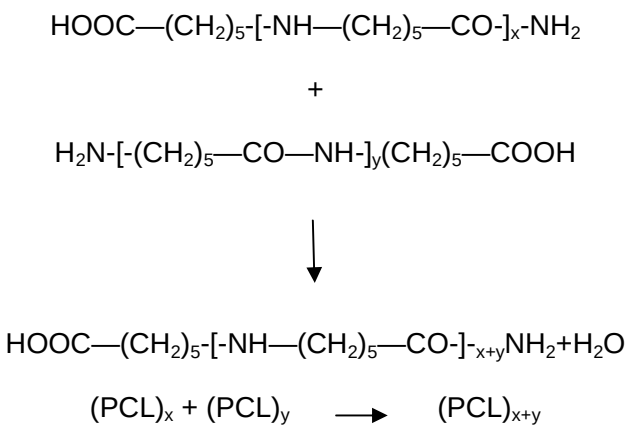

2.4. Nanoparticle based nanocomposite

Inorganic particles are used in different matrices for specific purposes [54]. For metals, fillers improve high temperature creep properties and hardness when compared with the pure metal. For ceramics, fillers are used to improve their toughness [53] and for polymers for the increase of stiffness, strength, electrical properties and occasionally for toughness. The fillers used in polymer nanocomposites are usually inorganic fillers, although carbon nano-tubes and carbon black are exceptions. Nano-fillers may possess different shapes: (a) spherical like silica and carbon black (b) rod or fiber like as synthetic whiskers, or carbon nano-tubes and (c) in sheet or platelet shape as in layer silicate such as montmorillonite. The incorporation of fillers into organic polymers may result in a brittle composite material. In addition, the amount of filler that can be incorporated is limited (thus, sometimes the addition of higher amounts of filler does not improve the mechanical properties of the material) and the filler may not be uniformly dispersed in the organic polymer. The efficiency of the filler to modify the properties of the polymer is primarily determined by the degree of dispersion in the polymer matrix.

2.4.1. Particle typically used

Nanoparticle-filled polymers are attracting considerable attention since they can induce property enhancement that is sometimes even higher than for the conventional micro-sized fillers applied in the polymers at volume fractions in the range of 1–5% [61]. Different particles have been used to prepare polymer/inorganic particle nanocomposites, including:

. Metal (Al, Fe, Au, Ag, etc.)
. Metal oxide (ZnO, Al_2O_3, $CaCO_3$, TiO_2 etc.)
. Non-metal oxide (SiO_2) [48]
. Other (SiC)

In literature there are quite a lot of materials used as filler [65- 70], while the selection of nanoparticles aims on the desired thermal, mechanical, and electrical properties of the nanocomposites. For example, Al nanoparticles are often selected due to their high conductivity; calcium carbonate particles are chosen because of the relative low cost of the material, and silicon carbide (SiC) nanoparticles are used because of their high hardness, corrosion resistance, and strength [64].

A variety of inorganic materials, especially nano-ceramic powder materials such as titanium oxide (TiO_2), zirconium oxide (ZrO_2), aluminum oxide (Al_2O_3), silicon carbide (SiC), silicon dioxide (SiO_2), etc. have been successfully used as additives for reinforcement in order to improve the stiffness and strength of polymers .

2.4.2. Silica

Silica has been used in different polymers as a reinforcement material. Examples are in methacrylate [61-72], polyimide [6, 73], polyamide [74], rubbery epoxies [75], and acrylic [76]. Particularly, Rong et al. have reported for polypropylene composite an improvement of tensile performance filled by a low amount of SiO_2 nanoparticles [78]. Li et al. have incorporated SiO_2 nanoparticle to polyaniline to produce an electrical conducting nanocomposite. The specific function of the filler is based on the specific resin system, particle size, surface area, loading and surface modification. Because of the high bond energy in the Si-O bond, SiO_2 has extremely high thermal stability. SiO_2 also possesses a very low thermal expansion coefficient.

2.5. Organic-inorganic nanocomposite

Polymer nanocomposites constitute a class of hybrid materials composed of a polymer matrix and an inorganic filler component which has at least one dimension in the nanometer (100 nm) size domain [77- 79]. The properties of a polymer-reinforced composite are mostly influenced by the size, shape, composition, state of agglomeration, and degree of matrix filler adhesion [80]. Optimum surface curvature at the polymer-filler interface can be realized when large surface areas are created, which is possible when the filler particles are sufficiently small [81]. Decreasing the particle size to the nano-size dimension influences the macroscopic properties of the polymer because a breakdown of the common rule-of-mixture theory occurs [82]. A major challenge remains, however, to effectively incorporate mono-disperse nanoparticles inside a polyamide matrix since a drawback of such small particles is their tendency to aggregate, particularly when higher particle concentrations, intimate mixing and prolonged heating are part of the reaction conditions. Presently, researchers mainly focus on the following three different methods in order to prepare polymer/inorganic particle nanocomposites, including: in-situ polymerization [83], melt compounding by twin-screw extrusion [84, 85], solution blending [86], and high shear mixing with three roll milling.

2.5.1. Melt intercalation

Melt intercalation is the most widely used method in polymer/ particle nanocomposite preparation, and it has tremendous potential for industrial application. An advantage of this method over the others is that no solvent is required. The melt intercalation process involves mixing the particles by annealing, statically or under shear, with polymer pellets while heating the mixture above the melting point of the polymer [8]. Schematic representation of the flow diagram for melt-intercalation process is as shown below in Figure 2.3.

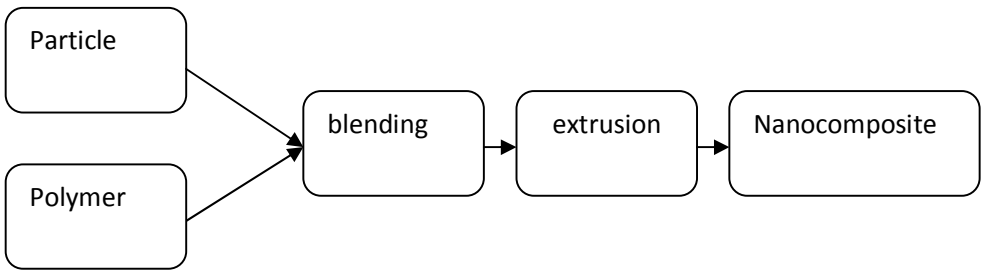

Figure 2.3 Flow diagrams for melt-intercalation process.

2.5.2. Solution intercalation

In nanocomposites prepared via solution blending, the filler is suspended in suitable solvent under vigorous stirring condition. In addition to mechanical mixing, ultrasound can be used to separate the filler particles. When the dispersion is satisfactory and the polymer is solved, the solvent is evaporated to yield the filled polymer. This method is suitable for systems that consist of a polymer which is soluble in a common solvent, in which also the nano-filler can be dispersed well. Figure 2.4 represents the steps involved in the solution process.

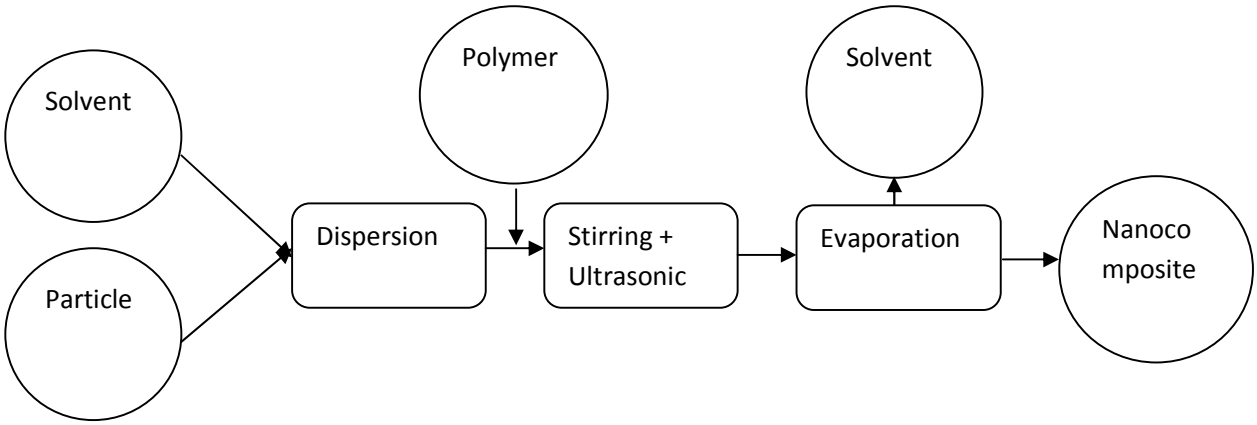

Figure 2.4 Flow diagrams represents the steps involved in the solution process.

2.5.3. in-situ polymerization

In -situ polymerization involves the dispersion and distribution of particle in the monomer followed by polymerization. The particle is swollen within the liquid monomer or a monomer solution so that polymer nanocomposite formation can occur during polymerization process. Polymerization can be initiated either by heat or radiation, diffusion of a suitable initiator, or by an organic initiator [8]. Flow diagram for In-Situ Polymerization process is as shown Figure 2.5

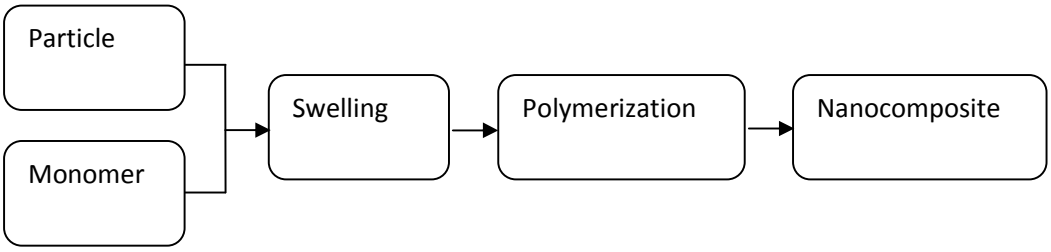

Figure 2.5 flow diagrams for In- Situ polymerization process

2.6. Polyamide 6/SiO_2 nanocomposite and nanocomposite fiber

Polymer fibers are commonly applied as textiles, carpets, or as additives to reinforce or modify material properties [87-91]. As an additive, they modify bulk polymer properties by blending; they enforce the stability of tires in automobile industry or the flexibility of hardened cement as additive for construction [92]. Already the properties of the fibers themselves depend on their composition and processing conditions [93]. Common melt spun polymer fibers are made from polymers like polypropylene, polyethylene, polyesters, or polyamides [88-91]. In addition, some fibers are modified by being blended with other polymers [94] or by being compounded with very small amounts of inorganic components, [95] e.g., for dyeing. In contrast to the polymer fibers, bulk polymers are easy to be modified by inorganic additives like minerals (e.g., kaolin, quartz), exfoliated layer minerals (montmorillonite nanocomposites), nano-fibers (carbon or mineral nano-fibers), or by spherical inorganic particles (amorphous Al_2O_3, $CaCO_3$, fumed silica, pigments) [96-98]. Despite successful attempts to transfer carbon nano-fiber and montmorillonite-modified polymer nanocomposites[99-102] into fibers, difficulties result from particle aggregation, from polymer degradation catalyzed by the additives or from the increased crystallization velocity and crystalline polymer [101,103], resulting in brittle fibers. Good processability during the preparation and drawing of composite fibers requires a homogeneous distribution of the filler in the polymer matrix. As a consequence, a high compatibility between the fiber forming polymer and the inorganic filler is generally preferred. A modification of polymer fibers with inorganic fillers by avoiding these problems will give access to a new class of fibers with changed material properties. While nano-sized silica, aluminum oxide, and $CaCO_3$ particles were already used as fillers for polymer compounding [98, 104] or as scratch resistant coatings, [105, 106] only few papers are published on fibers filled with inorganic particles, apart from TiO_2.

Commonly just low amounts of that filler (pigments) are applied for delustring. Nevertheless, there are already polymer fibers filled, e.g., with exfoliated montmorillonite [101, 102] and carbon nano-fibers [99, 100] reported in the literature. Problems arise from the weak ionic bonds between the montmorillonite and the applied cationic surfactants (e.g., alkyl ammonium salts) used as a compatabilizer to the polymer matrix. As a result in part filler re-aggregation occurs during fiber spinning and homogeneity of the filler dispersion is reduced especially after drawing. Here, surface modified and unmodified silica nanoparticles were studied as fillers within polyamide nanocomposites and fibers. The compatibility between the different fillers and the polymer matrix and the changes (improvements) in the final fiber properties as obtained by melt spinning due to the filler surface modification were investigated in a more fundamental way.

Polyamide's toughness, low coefficient of friction and good abrasion resistance make it an ideal replacement for a wide variety of applications, replacing metal and rubber. The amide groups of polyamide are very polar, and hydrogen bonds can form between them. Because of these, and because the polyamide backbone is so regular and symmetrical, polyamides are often crystalline, and make very good fibers [107]. When polyamide is spun into fibers, the long chain-like macromolecules line up parallel to each other. The amide groups on adjacent chains then form strong bonds with each other called bridged hydrogen bonds. These hydrogen bonds hold the adjacent chains together, making polyamide yarn strong. When polyamide 6 polymerizes, the amide link present in caprolactam (starting monomer for polyamide 6) opens up and the molecules join up in a continuous chain, providing an ideal mechanism for interacting with nanoparticles. On the other hand, silica particles are formed by strong covalent bonds between silicon and oxygen atoms by sharing their electron pairs at the p orbital. The surface bound OH groups on the silica surfaces may also form stable bonds with polyamide during polymerization.

Chapter 3

Structures and properties of nanoparticles

3.1. Introduction

Fillers play important roles in the modification of the properties of various polymers and nanoparticles are without doubt one of the most outstanding and promising fillers that are being studied by many scientists all over the world, due to their high surface area, low density and high young's modulus, among other properties that can be transferred to the polymeric matrix if a good dispersion of the filler is ensured in the polymer [108, 109]. The transition from microparticles to nanoparticles can lead to a number of changes in physical properties. Two of the major factors are the increase in the ratio of surface area to volume, and the size of the particle moving into the area where quantum effects predominate. The increase in the surface area to volume ratio, which is a gradual progression as the particle gets smaller, leads to an increasing dominance of the behavior of atoms located on the surface of a particle over that of those located in the interior of the particle. This affects both the properties of the particle as such and its interaction with other materials. High surface area is a critical factor in the performance of catalysis and structure such as electrodes, allowing improvement in performance of such technologies as fuel cells and batteries. The large surface area of nanoparticles also results in a lot of interaction between the intermixed materials in nanocomposites, leading to special properties such as increased strength and/or increased chemical and heat resistance.

Nanoparticles are currently made out of a very wide variety of materials, the most common of the new generation of nanoparticles being ceramics, which are best split into metal oxide ceramics such as titanium, zinc, aluminum and iron oxide, to name a prominent few, and silicate nanoparticle [108, 109]. Silica plays an important role in nature, science and technical applications [113–116]. The special advantage of silica is that it exists in various kinds of its morphologies in natural sources or can be synthesized by various preparation techniques, e.g. nanoparticles, particles with random size, spherical hollow spheres, transparent films, mesoporous materials with narrow pore size distribution as well as solid materials without pores or flat surfaces of silicon wafers having a thin silica layer. The chemical properties of the silica surface are mainly determined by the various silanol and siloxane groups that are present on the external as well as internal surface.

3.2. Definition of nanoparticle

The definition of nanoparticles differs upon the materials, fields and applications concerned. In the narrow sense, they are regarded as the particle smaller than 10- 20 nm, where the physical properties of solid materials themselves would drastically change. On the other hand, the particles in the three digits range of nanometer from 1 nm to 1 μm could be called as nanoparticles. In many cases, the particles from 1 to 100 nm are generally called as nanoparticles, but here they will be regarded as the particle smaller than those called conventionally “submicron particle”, and concretely less than the wavelength of visible light (its lower limit is about 400 nm) as a measure, which need to treated differently from the submicron particles [110].

3.3. Definition of particle size

Particle size is the most important information in practical applications of powder-particles. Usually, powders are constituted of particles of various sizes and, therefore, it is necessary to obtain not only the mean particle size but also the size distribution for the characterization. A particle is usually three-dimensional and it may take various shapes. “Particle size” is a term to represent the three-dimensional particle in one-dimensional scalar value. The size of any spherical particle can be represented by its diameter with no ambiguity. For a particle with irregular shape, the size is represented by a geometrically obtained one-dimensional scalar value, geometric size, or an equivalent size in relation to practical methods of particle size measurements such as those based on laser diffraction and scattering, dynamic light scattering, and differential mobility analysis [111].

3.4. Silicium dioxide

The chemical compound silicon dioxide, also known as silica (from the Latin silex), is an oxide of silicon with the chemical formula SiO_2. It has been known for its hardness since antiquity. Silica is most commonly found in nature as sand or quartz, as well as in the cell walls of diatoms [113, 117]. Silicas are grouped into two major categories of natural mined silicas and synthetic silicas, which are significantly different from each other with respect to properties and functions. Silica is manufactured in several forms including fused quartz, crystal, fumed silica (or pyrogenic silica, trademarked Aerosil or Cab-O-Sil), colloidal silica, silica gel, and aerogel. Silicon dioxide is the most abundant mineral in the Earth's crust, and it is found across the world in various forms. Because of its abundance, it has been used in a number of different applications and is a prized

mineral. Without silicon dioxide, some of the things you may take for granted would have never been made. In solid form, silicon dioxide is white and powdery with a density of 2.2 grams per cubic centimeter. It mostly forms in nature as sand or quartz crystals, and it is renowned for its hardness. It is a mineral that is highly resistant to heat, with a melting point of 1650 degrees Celsius. Synthetic silicas are of five types: fumed, electric arc, fused, gel and precipitated. Fumed and electric arc silicas are produced by a vapor or pyrogenic process. Fused or vitreous silica is produced by fusing high-purity quartz at high temperature. Silica gel and precipitated silicas are produced by a liquid or wet process. Because in the wet process silicas are produce in water medium, these products are also known as hydrated silica. Pyrogenic process silicas are also called anhydrous silicas because of their production at high temperature and low water content. A flow diagram of the various types of synthetic silicas is given in Figure 3.1

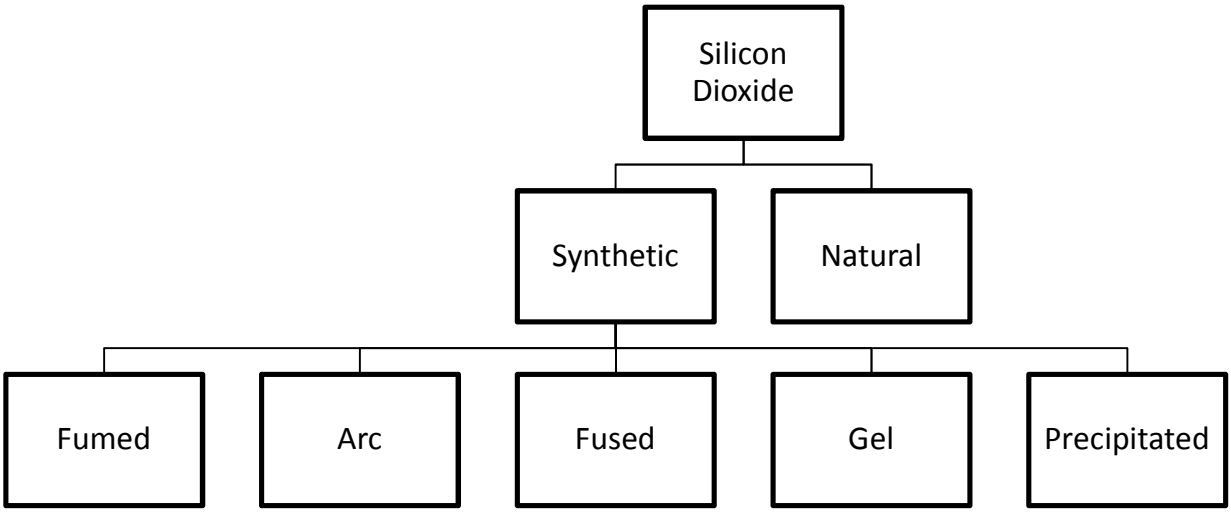

Figure 3.1 Types of synthetic silica [139]

Synthetic silicas are manufactured under controlled reaction condition to produce products consisting of very fine spherical particles, with typical primary particle size of 0.01 to 0.1 μm and a 50 to 800 m^2 /g surface area. The surface of synthetic silicas contains hydroxyl groups called silanol groups. Because of surface moisture and the presence of silanol groups, the synthetic silicas are hydrophilic in nature. The compatibility of synthetic silicas for their use in plastics and polymers can be improved by hydrophobizing the silica surface with suitable coupling agents

and chemical treatments. Synthesis silicas are considered as polymers of silicic acid in which the bulk structure is produced by interlinking the SiO_4 tetrahedra. At the surface, the structure terminates in siloxane groups (≡Si-O-Si≡) and one of the several forms of silanol groups (≡Si-OH). Regardless of method of preparation, all synthetic silicas are amorphous in nature, as determined by X-ray, and have the chemical composition of SiO_2. All synthetic silicas are colorless, odorless, tasteless, fine-particle and white powders. Silicas are chemically inert and insoluble powder except in strong alkali (NaOH) and hydrofluoric acid (HF).

3.4.1. Crystal structure of silica

In the vast majority of silicates, the Si atom shows tetrahedral coordination, with 4 oxygen atoms surrounding a central Si atom. The most common example is seen in the quartz crystalline form of silica SiO_2. In each of the thermodynamically most stable crystalline forms of silica, on average, all 4 of the vertices (or oxygen atoms) of the SiO_4 tetrahedron are shared with others, yielding the net chemical formula: SiO_2.

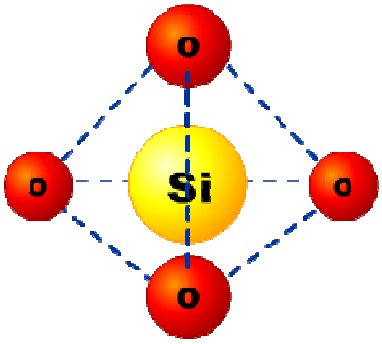

Figure 3.2 Tetrahedral structural unit of silica (SiO_4), the basic building block of the most ideal glass former

The amorphous structure of glassy silica (SiO_2) is in two-dimensions. No long-range order is present; however there is local ordering with respect to the tetrahedral arrangement of oxygen (O) atoms around the silicon (Si) atoms. Note that a fourth oxygen atom is bonded to each silicon atom, either behind the plane of the screen or in front of it; these atoms are omitted for clarity.

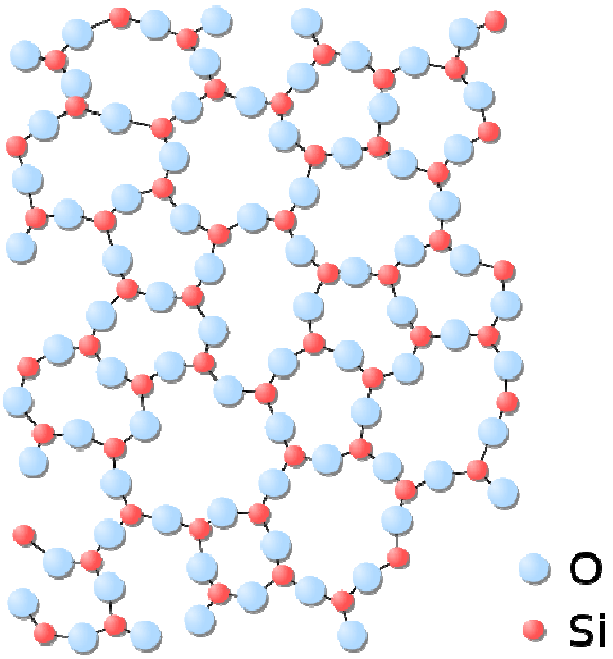

Figure 3.3 The amorphous structure of glassy silica (SiO_2) in two-dimensions. Note that a fourth oxygen atom is bonded to each silicon atom, either behind the plane of the screen or in front of it; these atoms are omitted for clarity

For example, in the unit cell of alpha-quartz, the central tetrahedron shares all 4 of its corner O atoms, the 2 face-centered tetrahedra share 2 of their corner O atoms, and the 4 edge-centered tetrahedra share just one of their O atoms with other SiO_4 tetrahedra. This leaves a net average of 12 out of 24 total vertices for that portion of the 7 SiO_4 tetrahedra which are considered to be a part of the unit cell for silica (see 3-D Unit Cell). SiO_2 has a number of distinct crystalline forms (polymorphs) in addition to amorphous forms. With the exception of stishovite and fibrous silica, all of the crystalline forms involve tetrahedral SiO_4 units linked together by shared vertices in different arrangements. Silicon-oxygen bond lengths vary between the different crystal forms, for example in α-quartz the bond length is 161 pm, whereas in α-tridymite it is in the range 154–171 pm. The Si-O-Si angle also varies between low values of 140° in α-tridymite, up to 180° in β-tridymite. In α-quartz the Si-O-Si angle is 144° [118].

3.4.2. Chemistry of silica

Silicon dioxide is formed when silicon is exposed to oxygen (or air). A very shallow layer (approximately 1 nm or 10 Å) of so-called native oxide is formed on the surface when silicon is exposed to air under ambient conditions. Higher temperatures and alternative environments are used to grow well-controlled layers of silicon dioxide on silicon, for example at temperatures between 600 and 1200 ℃, using so-called dry or wet oxidation with O_2 or H_2O, respectively [119]. The depth of the layer of silicon replaced by the dioxide is 44% of the depth of the silicon dioxide layer produced [119].

Alternative methods used to deposit a layer of SiO_2 include [120]

- Low temperature oxidation (400–450 ℃) of silane

$$SiH_4 + 2\ O_2 \rightarrow SiO_2 + 2\ H_2O.$$

- Decomposition of tetraethyl orthosilicate (TEOS) at 680–730 ℃

$$Si(OC_2H_5)_4 \rightarrow SiO_2 + 2\ H_2O + 4\ C_2H_4.$$

- Plasma enhanced chemical vapor deposition using TEOS at about 400 ℃

$$Si(OC_2H_5)_4 + 12\ O_2 \rightarrow SiO_2 + 10\ H_2O + 8\ CO_2.$$

- polycondensation of tetraethyl orthosilicate (TEOS) at below 100 ℃ using amino acid as catalyst.[121]

3.4.3. Silica nanoparticles

Among the numerous inorganic/organic hybrid materials, silica-polymer hybrid materials are one of the most commonly reported in the literature. This may be attributed to their wide use and the ease of particle synthesis. Silica nanoparticles have been used as fillers in the manufacture of paints, rubber products, and plastic binders [122]. Stöber and co-workers [123] reported a simple synthesis of monodisperse spherical silica particles. Silica nanoparticles were prepared by hydrolysis and condensation of TEOS in ethanol, and in presence of ammonia as catalyst. The hydrolysis and condensation reactions provide precursor species and the necessary supersaturation for the formation of particles will be briefly described as follows. During the hydrolysis reaction, the ethoxy group of TEOS reacts with the water molecule to form

intermediate [Si $(OC_2H_5)_{4-X}(OH)_X$] with hydroxyl group substituting ethoxy groups. Moreover, ammonia works as a basic catalyst to this reaction; the hydrolysis reaction is probably initiated by the attacks of hydroxyl anions on TEOS molecules. The chemical reaction is expressed as follows:

$$Si(OC_2H_5)_4 + xH_2O \rightarrow Si(OC_2H_5)_{4-x}(OH)_x + xC_2H_5OH$$

Following the hydrolysis reaction, the condensation reaction occurs immediately. The hydroxyl group of intermediate [Si $(OC_2H_5)_{4-X}(OH)_X$] reacts with either the ethoxy group of other TEOS (alcohol condensation) or the hydroxyl group of another hydrolysis intermediate (water condensation) to form Si-O-Si bridges. Furthermore, it was also claimed [331] that the rate of water condensation is thousands times faster than the alcohol condensation. Both condensation reactions can be expressed as follows:

$$\equiv Si - OC_2H_5 + HO - Si \equiv \rightarrow \equiv Si - O - Si \equiv + C_2H_5OH$$

$$\equiv Si - OH + HO - Si \equiv \rightarrow \equiv Si - O - Si \equiv + H_2O$$

The overall reaction can then be depicted as follows:

$$Si(OC_2H_5)_4 + 2H_2O \rightarrow SiO_2 + 4C_2H_5OH$$

As going to be reported in this thesis the main particles used as filler in polyamide matrix are fumed silica nanoparticles (commercially AEROSIL). Alumina (commercially AEROXIDE) and Ceria (commercially AdNano® Ceria) particle are also used for comparison of the results.

Fumed silica

Fumed silica, also known as pyrogenic silica because it is produced in a flame by a vapor process at high temperature, consists of microscopic droplets of amorphous silica fused into branched, chainlike, three-dimensional secondary particles which then agglomerate into tertiary particles. Fumed silicas are fluffy, white powder of amorphous structure. Because of their extremely small particle size and spherical morphology, high surface area, unique surface chemistry, and high purity, these products are used in a multitude of industrial applications. The average diameter of the spherical primary particles can be varied from 7 to 40 nm by using

different reaction conditions during flame hydrolysis. This produces fumed silica grades with BET surface area between 50 and 380 m^2 /g. Fumed silicas with a surface area below 300 m^2/g are nonporous; products with surface area above 300 m^2/g can have micro porosity. Fumed silicas were invented by Degussa in the early 1940s and are offered under the name Aerosil®.

Fumed silicas are divided into three groups:

- Hydrophilic silicas: those products that can be wetted with water. These silicas are produced through the normal flame hydrolysis of silicon tetrachloride.
- Hydrophobic silicas: those products that cannot be wetted with water. These silicas are produced from reacting hydrophilic silicas with organosilanes.
- Mixed oxide: those products that are formed through flame hydrolysis of silicon tetrachloride mixed with another volatile compound such as aluminum chloride or boron chloride.

Siloxane (≡Si-O-Si≡) and silanol (≡Si-OH) groups are situated on the surface of fumed silica particles. This latter type (i.e. silanol) of functional groups in particular is responsible for the hydrophilic behavior of non-after treated fumed silica types. Figure 3.4 shows the surface groups of hydrophilic AEROSIL fumed silica. AEROSIL fumed silica can be surface-modified by reacting the silanol groups with suitable compounds such as silanes. For example Aerosil R972, is produced by reacting hydrophilic silica with dimethylchlorosilane as shown in Figure 3.5 .this product exhibits chemically bound dimethyl silyl groups on its surface and can no longer be wetted with water – in other words, it is hydrophobic.

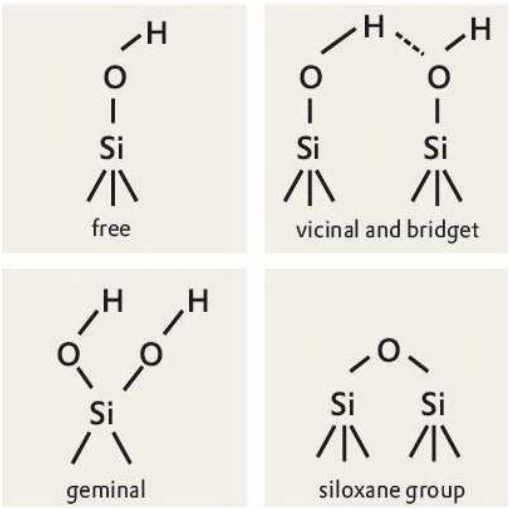

Figure 3.4 potential SiO_2 surface groups of hydrophilic silicas [140]

AEROSIL R 972 became the first hydrophobic silica to be manufactured on an industrial scale in 1962. Further hydrophobic AEROSIL grades are now available, produced by similar industrial-scale methods using corresponding silanes. Figure 3.5 provides a sampling of the many hydrophobic grades available and highlights the difference between them and hydrophilic AEROSIL grades according to the schematically represented surface groups. All hydrophobic AEROSIL types carry the suffix “R“ to indicate their water-repellent character.

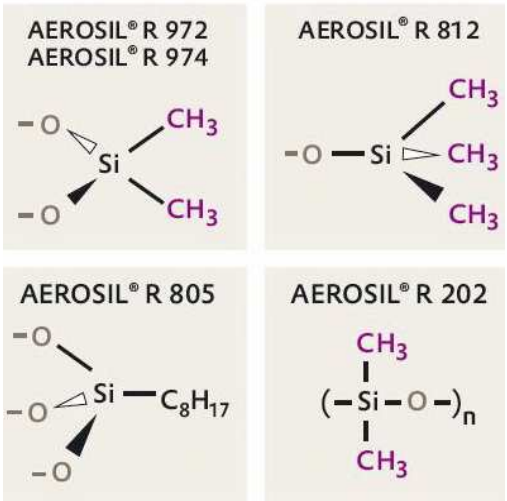

Figure 3.5 Hydrophobic Aerosil grade and their surface groups [140]

Hydrophilic and hydrophobic fumed silica grades have proven effective for numerous areas of application. In view of their use in the plastics industry, the principal properties of fumed silicas are listed below:

• Reinforcing fillers
• Thickening and thixotropic agent for resins
• Anti-sedimentation agent for cast resins and adhesives
• Free flow aid for powder coatings In contrast to silicas of mineral origin, meaning quartz powder which is used mainly as a “filler“ in the true sense of the word, the desired effects can be obtained by adding only relatively small amounts of synthetic silicas.

Fumed silica manufacturing [122]

Fumed silica is prepared by a vapor process at high temperature. Fumed silica was first prepared in 1941 by a German chemist, Dr. Harry Klopfer [141] as he was trying to develop white reinforcing filler comparable to properties of channel blacks in rubber. At present fumed silica is prepared by the hydrolysis of silicon tetrachloride vapor in a flame of hydrogen and oxygen at a temperature of 1000℃ or higher:

$$2H_2 + O_2 \rightarrow 2\ H_2O$$

$$SiCl_4 + 2H_2O \rightarrow SiO_2 + 4HCl$$

$$2H_2 + O_2 + SiCl_4 \rightarrow SiO_2 + 4HCl$$

The primary particles of silica are formed when silicon tetrachloride is burned in a flame of hydrogen and oxygen. While still molten, the primary particles fuse irreversibly into secondary particles called aggregates. The key properties, such as particle size and surface area, of the resulting fumed silica are controlled by varying the ratio of reactants: silicon tetrachloride, hydrogen and oxygen (in the form of dry air).before the silica particles are separated from the HCl-containing combustion gases by means of cyclones or filters. The reaction mixture passes through a coagulation and cooling zone. The residual HCl, which is physically absorbed by the high surface fumed silica, is removed by treating the silica with moist hot air. This treatment lowers the residual HCl content in the silica product to less than 0.025%.

The flow diagram used in the fumed silica manufacturing process is shown in Figure 3.6

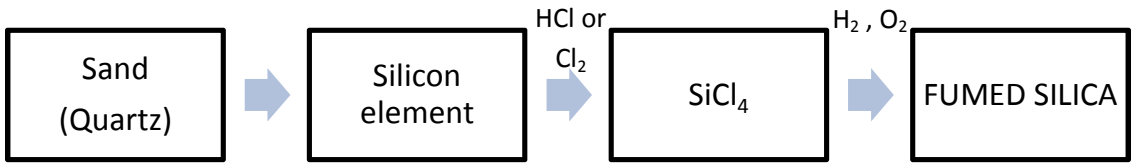

Figure 3.6 Fumed silica manufacturing process. [139]

3.4.4. Functionalization of silica nanoparticle

Although some nanomaterials have excellent physical and chemical bulk properties, but due to their high surface area and their dangling bonds, nanoparticles have a tendency to agglomerate, hence they do not possess suitable surface properties for specific applications. Consequently, it may be necessary to modify the surface of such materials [124, 125]. The most common way to do so is to attach suitable organic groups to the surface atoms. First, surface modification can stabilize nanoparticles against agglomeration [126, 127]. A second aspect for modifying nanoparticles is to render them compatible with another phase. For example, metal particles can be made water-soluble when appropriate groups are attached [128]. Another example is the use of modified inorganic (nano-) fillers in organic polymers. The modification can avoid homogeneity and compatibility problems between the two phases and thus improve the mechanical properties of the composite [129]. A third interest in nanoparticles modification is to enable their self-organization [126]. A relatively unexploited additional possibility is the functionalization by the organic groups. While simple organic groups are sufficient to protect nanoparticles against agglomeration, functional organic groups on the particle surface may allow deliberate interaction of the nanoparticles with molecules, other nanoparticles, surfaces, or solids. The mentioned possibilities are synergetic. For example, surface functionalities also protect the nanoparticles against agglomeration and may be required to enable their self-organization. Various organic compounds are potential silica modifiers, among them, as for metal nanoparticles, are thiols, carboxylic acids and amines [130, 121]. However, amines and thiols are relatively rarely used. The main compounds used for modifying silica nanoparticles are silanes. Silanes are the most

often used modifiers for metal oxide surfaces. This includes alkoxysilane, ≡Si–OR (R = alkyl), hydrogenosilane, ≡Si–H, or chlorosilane, ≡Si–Cl, reagents. As a matter of fact, there is a broad variety of commercially available silanes, and others are readily synthesized or modified. One of the main advantages of silanes is that they can bear numerous functionalities, for example amino, cyano, carboxylic acid, epoxy groups, etc. [124, 132-136].

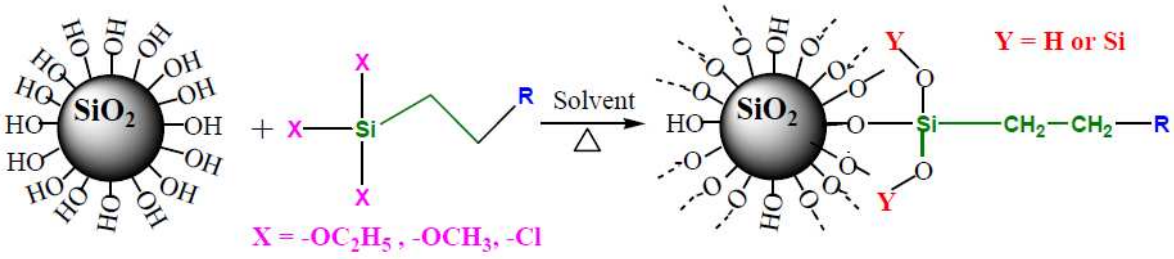

Figure 3.7 Surface modification of silica nanoparticle [137]

The organosilanes are used to modify the surface of silica nanoparticles. Organosilanes have the ability to incorporate both organic- and inorganic-compatible functionality within the same molecule. The inorganic compatibility comes from the alkoxy groups attached to the silicon atom. This bond is hydrolytically unstable and in the presence of moisture hydrolyzes to an intermediate Si–OH bond which then condenses with surface bound OH groups on inorganic surfaces to form stable Si–O–Si bonds. The molecular structure of organosilane and its interaction with silica substrates is depicted in Figure 3.7. The final result of reacting an organosilane with a substrate is to utilize the substrate to catalyze chemical transformations at the heterogeneous interface, ordering the interface region, and modifying its partition characteristics. Most importantly, it includes the ability to affect a covalent bond between polyamide and SiO_2 particles.

3.5. Aluminum oxide

Aluminum oxide is the family of inorganic compounds with the chemical formula Al_2O_3. It is an amphoteric oxide and is commonly referred to as alumina, corundum as well as many other names, reflecting its widespread occurrence in nature and industry. Its most significant use is in the production of aluminum metal although it is also used as an abrasive due to its hardness and as a refractory material due to its high melting point. The most common form of crystalline

alumina is known as corundum. The oxygen ions nearly form a hexagonal close-packed structure with aluminum ions filling two-thirds of the octahedral interstices. Each Al3+ center is octahedral. In terms of its crystallography, corundum adopts a trigonal Bravais lattice with a space group of R-3c (number 167 in the International Tables). The primitive cell contains two formula units of aluminium oxide. Alumina also exists in other phases, namely η-, χ-, γ-, δ- and θ-aluminas. Each has a unique crystal structure and properties. The so-called β-alumina proved to be $NaAl_{11}O_{17}$.

3.6. Cerium oxide

Cerium (IV) oxide, also known as ceric oxide, ceria, cerium oxide or cerium dioxide, is an oxide of the rare earth metal cerium. It is a pale yellow-white powder with the chemical formula CeO_2. Cerium (IV) oxide is formed by the calcination of cerium oxalate or cerium hydroxide. Powdered ceria is slightly hygroscopic and will also absorb a small amount of carbon dioxide from the atmosphere [138]. Cerium also forms cerium (III) oxide, Ce_2O_3, but CeO_2 is the most stable phase at room temperature and under atmospheric conditions. Ceria has been extensively looked at over the past 15 years as a solid oxide electrolyte mainly due to its higher ionic conductivity at lower temperatures than Yttria-stabilized zirconia (YSZ), the more widely used solid oxide electrolyte. The use of CeO_2 – based materials has attracted considerable attention in recent years, particularly in applications such as environmental catalysis, where it has found widespread use. Ceria is also well known as a highly effective polishing agent for glass. More recent applications can be found in the field of chemical mechanical polishing (CMP) where ceria plays an important role in the planarization of integrated circuit (IC) wafers.

Chapter 4

Physical structure and polymorphism of polyamide 6 nanocomposites

4.1. Introduction

The amide group is one of the most important building blocks of nature and exists in the structure of all proteins. The group is essentially planar due to the partial double bond character of the C–N bond. The ability of the NH group to form strong hydrogen bonds (H-bonds) with the CO group is the determining factor for the crystal structures found in polyamides. The chains are oriented in such a way as to maximize hydrogen bonding. For polyamide 6 all H-bonds can only be formed in a planar conformation if adjacent molecules are antiparallel. If adjacent molecules were of the same direction (parallel) only half of the H-bonds could be formed, in contrast to the experimental observations of almost complete H-bond formation [142].

Polyamide 6 exhibit polymorphic structures that contained two types of stable crystal form: monoclinic α-form and monoclinic (or pseudohexagonal) γ-form [143-147], which are very sensitive to the way in which the samples are prepared. Previous studies have also shown that a partially disordered structure of PA6, mesomorphic β-form, could be obtained by cooling the samples rapidly from the melt state [148], while the α-form crystal of PA6 result from slow cooling from the melt state [149].

4.2. The α-structure

The structure of polyamide 6 was determined by Bunn and Garner [153], who described the α-structure for the first time. The polymer chains in the α-structure are in the fully extended planer zig-zag conformation and grouped into essentially planar, H-bonded sheets. The H-bonded sheets are, however, staggered up and down instead of always being displaced in the same direction. The resulting structure is monoclinic instead of triclinic as observed in polyamide 66. Because of crystallographic convention for monoclinic structure, the direction along the molecular chain (the “fiber” axis) is labeled the b-axis rather than the c-axis as in the case for the triclinic PA66. Because there is four rather than one chemical repeat unit in the unit cell, the Miller indices are doubled for non-fiber axes. Thus, the intense equatorial reflections of PA6 are indexed as (200) and the (002), (202) doublet.

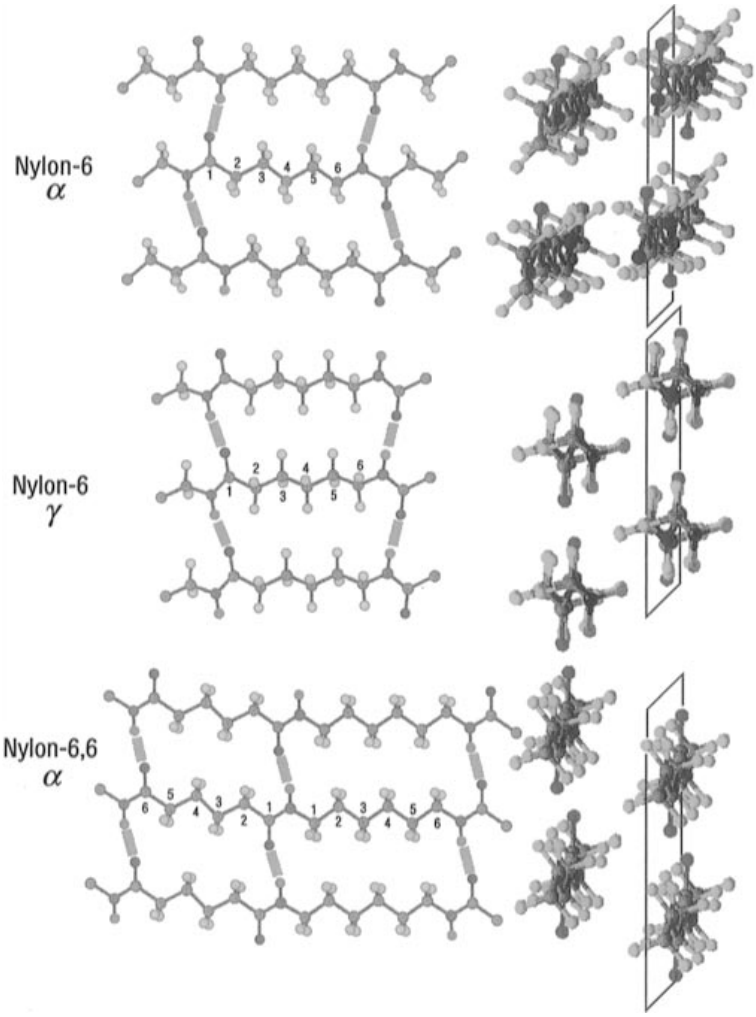

Figure 4.1 Structures of the α- and γ-forms of PA6 and PA66. The left side shows the view of the hydrogen-bonding planes, and the right side shows the view down the chain axis. For the α-form of PA6, the adjacent chains are antiparallel and the hydrogen bonding is between adjacent chains within the same sheet (bi-secting the CH_2 angles). For the γ-form of PA6, the chains are parallel and the hydrogen-bonding is between chains in adjacent sheets. In PA66, the chains have no directionality [155].

4.3. The γ-structure

The second stable crystal structure observed in polyamides is the γ-structure which was initially suggested by Kinoshita [154] as a way to adapt to the experimental evidence for complete H-bond formation in polyamides. The γ-structure of polyamide 6 is shown in Figure 4.1.Compared to the α-form, the γ-form has a shorter chain axis due to a 30° tilting of the amide group with respect to the chain axis. The tilting allows all H-bonds to be formed without strain. The energy cost to expend to twist the amide groups in γ-crystals is compensated by the stability of the fully H-bond structure. The H-bonds are not co-linear anymore and are disposed on pleated extended sheets. The crystal structure is usually monoclinic, and the X-ray pattern consists of a single strong equatorial reflection as opposed to two reflections in the case of the α-form. The comparison of the two fiber scans for PA6, a polyamide that can be obtained in both forms, is given in Figure 4.2.

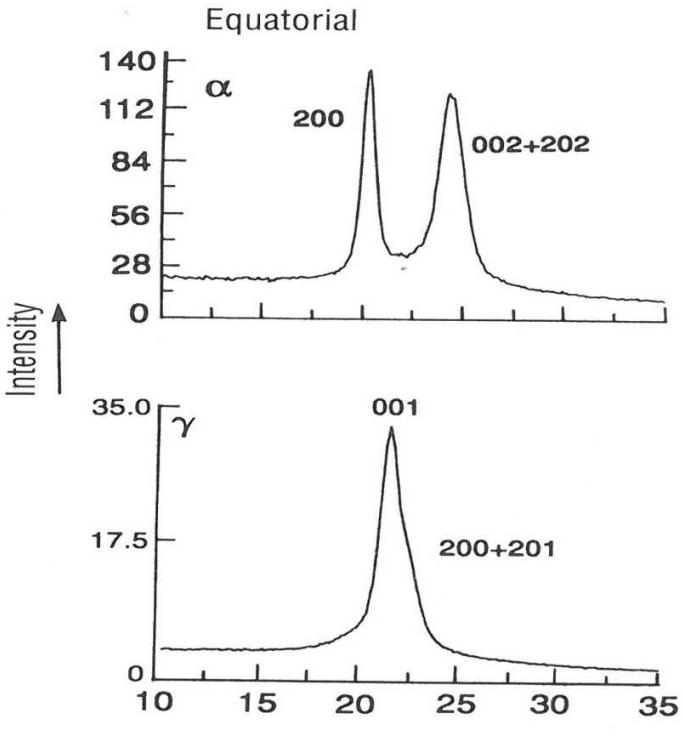

Figure 4.2 X-ray diffraction of pure α form and pure γ crystal form of PA6 [142]

On a cross section normal to the c-axis, the chains are at the corners of a hexagonal unit cell. This indicates hexagonal packing of crystal stems and if the chains were structureless cylinders

it would also imply hexagonal symmetry. Alternatively hexagonal symmetry could be found if there was complete rotational freedom about the axes. This is prohibited by the presence of the H-bonds. In fact, the γ-form of polyamide is not mobile and the planar zig-zag structure in the methylene sequences is retained. The structure is therefore termed pseudohexagonal. (Figure 4.3)

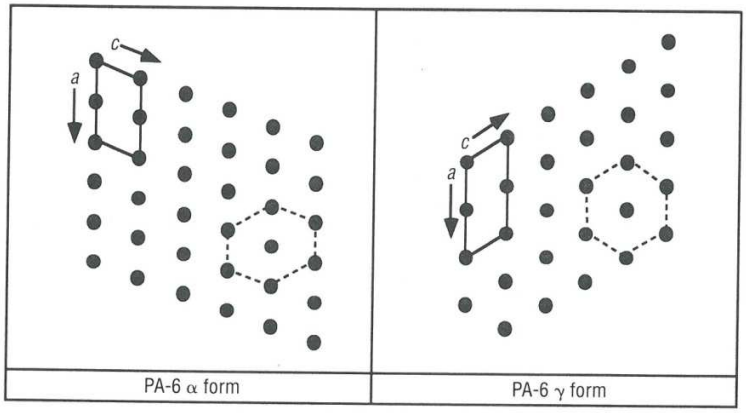

Figure 4.3 Cross-section of chain (a-c planes) illustrating the hexagonal packing of the chain stem in γ- PA6, that is, the pseudohexagonal structure [142].

4.4. Polymorphic Transformations

Polyamides exhibit more varied polymorphism than most other classes of polymers. The polymorphic structures of polyamide resulted from the different spatial arrangement in the hydrogen bonding between the oxygen in the carbonyl group of one polyamide molecular chain and the hydrogen attached to the nitrogen in the neighboring polyamide molecular chain. The γ-form polyamide crystal was constituted by polyamide molecules adopting the parallel-chain-arrangement hydrogen bonds, whereas the polyamide molecules in the monoclinic α-form crystal have taken the more stable antiparallel-chain-arrangement hydrogen bonds. The α-form is more stable than the γ-form because of shorter hydrogen bonds. The third form, mesomorphic β-form, although unstable, also existed. The formation of a stable crystal form by polyamide molecules was determined by the flexibility of their molecular chains. For containing even numbers of methylene group in the repeating unit of polyamide, the packing interaction between the methylene groups in polyamide determined their crystal structures. For PA6, the α-form

crystal is more stable, while for polyamide with more carbons, the γ-form crystal of polyamide is more stable [156].

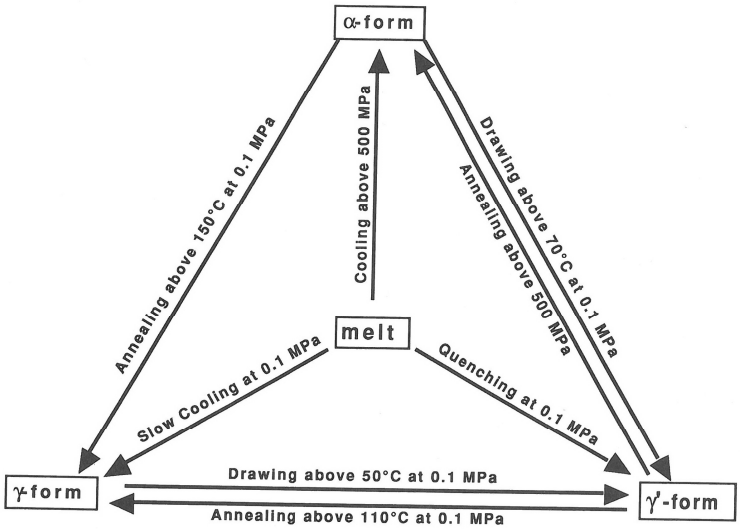

Figure 4.4 Schematic phase transformations of polyamide under various thermomechanical and pressure treatments [157].

In practice, PA6 can exhibit either the α-form crystal under slow cooling [149] or the mesomorphic *β*-form under quenching from the melt state [148] as a result of the large difference in the crystallization time in achieving the crystal form. Figure 4.4 shows that the *γ*-form crystal of PA6 can be transformed into the α-form crystal by annealing PA6 or by drawing and then by annealing PA6 or by treating PA6 with a phenol aqueous solution [150, 151]. Conversely, the α-form of PA6 can be transformed to the γ-form by treating PA6 with iodine-potassium aqueous solution. [156,152].

4.5. Polymorphic Transformations in nanocomposites

As explained in previous section, one of the most remarkable features of polyamide 6 is that these semicrystalline polymers exhibit polymorphism depending on the thermal history, processing conditions, mechanical stress, and crystallization condition. Since the importance of polymorphic form on elevated temperature properties, such as heat distortion temperature, softening, dimensional stability, and warp, the polymorphism and polymorphic transformations of

polyamide 6 nanocomposites have drawn considerable research interests. Studies on the crystal structure of polyamide 6 in nanocomposites were first carried out by Kojima et al. [158] who reported that both α- and γ-crystals were present in nanocomposites. However, after annealing under elevated pressure, they found that the fraction of γ-phase decreased. Early investigations by Liu et al. [159] suggest that the formation of γ-crystalline form is enhanced by the addition of particle. This is significant since crystalline structure may affect physical and mechanical properties. Mathias et al. [160] reported that when both crystal forms were present in nanocomposites, those annealed at 200℃ under vacuu m produced only γ-crystals. Fornes and Paul [161] found that there were significant differences in crystal type within the core and skin regions of injection-molded nanocomposites. The skin region contains only the γ-crystalline form; the core region, on the other hand, contains both α- and γ-forms of polyamide 6. Wu et al. [162] showed from his DSC and XRD results that the polymorphic behavior in polyamide 6/clay nanocomposites depends on the content of clay and the cooling rate from melt. Thermal treatment of polyamide 6 and polyamide 6/clay nanocomposites at various temperatures promotes mostly the α-form crystalline formation. Okamoto et al. [163] investigated the effect of crystallization temperature (T_c) on crystal structure of polyamide 6 and its nanocomposite. Their results show that at lower T_c, both α- and γ-crystal structures are formed in polyamide 6, with increasing T_c, the γ-form gradually disappeared. On the other hand, only the γ-crystal is pronounced for the polyamide 6 nanocomposites throughout the whole T_c range studied. Although intensive research efforts have been devoted to this system, to our knowledge, most research mainly focus on the effect of particle and the annealing temperature on crystallization behavior of polyamide 6 matrixes [164, 165-170, 171, 172], The effect of annealing on thermal behavior of polyamide 6/particle nanocomposites is still an interesting subject needed to be further identified, since some microstructural changes may occur at such high annealing temperature, which would have a significant impact on properties of polyamide 6/particle nanocomposites. Some characteristic properties of the α- and γ-forms of polyamide 6 are listed in Table 4.1 [173- 187]. The heats of fusion, ΔH_f°, are the values reported by Illers [184]. It should be noted that other values for the α-form have been reported in the literature [180, 184, 186, 188-191] and Wunderlich has suggested a value of 230 J/g based on a compromise of various reports in the literature [192]. The effect of crystallization temperature and time on the formation of the α- versus γ-forms has been widely studied [185, 193, 194]. Gurato and his coworkers have shown that crystallization for extended periods of time below ~130 ℃ leads only to the γ-crystallites while above ~190 ℃ only the α-form is produced. Temperatures in between these limits result in a mixture of the two forms, with higher fractions of α-form being

produced at higher temperatures. The disappearance of the γ-form at ~190 ℃ has been commonly referred to as the Brill transition, a phenomenon first observed in polyamide 66 [195]. This transition corresponds to the merging of the two reflections of the α-form into a single peak in plots of X-ray diffraction intensity versus 2θ [196-199] as the sample is heated. Kyotani and Mitsuhashi [194] also found that very short crystallization times at either 100 or 200 ℃ lead to both crystalline forms, while longer times produced predominantly γ- and α-form, respectively. In general, rapid cooling or quenching from the melt produces the γ-form [196, 200-202]. Annealing also affects the crystal structure. For example, annealing of quenched samples or those crystallized between 100 and 150 ℃, at 200 ℃ for extended times leads to the conversion of the γ- into α-form [194]. Gogolewki et al. [186] and Gurato et al. [193] demonstrated similar annealing results. Based on the above, it is clear that, in general, rapid cooling and low temperature crystallization promotes the γ-form of polyamide 6, while higher crystallization temperatures or slow cooling leads to the α-form. Kyotani and Mitsuhashi [194] attribute the temperature dependence to the crystallization rates of the two forms; i.e. at temperatures below 130 ℃ the rate of formation of γ is faster, while above ~190 ℃ the crystallization rate of α-form is faster, while at intermediate temperatures, the rates are comparable. Interestingly, the maximum crystallization rate of polyamide 6 occurs at approximately 140 ℃ [203]. The temperature dependence of the crystallization rate above this maximum is dominated by the driving force for crystallization, i.e. the degree of undercooling, while below, the rate is dominated by the resistance to crystallization, i.e. polymer chain mobility. Therefore, it may be postulated that conditions of limited polymer chain mobility favor the crystallization of the γ-form for polyamide 6.

Studies of polyamide 6-based nanocomposites have caused renewed interest in the factors affecting the crystalline structure. As mentioned above, Kojima et al. [203] and Liu et al. [165] reported that when the one nanometer thick platelets of montmorillonite are dispersed in polyamide 6 the polymer crystallizes in the γ-form. Wu and coworkers [204-207] examined the influence of thermal treatment on the crystallization behavior of melt processed nanocomposites using FTIR, WAXD, and DSC. From FTIR measurements on thin film samples, it has been claimed that the hydrogen bonding in both crystalline forms of polyamide 6 is weakened by the presence of the clay. WAXD analysis revealed that nanocomposites films exhibit both crystalline forms when slowly cooled from the melt; whereas, pure polyamide 6 gave predominantly the α-form. Methods that permit higher cooling rates, e.g. air and water-cooling, have increased the content of the γ-phase especially for the nanocomposite. Further WAXD investigations conducted on samples that had been annealed at different temperatures showed the onset of

the γ- to α- transition, normally observed around 130 ℃ for p ure polyamide 6, in this case at 120 ℃, occurred approximately 40 ℃ higher for the nan ocomposite. Interestingly, an unexpected higher amount of γ-form was observed after annealing at 200 ℃ than a t 180 ℃. Lastly, non-isothermal crystallization surprisingly showed that the degree of crystallinity increased with increasing cooling rate for the nanocomposites, in contrast to what is observed in pure polyamide 6 and other polymers.

Table 4.1 Miscellaneous data for the α- and γ-crystalline forms of polyamide 6

Property	**α**	**γ**	**Reference(s)**
Crystal structure	Monoclinic	Hexagonal/pseudohexagonal	
Lattice constants	*a=0.956* nm	*a=0.472* nm[a]	[174-175]
	b=1.724 nm (fiber axis)	*c=1.688* nm[a]	
	c=0.801 nm	*γ*=120°[a]	
	β=67.5°		
Crystallographic reflection(s)	(200)	(001)	[173, 175, 176]
	(002/202)	$(200/201)_{\text{-minor}}$	
Characteristic d-spacings	$d_{200} \cong 0.370$ nm	$d_{001} \cong 0.413$ nm	[174, 175, 177, 178]
	$d_{002+202} \cong 0.440$ nm		
Density, *ρ* (g/cm^3)	1.23 (experimental)	1.16–1.19 (experimental)	[175, 177, 176-186], amorphous *ρ*=1.09
	1.23 (calculated)	1.16 (calculated)	
Heat of fusion, $\Delta H_f°$ (J/g)	241	239	[183]

[a] Hexagonal lattice constants were calculated based on the monoclinic parameters *a=0.933*nm, *b=1.688*nm, and *c=0.478*nm and *β*=121°. The hexagonal lattice constant, *a*, was taken as the average of *a* and half of *b* of the monoclinic unit cell. The constant *c* representing the fiber axis remained fixed [161].

4.5.1. Effect of particle concentration

Wu and Liao examined the effect of thermal history and filler concentration on the crystal structure of polyamide 6 nanocomposites formed by in situ polymerization using synthetic saponite and natural montmorillonite [208, 209]. Similar crystalline behavior was observed for the pure and nanocomposite materials when samples were slowly or rapidly cooled from the melt; however, nanocomposites containing a low concentration of saponite, i.e. 2.5 wt. %, favored the formation of the α-form regardless of the cooling conditions, whereas by increasing silica content γ-form is more dominant (Figure 4.5). Annealing studies showed that higher amounts of γ were present in the nanocomposite than in pure polyamide 6 after annealing at high temperatures, except at low saponite contents.

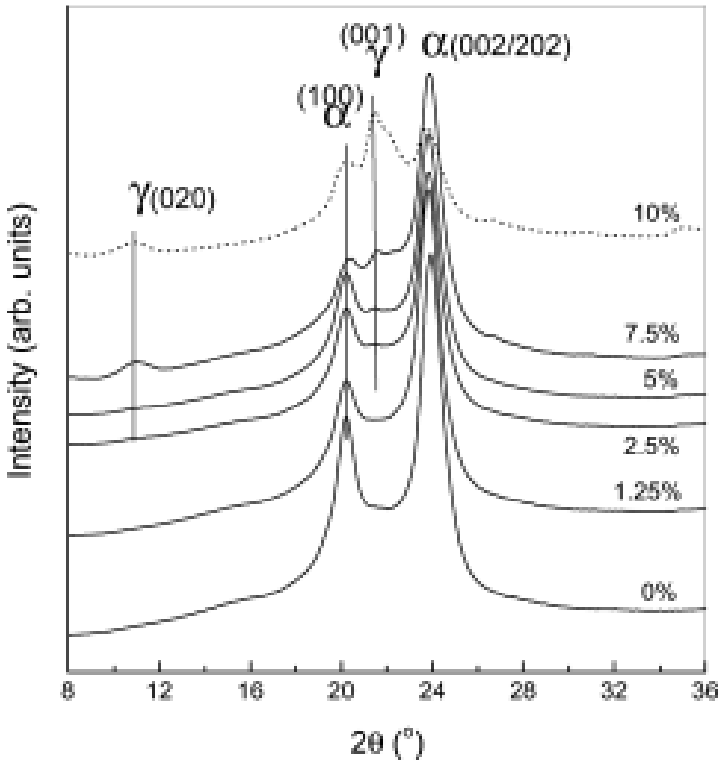

Figure 4.5 XRD pattern of pure PA6 and the nanocomposite samples as a function of silica concentration

4.5.2. Effect of take- up velocity

In many studies on the high-speed melt spinning and the structure of PA 6, the existence of three crystalline phases is considered: monoclinic α, pseudohexagonal γ, and hexagonal [211-213]. The γ-form and hexagonal form give similar WAXD patterns, and it is difficult to distinguish these two forms unless the sample has highly ordered crystalline structure. In the equatorial WAXD scan, the peak of 011 and 200 planes of the γ-phase appear at 2θ =21.5° and 22.3°, respectively. These two peaks are closely located and usually are observed as a single peak. On the other hand, the 200 and 002/202 peaks of the α-form crystals are located approximately at 20.5° and at 24°.

The equatorial WAXD diagram of polyamide 6 is shown in Figure 4.6.

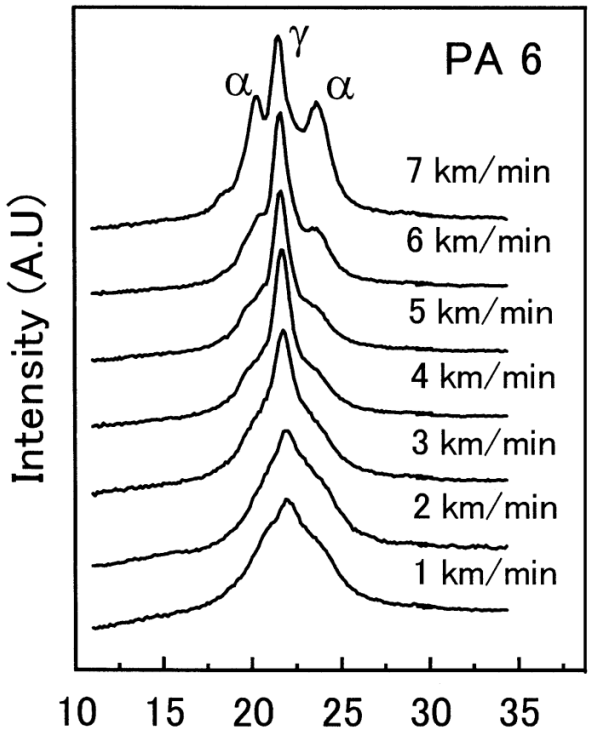

Figure 4.6 X-ray diffraction of polyamide 6 at different take-up velocity

Giza et al. [210] reported that at low take up velocity γ-phase dominate and by increasing take up velocity and drawing the α-phase also appear and at sufficiently high take-up velocity (in the neighborhood of 7 km/min), the direct formation of α-form crystals in the spin line takes place.

4.5.3. Effect of thermal after-treatment

As explained particle addition promoted the α→γ crystal-phase transformation. But in some further process with thermal after treatment like extrusion process, the crystal phase converted again to α-form crystal.

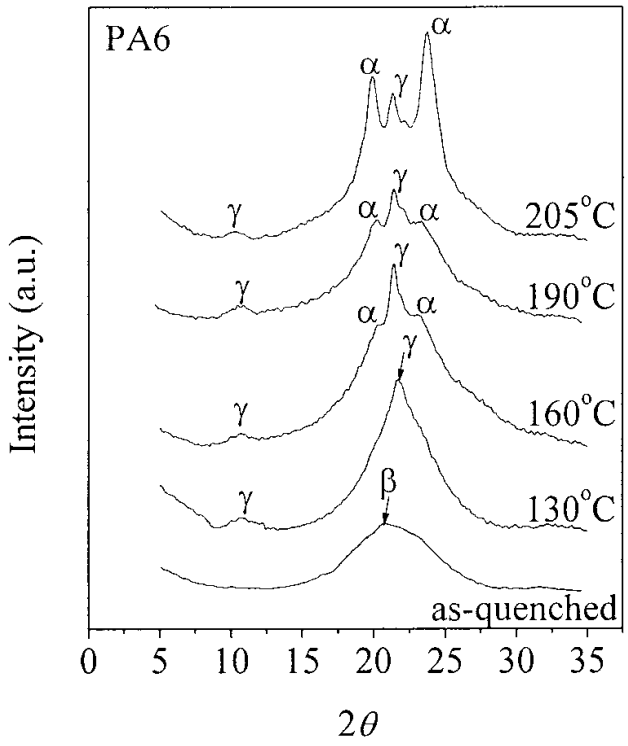

Figure 4.7 X-ray diffractions of polyamide 6 annealed at different crystallization temperature [143, 167]

Figure 4.7 shows X-ray diffraction scans of polyamide 6 after has been thermally annealed at various temperatures and then rapidly cooled to room temperature. In both cases, the γ- form diffraction peak at 21.5° gradually disappears and the α- form diffraction peaks at around 20.5° and 24° become sharper as the annealing temperature s increase. Since the structure of polyamide 6 shows the Brill transition over a broad range of temperatures starting from 160℃ to about 190℃, it is possible to induce the crystal -crystal transition during the annealing process in the range of 160-205℃. These thermal treatments favor the formation of the α- form rather than the γ- form in polyamide 6 as the α- form is the thermodynamically more stable crystalline form.

Therefore the effect of thermal annealing at various temperatures on the crystalline structure of polyamide 6 is to promote the α-form crystalline formation during the process.

4.5.4. Effect of preparation method

Some studies have explored the differences between polyamide 6 nanocomposites formed by in situ polymerization and by melt processing. Based on DSC and solid state NMR studies, VanderHart et al. [214, 215] concluded that the silicate layers promote the γ-form regardless of the formation technique, and that γ-crystallites reside near the polyamide/clay interface. Lincoln et al. [164] used small angle X-ray scattering, in addition to WAXD and DSC, to infer about the crystalline morphology of these two types of nanocomposites. They concluded that the clay platelets disrupt the formation of crystallites and the extent of platelet-crystallite interactions is dependent upon the technique used to form the nanocomposites. In other words, the nature of the bond between the clay and polyamide chains seems to influence clay–crystallite interactions.

4.6. Characterization of the Crystalline Phases by Infrared Spectroscopy

The effect of particles on crystallization of polyamide 6 is investigated by FTIR [216-218]. A polymer can be quickly identified as a polyamide by its IR spectra. It is known that polyamide 6 is semi crystalline and generally exhibits two kinds of crystal forms depending on the thermal and processing conditions (preparation method, particle percentage, etc.) in correlation with the requirement to maximize the number of H–bonds. One is the *α*-phase, which consists of molecules aligned in a regular extended-chain conformation (all-*trans*) and the other is the γ - type crystal structure (quasi-hexagonal form) in which the chains are helical twisted because of somewhat irregular intermolecular hydrogen bonding via amide groups [219]. The crystalline structure of PA6 under equilibrium conditions and at room temperature is the α-phase. And γ-form is an unstable form which can be transformed into the α-form by annealing [220, 221] or by treatment with a phenol aqueous solution [222, 223]. The characteristic absorption peaks of the α-phase are 1478 cm^{-1} (CH_2 scissor vibration), 1416 cm^{-1} (CH_2 scissor vibration), 1373 (amide III and CH_2 wag vibration), 1199 cm^{-1} (CH_2 twist –wag vibration), 959 cm^{-1} (CO-NH in plane vibration) and 928 cm^{-1} (CO-NH in plane vibration). The characteristic peaks of γ-phase were 1439 cm^{-1} (CH_2 scissor vibration), 1369 cm^{-1} (CH_2 twist –wag vibration), 1236 cm^{-1} (CH_2 twist – wag vibration), 976 cm^{-1} (CO-NH in plane vibration), 712 cm^{-1} (amide V) [221]. Wu et al. have studied the effect of particle on crystallization of PA6-clay nanocomposite in various cooling condition. Figure 4.8 shows the FT-IR spectra of PA6 nanocomposite under different cooling

conditions. Similarly, the PA6 nanocomposite quenched in 20 ℃ water, cooled in 20 ℃ air or cooled down in oil bath from 250 to 20 ℃ are desig nated as W (water), A (air), O (oil). In sharp contrast to PA6, all the PA6 nanocomposite samples, regardless of cooling history, revealed the presence of γ-phase since peaks were observed at 1439 and 1236 cm^{-1}. No peaks associated with the α-phase were observed for nanocomposite (W). In nanocomposite (A), there were weak signals of the α-phase at 1478, 1199, 959 and 928 cm^{-1}. The intense α-peaks in nanocomposite (O) implied coexistence of two crystalline phases. In summary, the γ-phase becomes the dominant phase in the nanocomposite system. This phenomenon has been verified [224-229] by means of XRD or NMR. The reason why the particles favor the formation of γ-phase in PA6 still remains unclear. Vaia et al. suggested that the addition of clay layers forces the amide groups of PA6 out of the plane formed by the chains. This result in conformational changes of the chains, which limits the formation of H-bonded sheets and the γ-phase, is favored [230].

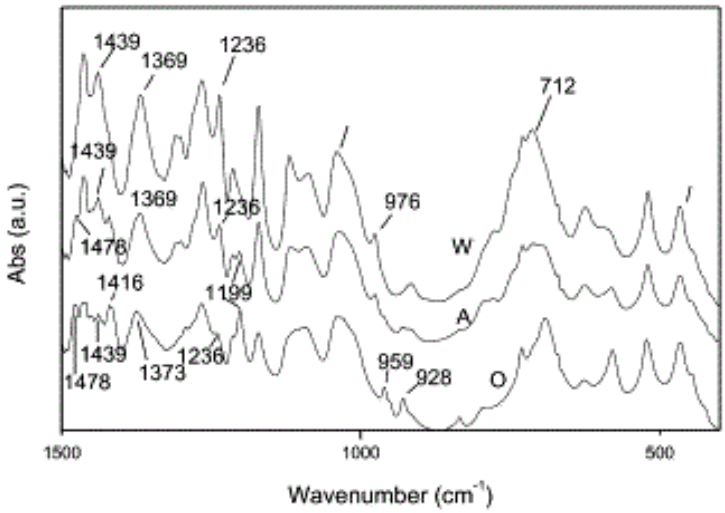

Figure 4.8 FT-IR spectra of PA6/clay nanocomposite under various cooling conditions; (W): removed from the 250 ℃ oil bath and quenched in a water bath at 20 ℃; (A): removed from the 250 ℃ oil bath and cooled in 20 ℃ air; (O): coole d down in oil bath from 250 to 20 ℃ by natural convection.

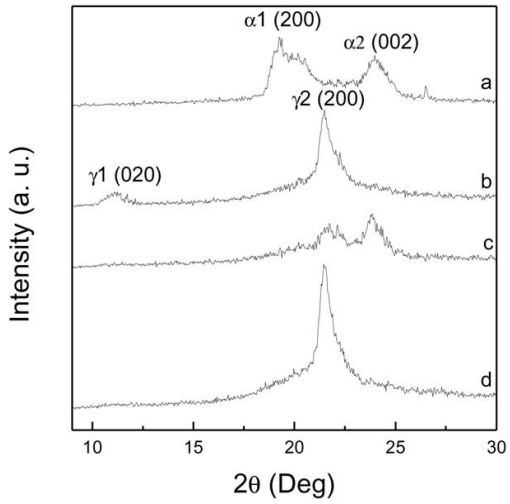

Figure 4.9 XRD patterns of (a) α-phase PA6; (b) γ-phase PA6; (c) N5O (PA6CN is cooled down in oil bath from 250 to 20 ℃ by natural convection); (d) N5W (PA6CN is removed from the 250 ℃ oil bath and quenched in a water bath at 20 ℃.

VASANTHAN and SALEM [231] also have applied FTIR method to the quantitative analysis of phase changes during thermal treatment and the drawing of polyamide-6. They confirmed that crystallization during thermal treatments involved increases in both phases and did not involve crystal-to crystal transformation, whereas drawing involved both crystallization of the amorphous phase in the α form and γ →α transformation. They showed that the α-crystal formation occurs by increasing heat-treatment temperature during thermally induced crystallization as well as increasing the draw ratio. (Figure 4.10)

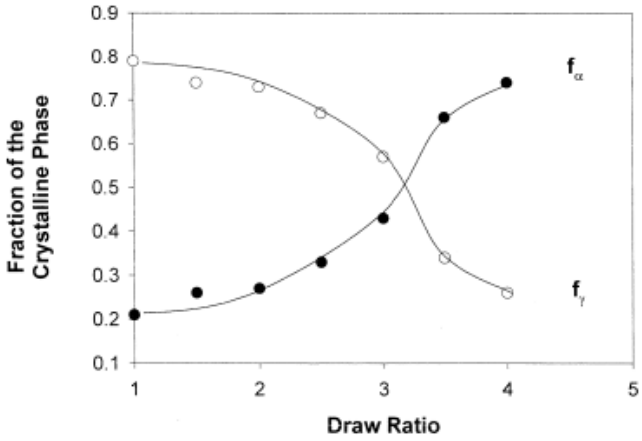

Figure 4.10 Fraction of α- and γ-crystalline phases in the total crystallinity of polyamide-6 fibers drawn to different draw ratios versus draw ratio.

Figure 4.11 shows the XRD pattern for the polyamide-6 fibers drawn at different draw ratios. A strong reflection at 23° is observed for the undrawn (as-spun) fiber (sample a), indicating that it contains predominantly the γ-crystal form. As the draw ratio increases, new reflections (2θ ~ 21 and 24°) appear as shoulders on both sides of the γ reflection. These reflections become predominant at higher draw ratios, indicating that the α-crystal content increases with an increasing draw ratio.

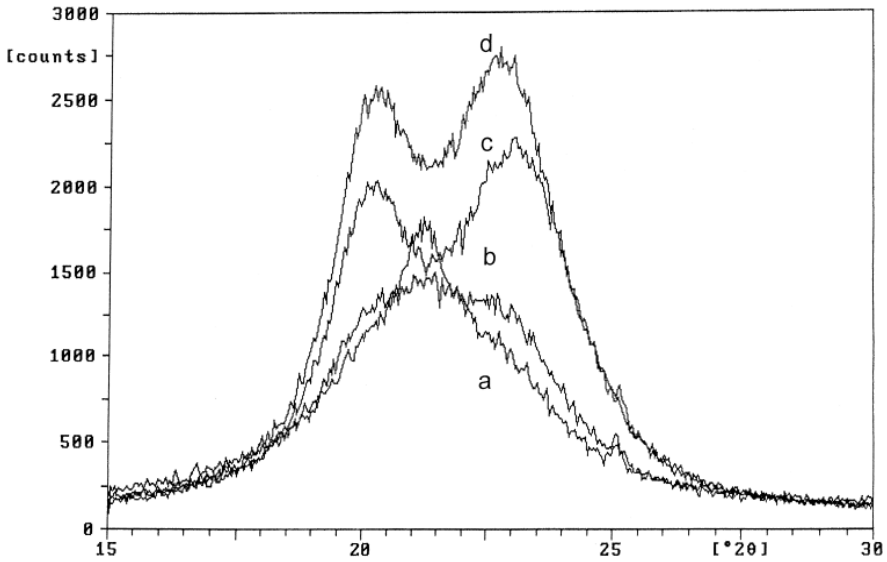

Figure 4.11 Wide-angle X-ray diffraction pattern (equatorial scan) of polyamide-6 fibers drawn at different draw ratios: (a) DR1, (b) DR2, (c) DR3, and (d) DR4.

Chapter 5

Characterization techniques applicable to nanocomposite

5.1. Introduction

In the general research area of polymer nanocomposites, a number of critical issues need to be addressed before the full potential of polymer nanocomposites can actually be realized. While a number of advances have recently been made in the area of polymer nanocomposites, the studies on understanding of the effects of processing parameters on the structure, morphology, and functional properties of polymer nanocomposites are essential. There is a need for characterization techniques to quantify the concentration and distributions of nanoparticles as well as to assess the strength at the interface between the polymer and nanoparticles. Also, there is a need for the development of better models which are able to predict the mechanical properties of the polymer nanocomposites as a function of many factors, including nanoparticle orientation, the type of functional groups, and the molecular weight of polymer matrix. The relationship between the structural distributions of the nanoparticles and the ultimate properties of the polymer nanocomposites also needs to be elucidated. Therefore, for developing and assessment of research results, characterization and acquaintance with characterization techniques is a must.

Characterization of the nanocomposites is essential for achieving meaningful results; therefore characterization is required at the following stages.

1- Characterization of physical structure and morphology, specially the parameters which govern the properties of polymers and fibers.
2- Characterization of thermal properties, namely the measurement of temperature of melting, crystallization and decomposition.
3- Characterization at the molecular level, which involves measurement of molecular weight and some time also the characterization of chemical structure.

5.2. X-ray diffraction (XRD) [232-235]

X-ray powder diffraction is a powerful non-destructive testing method to study the morphology and structural evolution of polymeric materials from micro to nano levels. The X-ray diffraction method is the most powerful technique available for the examination of polymers in the solid state. In general, useful information can be obtained only if the polymer forms oriented fibers or yields single crystals. The following type of information can be obtained from X-ray diffraction experiments:

1- Estimate of the degree of crystallinity of a polymer sample.
2- Determination of the extent of orientation of crystallites in a polymer.
3- Analysis of the macrostructure of the polymer – the way in which the crystallites or bundles of chains are packed together.
4- Determination of the molecular structure, including the chain conformation and the position of individual atoms. This aspect is the most involved but yields the greatest amount of useful fundamental information.

X-rays, with wavelengths comparable to interatomic distances, are quite appropriate for measuring the crystalline structure of polymers. A large number of sets of parallel planes can be considered to pass through any regular three-dimensional array of atoms. Some of these are more sensitive than others to the reflection of a X-ray beam, depending on the total electron density of the atoms in the set of planes. Thus the incident X-ray beam reflected through such sets of planes may interfere constructively to produce enhanced intensity, which produces a diffraction point on a photographic plate or a maximum in the diffraction pattern recorded through a detector. The condition for such constructive interference, or the occurrence of a diffraction maximum, is described by Bragg's equation:

$$2d \sin\theta = n\lambda$$

Where d is the interplannar spacing, θ is the Bragg angel (or half the angle between incident and diffracted beam directions), λ is the wavelength of the X-rays and n is the order of diffraction (usually n =1 for the most intense diffraction maxima.)

Fibers possess a high degree of crystallite orientation; hence in practice their diffraction patterns are recorded using two types of samples:

1. Powdered samples, where the fibers are cut into small pieces (almost like a powder) and mixed randomly to form a compressed pellet. Thus the crystallites are randomly oriented and one obtains the diffraction maxima in the form of uniform intensity circles.

2. Fiber samples, where the fibers are held mutually parallel and straightened along their fiber axis in a brunch. Owing to the preferred orientation of crystallites, the diffraction maxima appear as arcs with arc length depending on the degree of orientation. The greater the degree of orientation, the smaller is the arc length.

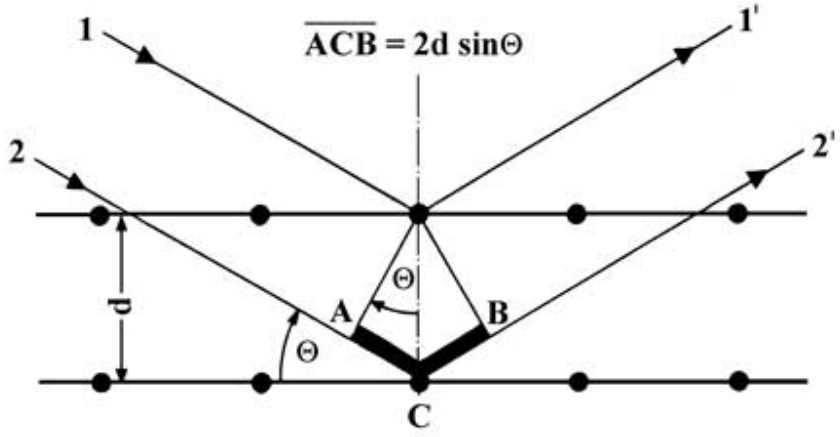

Figure 5.1 Schematic representation of the XRD process

5.3. Microscopic techniques [236-238]

Microscopic observations enable the characterization of polymers and fibers in various ways, depending on magnification ranges and radiation used [239]. The microscopic techniques are of three types: light microscopy, electron microscopy and atomic force microscopy with the two latter extensively used in polymer nanocomposite researches. Within this work the focus is more on electron microscopy technique. Electron microscopy is a process of obtaining images using electrons and is frequently used when the magnification required is much larger than what can be achieved by light microscopes that means; when the particles to be monitored are smaller than the wavelength of the visual light (< 400 nm). The physical effect behind this principle is based on wave-particle duality of electrons. The emitted electrons are high-energy matter having wavelength much smaller than that of light and this allows for the resolution of smaller objects. Moreover, the electrons interact with samples in various ways and this allows for the determination of detailed information about them. The advantages of electron microscopy over X-ray crystallography are, that the specimen need not be a single crystal or even a polycrystalline powder, and also that the Fourier transform reconstruction of the object's magnified structure occurs physically and thus avoids the need for solving the phase problem faced by the X-ray crystallographers after obtaining their X-ray diffraction patterns of a single crystal or polycrystalline powder. The major disadvantage of the transmission electron is the need for extremely thin sections of the specimens, typically less than 100 nanometers.

The two main electron microscopic techniques available for nanocomposite imaging are the scanning electron microscopy (SEM) and transmission electron microscopy (TEM).

5.3.1. Scanning electron microscopy (SEM)

A scanning electron microscope (SEM) is a type of electron microscope that images a sample by scanning it with a high-energy beam of electrons in a raster scan pattern. The electrons interact with the atoms that make up the sample producing signals that contain information about the sample's surface topography, composition, and other properties such as electrical conductivity. In SEM scanning is done on the surface of the specimen in the reflection mode, hence the surface has to be natural without any markings of the knife or microtome blade.

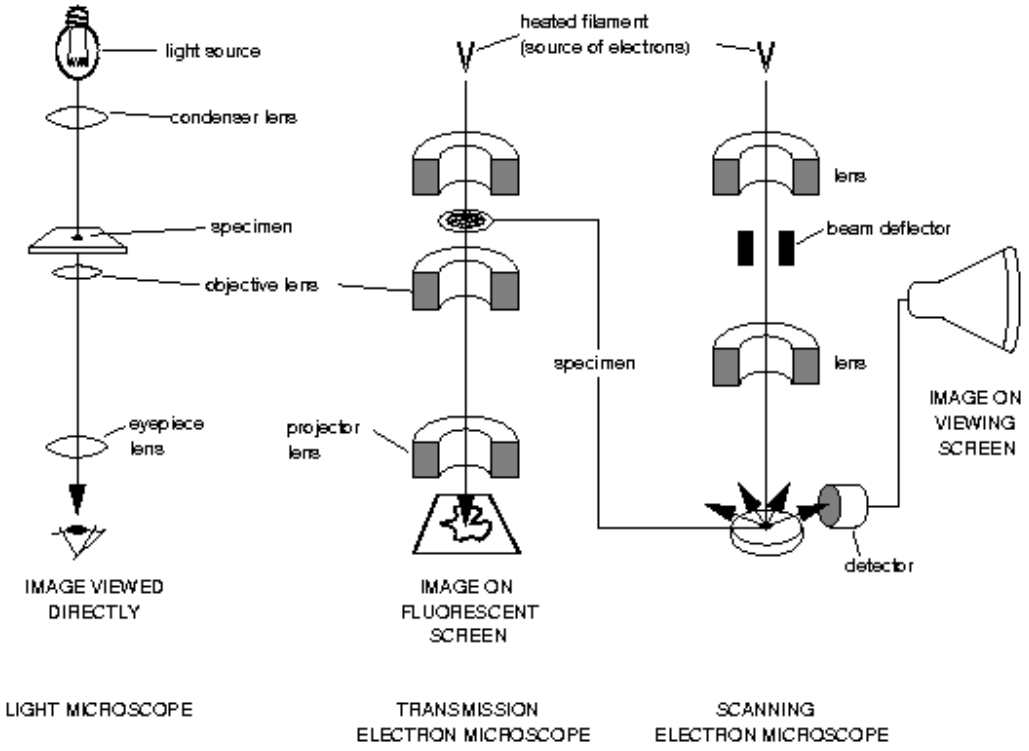

Figure 5.2 Comparison of the light microscope with TEM and SEM.

5.3.2. Transmission electron microscopy (TEM)

Transmission electron microscopy (TEM) is a microscopy technique whereby a beam of electrons is transmitted through an ultra thin specimen, interacting with the specimen as it passes through. An image is formed from the interaction of the electrons transmitted through the specimen; the image is magnified and focused onto an imaging device, such as a fluorescent screen, on a layer of photographic film, or to be detected by a sensor such as a CCD camera.

The samples used for TEM have to be very thin to allow sufficient transmission of the electrons. Thin sections cut on a microtome or thin films grown on substrates are used for this.

5.4. Spectroscopic technique [240, 241]

Spectral techniques are generally used to probe the chemical make-up of macromolecular materials such as functional groups, structural conformation and component concentration. The main spectral techniques applied in polymer nanocomposite research are Fourier transform infra-red spectroscopy (FTIR), nuclear magnetic resonance (NMR) and ultraviolet (UV) spectroscopy.

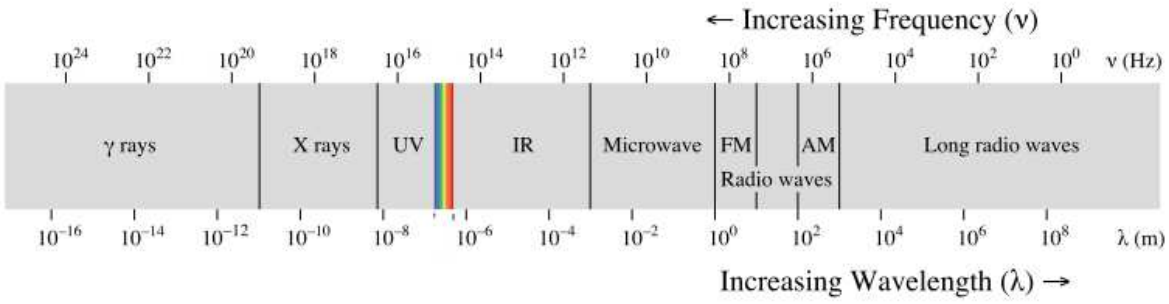

Figure 5.3 EM Spectrum showing the range of frequencies and wavelength of radiation.

Spectral techniques involve the interaction of molecules of a specimen or sample with electromagnetic (EM) radiation. It essentially monitors changes in energy states of molecules in response to EM radiation. Figure 5.3 shows the EM spectrum and the corresponding wavelength of the various radiations. Important is to understand the energy state of molecules when EM radiation is observed. Basically, when an atom or a molecule absorbs energy, it proceeds from the initial or ground state to a higher or excited state. These energy states are said to be quantumized and a particular value exists for each state. This could be related to the “spinning” of the sub-atomic particles, vibration of the chemical bonds, and so on.

Fourier transform infra-red spectroscopy (FTIR)

FTIR is a technique that utilizes the vibration response of molecules when exposed to infrared (IR) radiation. It is the absorption measurement of different IR frequencies by a sample positioned in the path of an IR beam. The infrared spectrum represents a fingerprint of a sample with absorption peaks, which corresponds to the frequencies of vibrations between the bonds of the atoms that make up the material. The main goal of IR spectroscopic analysis is to determine the chemical functional groups in the sample. Different functional groups absorb characteristic frequencies of IR radiation. Using various sampling accessories, IR spectrometers can accept a

wide range of sample types such as gases, liquids, and solids. Thus, IR spectroscopy is an important and popular tool for structural elucidation and compound identification.

5.5. Thermal characterization [242-244]

Thermal characterizations are generally defined as techniques in which a property of a specimen is continuously measured through a pre-determined temperature. Thermoanalytical techniques are used for characterization of glass transition and melting temperature, thermal stability and other properties as a function of temperature of polymers and fibers. The main thermal techniques are differential scanning calorimetry (DSC), thermal gravimetric analysis (TGA), dynamic mechanical analysis (DMA) and heat distortion temperature (HDT). Thermal analysis is based on the detection of changes in the heat content (enthalpy) or the specific heat of a sample with temperature.

5.5.1. Differential Scanning Calorimetry (DSC)

Differential scanning calorimetry is a thermo-analytical method that measures the difference between the amount of heat necessary to raise the temperature of sample and reference. It is used to study thermal transitions of a polymer. As thermal energy is supplied to the sample, its enthalpy increase and the temperature rises by an amount determined by the specific heat of the sample. The specific heat of the material changes slowly with temperature in a particular physical state, but alter sharply or discontinuously when a change of the state of the matter takes place. Apart from increasing the sample temperature, the supply of thermal energy may also induce physical or chemical changes in the sample (e.g. melting or decomposition) accompanied by a change in enthalpy in the form of the latent heat of fusion, heat of reaction, or others. Such enthalpy changes may be detected by thermal analysis and can be related to the processes occurring in the sample.

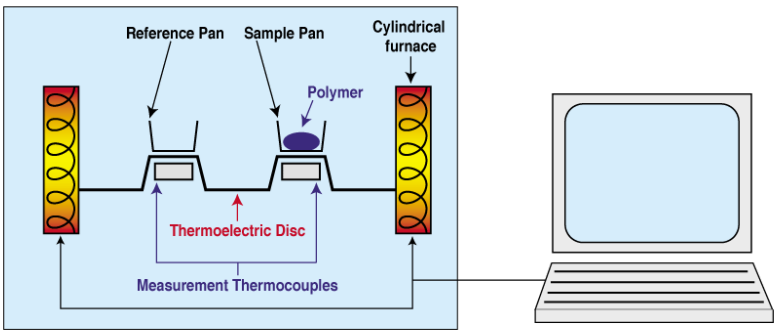

Figure 5.4 DSC experimental arrangement

Based on mechanism of operation DSC can be classified into two types.

1. Heat flux DSC
2. Power Compensated DSC

Heat Flux DSC

In a heat flux DSC, the sample material, enclosed in a pan and an empty reference pan are placed on a thermoelectric disk surrounded by a furnace. The furnace is heated at a linear heating rate and the heat is transferred to the sample and reference pan through thermoelectric disk. However owing to the heat capacity of the sample there exists a temperature difference between the sample and reference pans which is measured by area thermocouples and the consequent heat flow is determined by the thermal equivalent of Ohm's law,

$$q = \frac{\Delta T}{R}$$

Where q is sample heat flow, ΔT is temperature difference between sample and reference and R is resistance of thermoelectric disk.

Power Compensated DSC

In power compensated calorimeters, the sample and reference pan are in separate furnaces heated by separate heaters. Both the sample and reference are maintained at the same temperature and the difference in thermal power required to maintain them at the same temperature is measured and plotted as a function of temperature or time. DSC is used to determine glass transition, melting temperature, heat of fusion, percent crystalline and crystallization kinetics and phase transitions. The areas of crystallization or melting peaks are proportional to the heat involved in the process, and the areas can be accurately calibrated in terms of heat by using known standard sample. From the heat of melting of a given experimental sample (ΔH_c), one may calculate the degree of crystallinity,X_c, from the enthalpy involved during crystallization using following equation:

$$Xc = \frac{\Delta Hc}{(1-\phi)\Delta Hm} \times 100$$

Where X_c, is the degree of crystallinity, ΔH_c is the integrated heat below the melting peak, ΔH_m is the melting enthalpy of the crystalline polymer and ϕ is the weight fraction of particle in the mixture.

5.5.2. Thermal gravimetric analysis (TGA)

Thermogravimetric Analysis (TGA) is a type of testing that is performed on samples to determine the amount and rate of change in the weight of a material as a function of temperature or time in a controlled atmosphere. Measurements are used primarily to determine the composition of materials and to predict their thermal stability at temperatures up to 1000℃. The technique can characterize materials that exhibit weight loss or gain due to decomposition, dehydration, or oxidation. TGA is commonly employed in research and testing to determine characteristics of materials such as polymers, in order to determine: degradation temperatures, thermal stability of material, oxidative stability of material, moisture and volatiles content of materials, the level of inorganic and organic components in materials, decomposition points of explosives, and solvent residues. It is also often used to estimate the corrosion kinetics in high temperature oxidation.

5.6. Molecule weight determination [245-248]

Hence polymers are aggregates of large molecules comprising well-defined repeat units. The number of times the repeat unit occurs in a molecule is called degree of polymerization (DP), and DP multiplied by M_0 (molecular weight of repeat unit) is equal to the molecular weight of the polymer. Polymer molecular weight is important because it determines many physical properties. Some examples include the temperatures for transitions from liquids to waxes, to rubbers, to solids, and mechanical properties such as stiffness, tensile strength and elongation at break of fibers, as well as viscoelasticity, toughness, and viscosity. If molecular weight is too low, the transition temperatures and the mechanical properties will generally be too low for the polymer material to have any useful commercial applications. For a polymer to be useful it must have transition temperatures to waxes or liquids that are above room temperatures and it must have mechanical properties sufficient to bear design loads.
An important feature of polymers is that all their molecules are not of identical molecular weight. Thus, the molecular weight distribution, which influences the properties of the final product, has to be controlled through appropriate variation of process parameters and must be characterized. Moreover, owing to the existence of a molecular weight distribution (MWD) in any polymer sample, the measured molecular weight is an average value; the different kinds of average of molecular weight are defined below.

(a) Number average molecular weight
Number average molecular weight ($\bar{M}_n$) is defined as the total weight of all the molecules in a given sample divided by the total number of molecules

$$\bar{M}_n = \frac{\sum_i NiMi}{\sum_i Ni}$$

Where N_i and M_i are the number and molecular weight of the ith species of the molecules, respectively.

(b) Weight average molecular weight

Weight average molecular weight ($\bar{M}_w$) is defined as the total of the number of molecules multiplied by the square of molecular weight of all the species divided by the total weight of all the species of the molecules present in the given sample:

$$\bar{M}_w = \frac{\sum_i NiMi^2}{\sum_i NiMi}$$

(c) z Average molecular weight

This is a higher power average as defined by the following expression, and is useful in the interpretation of certain properties such as melt flow of polymer:

$$\bar{M}_z = \frac{\sum_i NiMi^3}{\sum_i NiMi^2}$$

The molecular weight determine in different methods include e.g. end group analysis, viscometry and gel permeation chromatography, osmometry, or light scattering. In this study the three first methods have been applied.

5.6.1 End group analysis [249, 142]

The number average molecular weight M_n of certain linear polymers can be found by estimating the number of end groups by chemical analysis. The end groups are often acidic or basic in type, as exemplified by the carboxylic groups of PET and polyamide or the amino groups of conventional polyamides.

(a) Measurement of amino end groups in conventional polyamides

The amino end groups in polyamide are determined by dissolving 1 g of polymer in 25 ml methanol/phenol mixture (70% w/w phenol) by refluxing for 30 min. The contents are cooled and titrated against 0.02 N HCl using thermo blue as an indicator.

$$Amino\ end\ groups\ = \frac{(A-B) \times normality\ of\ HCl\ \times 100}{weight\ of\ the\ sample}$$

= NH_2 milliequivalent per kg

Where A is the volume in ml of 0.02 N HCl for the sample and B is the volume in ml of 0.02 N HCl for the blank.

(b) Measurement of carboxyl end groups in conventional polyamides

The carboxyl end groups in polyamide are determined by dissolving 1 g of sample in 25 ml benzyl alcohol by refluxing it for 30 minutes. The contents are then titrated with 0.02 N alcoholic KOH, using phenolphthalein as an indicator. A blank is also run.

$$COOH\ end\ groups = \frac{(A-B) \times normality\ of\ KOH\ \times 1000}{weight\ of\ the\ sample}$$

= COOH milliequivalent per kg

Where A is the volume in ml of 0.02 N KOH for the sample and B is the volume in ml of 0.02 N KOH for the blank.
The molecular weight $\bar{M}_n$ can be calculated from the end group analysis using the following relationship:

$$\bar{M}_n = \frac{(weight\ of\ polymer) \times (number\ of\ end\ groups\ per\ molecule)}{total\ number\ of\ end\ groups\ determined}$$

5.6.2. Viscosity

Viscosity is a measure of the resistance of fluid to an applied stress. Viscosity essentially describes a liquid's internal resistance to flow and may be thought of as a measure of its internal friction. Polymer solutions show very high viscosity which varies not only with concentration but also with molecular weight. This property of polymers has been used as a method of determining the molecular weight of polymers. A parameter called intrinsic viscosity [η] is strongly dependent on the molecular dimensions of the solute particles. Since molecular dimensions depend on molecular weight, suitable calibration curves have been developed which led to well-known relation called the Mark-Houwink equation:

$$[\eta] = K\bar{M}^{a}$$

Where k and a are constants and $\bar{M}$ is the molecular weight of the polymer. $\bar{M}$ may represent $\bar{M}_n$ or $\bar{M}_w$, depending on the molecular weight average used in the calibration curve. The intrinsic viscosity $[\eta]$ is defined as follow:

$$[\eta] = \lim_{c\to 0}\left(\frac{\eta - \eta_0}{\eta_0^{c}}\right) = \lim_{c\to 0}\left(\frac{\eta_{sp}}{c}\right)$$

Where η and η_0 are the viscosities of the solution and the solvent, respectively, and c is the concentration. The last expression on the right-hand side is simply to define the symbol η_{sp} (specific viscosity) in subsequent discussion. The intrinsic viscosity is therefore determined by plotting $\eta_{sp}/_{c}$ against c and extrapolating the plot to zero concentration, as shown in Figure 5.5

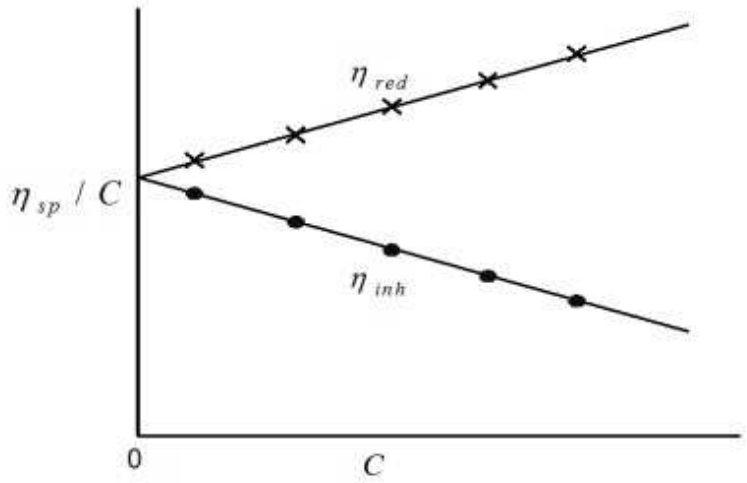

Figure 5.5 Typical plot of date for determining intrinsic viscosity

The Ubbelohde capillary viscometer

The most useful kind of viscometer for determining intrinsic viscosity is the "suspended level" or Ubbelohde viscometer, sketched below:

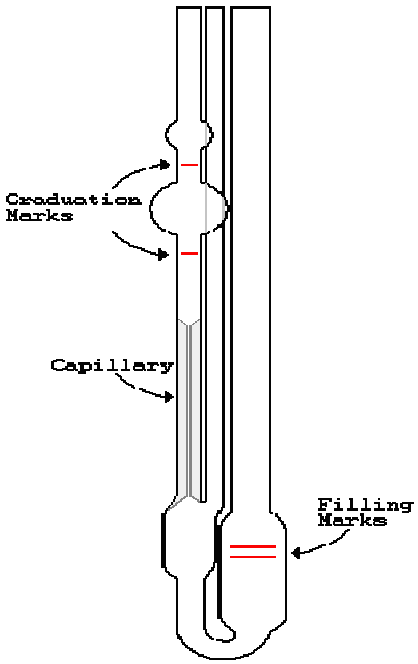

The viscometer is called "suspended level" because the liquid initially drawn into the small upper bulb is not connected to the reservoir as it flows down the capillary during measurement. The capillary is suspended above the reservoir. In conjunction with the pressure-equalization tube, this ensures that the only pressure difference between the top of the bulb and the bottom of the capillary is that due to the hydrostatic pressure i.e., the weight of the liquid. Other designs, e.g., the Cannon-Fenske viscometer, do not provide for this, and will give erroneous results in an intrinsic viscosity determination. Such viscometers are useful in other experiments--e.g., checking the stability of some polymer solution, where one is only interested in measuring a change in the flow time.

Basic Relations for Capillary Viscometry

Here is presented the basic relation of capillary viscometry, which is known as Poiseulle's law [250].

$$\eta = \frac{\pi R^4 P}{8Ql} \qquad \text{(Poiseulle's Law)}$$

Where:

- Q is the volumetric flow rate through the capillary in cm^3/s;
- P is the pressure head forcing the liquid through the capillary (usually, just the hydrostatic pressure of the liquid itself);
- R is the radius of the capillary;
- l *is the length of the capillary; and,*
- η is the viscosity

The bulb volume in the Ubellohde viscometer is fixed. Thus, the flow rate,Q, is just inversely proportional to the time between marks. Since P is usually the hydrostatic pressure, which is proportional to the density of the fluid, we have:

$$\eta \propto t\rho$$

This simple relationship is the "ideal gas law" of capillary

Use of the Ubbelohde viscometer

Capillary viscometry is conceptually simple: the time it takes a volume of polymer solution to flow through a thin capillary is compared to the time for a solvent flow. It turns out that the flow time for either is proportional to the viscosity, and inversely proportional to the density

$$t_{solvent} = \frac{\eta_{solvent}}{\rho_{solvent}}$$

$$t_{sol'n} = \frac{\eta_{sol'n}}{\rho_{sol'n}}$$

The relative viscosity is defined to be the ratio $\eta_{sol'n} / \eta_{solvent}$. For most polymer solutions at the concentrations of interest, $\rho_{sol'n} / \rho_{solvent} \approx 1$. Thus, to a very good approximation, the relative viscosity is a simple time ratio:

$$\eta_{rel} = t_{sol'n} / t_{solvent}$$

"specific viscosity" is also defined to be the fractional change in viscosity upon addition of polymer:

$$\eta_{sp} = \frac{\eta_{sol'n} - \eta_{solvent}}{\eta_{solvent}} \quad \text{(unitless)}$$

Both η_{rel} and η_{sp} depend on the polymer concentration, so to extract the "intrinsic" properties of the polymer chain itself, one must extrapolate to zero concentration. Measuring *at* zero concentration (c=0) would be useless, but this concept of extrapolating *to* c=0 is very important in polymer characterization and in thermodynamics generally. The two quantities that are commonly plotted versus concentration and extrapolated to c=0 are η_{sp} and $c^{-1} ln\ (\eta_{rel})$. A typical plot is Figure 5.5.

5.6.3. Gel permeation chromatography (GPC)

Gel permeation chromatography (GPC) is quite useful for routine estimate of molecular weight, owing to its convenience and the possibility of simultaneous evaluation of various averages of molecular weight, thus providing information about the molecular weight distribution.
The GPC technique is based on the separation of solute molecules according to their size by passing the polymer solution through a column packed with microporous gel particles. A known small volume of polymer solution is injected into an already stabilized current of the solvent through the column, and then the out flowing liquid from the column is analyzed for the concentration of the solute as a function of time. Separations of molecules occur by their preferential penetration into the pores of the gel filled in the column, depending on their sizes. Small molecules penetrate more easily than the larger one, while the very large ones may either partially penetrate or not penetrate at all. Thus, during the passage of the solution through the column the largest molecules will take the shortest time while the smallest one will take the longest time to elute from the column. The eluting liquid passing through the detector is measured for its solute concentration through its refractive index or optical density. The detector signal, which is proportional to the solute concentration, thus gives a trace as a function of time or elution volume, as shown in Figure 5.6 for a polydisperse polymer sample.

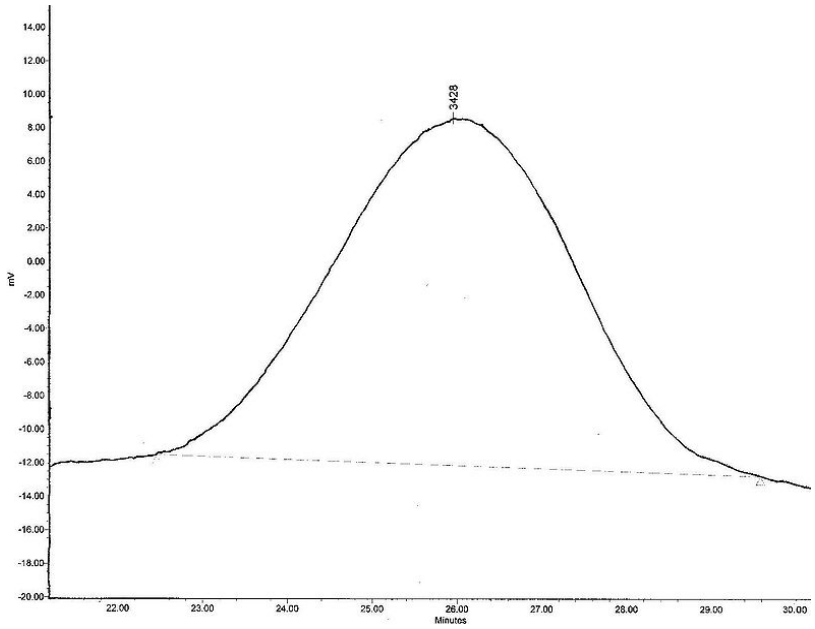

Figure 5.6 Typical GPC curve for a polydisperse polymer sample.

5.7. Tensile properties

Tensile properties of textile materials are measured using machines designed to impart, or transmit, force/extension to the material and measure the response of the material to the applied action. Tensile testing machine for textile materials are classified according to their operating principle as (1) Constant rate of extension (CRE), (2) Constant rate of traverse (CRT), (3) Constant rate of loading (CRL). Most fibers and filament yarn testers employ constant rate of extension (CRE) as the straining principle because there are difficulties in extension measurement on constant rate of loading (CRL) testers due to creep and the accuracy achieved using constant rate of traverse (CRT) testers is much lower than that achieved with other types of tester. The load-elongation characteristic curve obtained on CRE testers provide important information about the relationship between force and elongation during the time up to the fiber rupture and can be uses to determine a number of important tensile test parameters [44].

The following parameters are determined with reference to tensile tester equipment:

- *Breaking load*- the peak load that is reached during a tensile test (units: N, cN, mN).
- Elongation at break – the elongation at breaking load expressed as percentage of the original length (unit: %).
- Tenacity – the breaking load per unit linear density of the unstrained specimen (units: $Ntex^{-1}$, $cN\ tex^{-1}$, $cN\ dtex^{-1}$).
- Modulus of elasticity or Young's modulus – the slope of the stress-strain curve in the elastic region between the origin and the yield point. (units: $Ntex^{-1}$, $cN\ tex^{-1}$, $cN\ dtex^{-1}$).
- Work of rupture – the work done from the point of pretensional load to the point of breaking load. The energy required to bring a specimen to the breaking load can be obtained from the area under the load-elongation curve. Work of rupture is dependent on the linear density and length of specimen (units: N m, cN m)

Chapter 6

Synthesis and characterization of PA6/SiO_2 nanocomposites by Melt intercalation method

6.1. Introduction

The amide groups of polyamide are very polar, and hydrogen bonds can form between them. Because of these, and because the polyamide backbone is so regular and symmetrical, polyamides are often crystalline, and make very good fibers [142,161, 251-252]. Mixing and dispersing nanosized particles in polymer matrices provide the resulting materials with a variety of properties which are simply not available for bulk composites with high filler loading. In this study, we have aimed to produce nanocomposite fibers by compounding nanoparticles into polymer by melt intercalation technique. Therefore, spherical silica nanoparticles in two different particle sizes were incorporated into polyamide 6 and drawn into filaments through a melt-extrusion process. Alumina and ceria nanoparticles were used for comparison. There are two main problems during the preparation, spinning, and drawing of fibers, the difficulty of obtaining homogenous distribution of particles in the polymer and chemical compatibility of particles and polymers [13, 253-254]. Thus; appropriate way of mixing nanoparticles into the polymer is generally preferred. The three main ways of mixing nanoparticles into fiber-forming polymers are melt intercalation, solution intercalation, and in situ polymerization [253, 255]. Among these methods melt intercalation takes the advantages of traditional polymer processing techniques.

First nanoparticles and PA6 were mixed with a twin screw extruder before fiber spinning process to produce nanocomposite master batches. And then nanocomposite fibers were prepared by diluting master batch with polyamide 6 in order to reach three different weight percentages. Filaments with circular cross sections were spun using pilot melt spinning equipment. The thermal, structural and tensile properties of composite fibers were analyzed using differential scanning calorimetry (DSC), thermal gravimetric analysis (TGA) and tensile tests. The tensile properties of nanocomposite fibers were determined using a Statimat M (Textechno).The quality of particle dispersion was also studied by scanning electron microscopy (SEM).

6.2. Experimental

6.2.1. Raw material

Polyamide 6 granule (Ultramide B24 N03) was provided by BASF with Relative Viscosity (RV) 2.4 in sulfuric acid. The two different types of nanosilica (Aerosil OX50, Aerosil 150) of spherical shape which were used as filler being characterized by mean particle size of 40 nm , 14 nm and a specific surface area of 50 m^2 g^{-1} and 150 m^2 g^{-1}, respectively. Alumina (AEROXIDE Alu65) by mean particle size of 17 nm and surface area of 65 m^2g^{-1}, as well as Ceria (VP AdNano Ceria 50) by mean particle size 10 nm, were supplied by EVONIK Company and used as received. A brief description of the raw material used in this chapter is given in Table 6.1.

Table 6.1 Raw material used in chapter 6

Material	Commercial name	Description	Supplier
Polyamide 6 chip	B 24 N 03	RV =2.4	BASF
Silica (SiO_2)	AEROSIL OX50	40 nm , 50 m^2/g Powder , white	EVONIK
Silica (SiO_2)	AEROSIL 150	14 nm, 150 m^2/g Powder , white	EVONIK
Alumina (Al_2O_3)	AEROXIDE Alu65	17 nm , 65 m^2/g Powder , white	EVONIK
Ceria (CeO_2)	VP AdNano Ceria 50	10 nm , 50 m^2/g powder ,Yellowish	EVONIK

6.2.2. Sample preparation

6.2.2.1. Part one: master batch preparation

Prior to extrusion, nanoparticles are dried at 110°C in vacuum oven for 24 hours to minimize the effect of moisture [161, 252], and were kept in sealed desiccators. Polyamide chip were dried at 90℃ for 24 hours in a vacuum oven to remove the ab sorbed water due to the high moisture

absorption capability of polyamides. After drying, PA6/silica hybrid master batches were prepared by melt compounding technique using HAAKE twin screw extruder at a fixed rotational speed of 90 rpm. The temperature profile of barrel was set at 250°C – 255°C – 255°C degree from the hopper to the die. Finally melt strands were cooled in water bath and then pelletized with cutting machine. For comparison, pure PA6 was also extruded in twin screw extruder at the same process condition.

6.2.2.2. Part two: nanocomposite fiber preparation

In order to prepare nanocomposite fiber, the prepared master batches were mixed with polyamide 6 in order to reach final nanoparticle concentration 0.05, 0.2, 0.5 weight percent. The mixtures were dried at 90℃ for 24 hours in a vacuu m oven, and in order to be on the safe side, water content of samples measured according Karl Fischer method. Fiber melt spinning was carried out using a spinning apparatus (HAAKE single screw extruder) consisting of an extruder and a gear pump to control precisely the throughput rate, which was kept at 40 g/min for all polymers. Filaments extruded through a 24-hole spinneret with a diameter of 0.3 mm and at 275℃ were taken up by the high-speed winder SW46 o f BARMAG Company below the spinneret. Basic characteristics of polymers applied, and the spinning conditions are summarized in Table 6.2.

Table 6.2 Specification of material and fiber melt spinning

Material	Pure Polyamide 6	
	PA6/Aerosil OX50	0.05, 0.2, 0.5 wt. %
	PA6/Aerosil 150	0.05, 0.2, 0.5 wt. %
	PA6/Aeroxide Alu65	0.05, 0.2, 0.5 wt. %
	PA6/Ceria	0.05, 0.2, 0.5 wt. %
Spinning Temperature (℃)	275	
Throughput (g/min)	40	
Spinneret diameter (mm)	0.3	
Winding Speed (m/min)	4000	

6.3. Characterization

The crystal structures of the polyamide 6 and polyamide 6/nanocomposites was followed by X-ray diffraction analysis (XRD), using a PW 1050 Philips diffractometer (Ni—filtered Cu-K_α radiation of wavelength 0.1542 nm) in the reflection mode over the range of diffraction angles (2θ) from 5 to 35°, at room temperature. The voltage a nd tube current were 40 kV and 30 mA, respectively. The crystallization behavior of the PA6/particle hybrid nanocomposites was determined with Perkin Elmer 7 differential scanning calorimetry (DSC) over the temperature range of 30 to 250 °C at a heating rate of 10°C/min under nitrogen atmosphere and hold at that temperature for 2 minutes. Then the samples were cooled down very rapidly to 10 °C. The specimens were heated again to assess the effect of previous cooling scan. Heating scans were analyzed for the crystallization temperature, melting temperature T_m and heat of melt ΔH_f. Finally were cooled down slowly at 10 °C /min to 30℃ to complete crystallization. Crystal linity degree (X_c) of different samples was calculated by the ratio of heat of fusion of the sample to heat of fusion of the purely crystalline polyamide 6, i.e. 240 J/g. The 8 step program for DSC characterization is summarized in Table 6.3

Table 6.3 DSC Heating and cooling scan

1-	Hold for 2 min. at 30.0 °C
2-	Heat from 30 °C to 250 at 10 °C/min
3-	Hold for 2 min. at 250 °C
4-	Cool from 250 °C to 10 °C at 500 °C/min
5-	Hold for 2 min. at 10 °C
6-	Heat from 10 °C to 250 °C at 10°C/min.
7-	Hold for 2 min. at 250 °C
8-	Cool from 250 °C to 30 °C at 10°C/min.

In order to obtain the information on thermal stability, thermogravimetric analysis of PA6/silica nanocomposites was performed using a Perkin Elmer TGA7 under nitrogen atmosphere over the

range of 30℃ to 600 ℃ at a heating rate of 5 ℃/m in. The morphology of polyamide 6 nanocomposite was investigated by Scanning Electron microscope analysis using Zeiss DSM 962 microscope. Tensile properties of fibers were measured at standard climate conditions using STATIMAT M automatic tensile testing machine equipped with a 10N cell according to ASTM D-3822-07 [260]. The gauge length was 200 mm and the crosshead speed was 200 mm/min. An average of 25 reading for each fiber sample is reported.

6.4. Results and discussion

6.4.1. Melt viscosity and processability

For polymer composite systems, the size, shape and concentration of the filler can have a significant influence on the rheological properties in the melt stage. The absolute value of the melt viscosity of the nanocomposites is significantly lower than that of neat polyamide 6 [256]. The low viscosity of the nanocomposite implies good melt processability over a wide range of practical processing conditions such as extrusion and injection molding. However, it is not clear what mechanism causes the reduction of melt viscosity in the nanocomposite. One possibility is slip between polyamide 6 matrix and particles during high shear flow. Another possibility is a reduction of molecular weight of the polyamide 6 due to degradation in the presence of nanoparticle. The torque values of PA6 nanocomposite and pure PA6 as an indication of melt viscosity were measured using the Haake rheometer during melt compounding, and the results are shown in Figure 6.1. The variation in viscosity in conventional processing can be evaluated from the torque values [257-258]. As shown in Figure 6.1 by increasing of particle content the torque value decreased when compare to pure PA6.

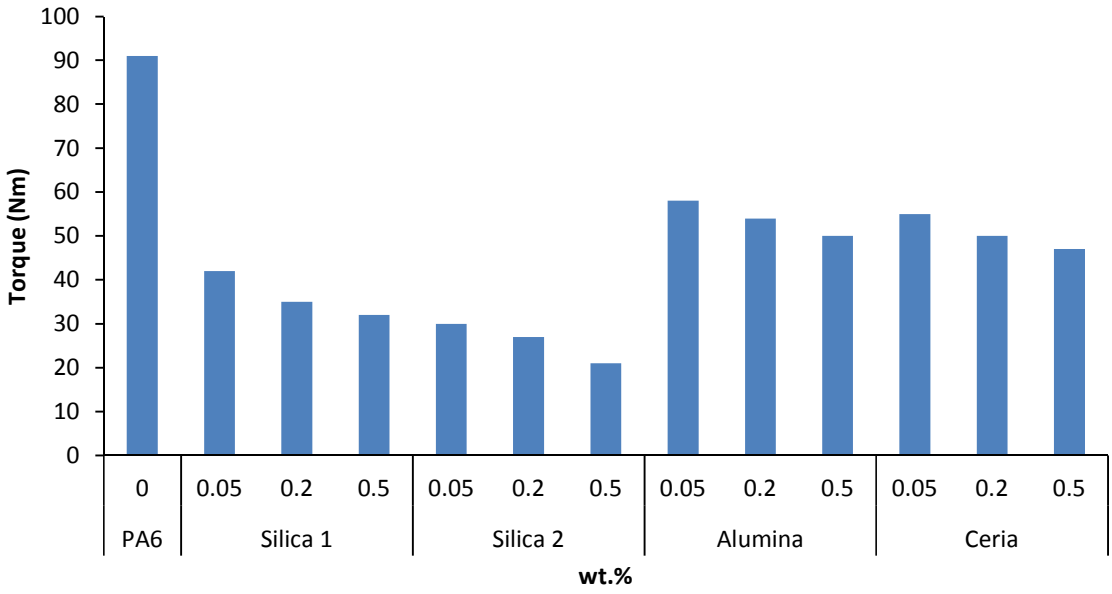

Figure 6.1 The torque values of pure Polyamide 6 and Polyamide 6 nanocomposite

Im et al. [259] have reported that when silica nanoparticles were used as filler, they acted as a lubricant rather than degrading the polymer matrix when exposed to the high shear forces and heat experienced during melt compounding. This is because the silica particles are spherical and have a smooth, non-porous surface, which lowers the coefficient of friction. The above properties allow for the possibility of improving the processibility, although decreasing the melt viscosity, have a direct effect on physical property of fibers. Furthermore the melt pressure of PA6 nanocomposites and pure PA6 measured at the head of extruder in addition proved that by incorporating particles the melt pressure, as an indication of melt viscosity, decreased as well (Figure 6.2).

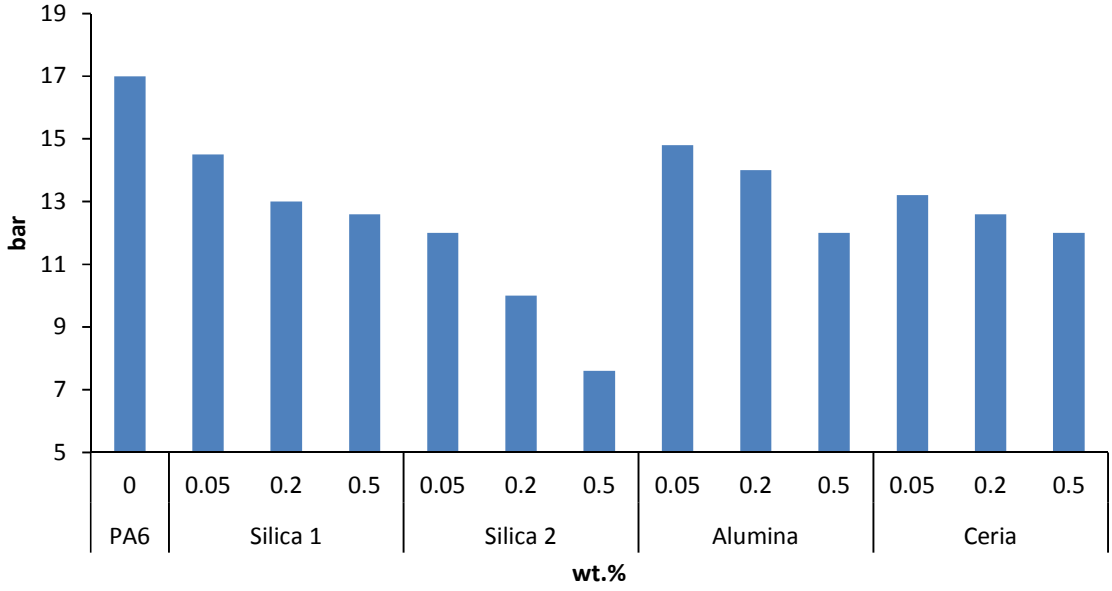

Figure 6.2 The melt pressure of pure PA 6 and PA 6 nanocomposites at head of extruder

6.4.2. Structure and crystallization Behavior of PA6/SiO_2 Nanocomposites fibers

As the mechanical properties of polymer composites are influenced by their morphology and crystallization behavior and as an incorporation of the SiO_2 plays a significant role in that, it is very important to characterize the crystallization and melting behavior of polymer nanocomposites. The presence of particle adds some complexity to the thermal behavior of the polymeric matrix. One of the most common effects is that the silica particle could serve as a nucleating agent, thus providing a large number of nucleation sites and allowing the polymer to crystallize at higher temperatures. This contributes to a change in the morphology of the system and in some cases, depending on the processing condition, a phase change occurs. The crystallization behavior of polymer composites and their crystallization kinetic as a function of particle incorporation and processing conditions are of great importance at polymer processing, particularly for the analysis and design of processing operations. Therefore, the crystallization behavior and performance of structure development of particle reinforcement polymer nanocomposites should be analyzed in order to realize the full potential of the SiO_2 for application in thermoplastic matrix-based polymer nanocomposites. Polyamide 6 is well known to crystallize into various phases, in PA6 fibers both of the most common crystal structure the α- and γ- structure are present. Often it is found the more stable α form rather than the γ form. The XRD study shows that the addition of nanoparticle has the effect of promoting the formation of

the γ form. Figure 6.3 shows XRD patterns of the polyamide 6 nanocomposites and the pure polyamide 6 matrix. Both the polymer matrix and nanocomposites exhibit two α crystalline diffraction peaks. However, besides these two peaks, the nanocomposites exhibit an additional distinct γ crystalline diffraction peak at 21.5° of 2 θ. The silica-induced γ crystalline form is also shown by the DSC heating scans. From Figure 6.4, it can be seen that the polyamide 6 matrix has one melting peak corresponding to α -form, but the nanocomposites system have two melting peaks, in which the high-temperature peak corresponds to the α form and the low-temperature peak corresponds to the γ crystalline form, which during annealing process in DSC measurement changed to α- crystal form.

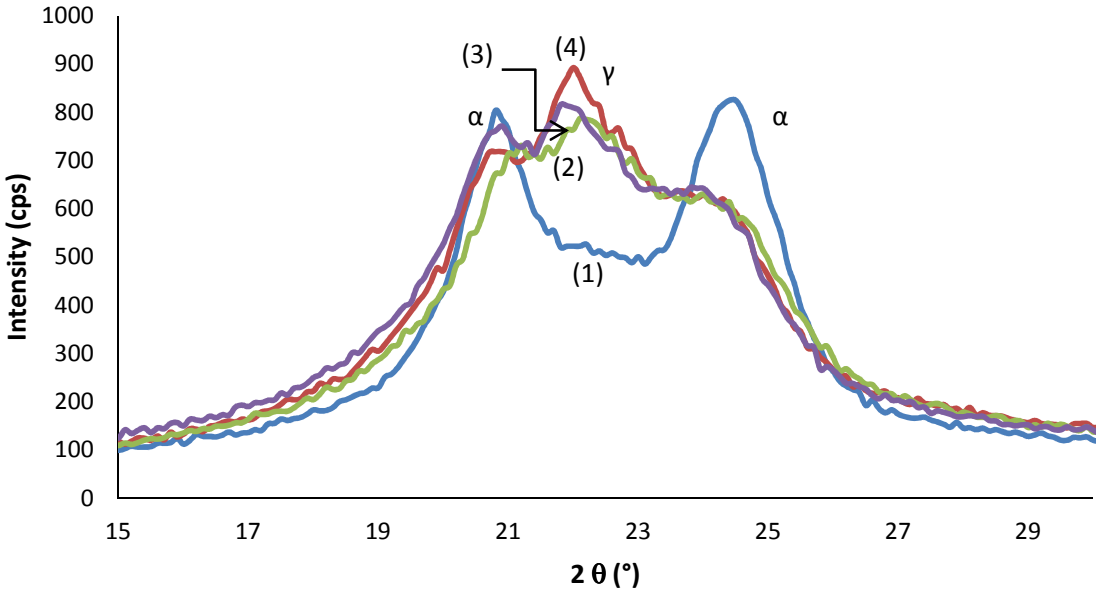

Figure 6.3 XRD pattern of Polyamide 6 and Polyamide 6/SiO_2 nanocomposite, (1): Pure PA6, (2),(3),(4): PSX with 0.05, 0.2, 0.5 wt. % respectively.

It is also worthwhile to note from Figure 6.5 that the α-form crystal is the most predominant phase and melting peaks corresponding to α-form crystals are greatly enhanced with increasing annealing time, whereas the melting peaks corresponding to γ-form crystals are observed only as a less pronounced shoulder and finally disappeared as the annealing times exceeded 60 min. This is not surprising, since, in solid state, polymer chains or segments are allowed to arrange themselves into a better organization when suitable conditions such as temperature and time are given to keep the system in a relatively lower energy. As the processing of polymer nanocomposites involves complex deformation behaviors, which may affect the nucleation and

crystallization behavior of the polymer nanocomposites, it is important to characterize the nucleation and crystallization behavior of polymer nanocomposites to optimize the process conditions. Analysis of the crystallization behavior of polymer nanocomposites reinforced with inorganic nanoparticles would make it possible to realize their potential applications in many fields of industry. The DSC results of PA6 and PA6 nanocomposites fibers in different concentrations prepared by melt compounding method are summarized in Table 6.4.

Table 6.4 DSC data of PA6 nanocomposite fibers as function of nanoparticle content

		heat up			cool down	
Sample	SiO_2	T_g	T_m	ΔH	T_c	X_c
	wt. %	℃	℃	J/g	℃	%
PA 6	0	26.9	227.3	70.1	171.3	29.2
PSX05[1]	0.05	40.2	221.36	46.7	187.9	20.5
PSX2	0.2	44.8	220.65	45.5	186.6	23.7
PSX5	0.5	42.5	220.1	47.2	186.1	39.3
PSA05	0.05	39.8	219.2	46.1	186.8	20.2
PSA2	0.2	42.2	218.5	50.7	186.6	26.4
PSA5	0.5	41.5	218.2	50.0	185.5	41.6
PAL05	0.05	44.7	218.7	47.2	186.4	20.7
PAL2	0.2	37.5	219.2	47.9	186.9	24.9
PAL5	0.5	39.9	222.0	46.3	188.8	38.6
PCe05	0.05	44.1	218.9	49.4	186.2	21.6
PCe2	0.2	44.2	219.7	50.0	185.6	26.0
PCe5	0.5	45.7	219.5	50.6	186.4	42.1

[1] PSX05: polyamide 6 / Silica (Aerosil OX50), 0.05 wt. %

6.4.2.1. Effect of Silica concentration on glass transition temperature (T_g)

The glass transition temperature (T_g) plays an important role in dictating the behavior of polymers and fibers. Below T_g molecular movement other than bond vibration is very limited. Above T_g the molecules absorb more energy and movement of molecular segments become possible well below melting temperature. The influence of nanoparticles on the T_g of PA6 was

evaluated from DSC results as shown in Table 6.4. Incorporating of 0.05 wt. % silica nanoparticle in to PA6 slightly increases the glass transition temperature (T_g) in compare to pure PA6 due to interaction of silica particles and PA6 which restrict the mobility of polymer chain. However further increase in silica concentration does not affect the T_g of nanocomposite. Also results from Table 6.4 show that silica size has no significant effect on glass transition temperature as T_g of both silica type nanocomposites is almost the same.

6.4.2.2. Effect of Silica size and concentration on melting temperature

The endothermic melting peaks of PA6 and PSX nanocomposites fibers as a function of silica content were investigated using DSC as shown in Figure 6.4. For pure PA6 on heating scan there is one endothermic peak at about 227℃ which indicated that in the pure PA6 sample, the α- crystals were the dominant crystalline phase. While for nanocomposite samples there are two endothermic peaks at about 225℃ and 212℃ which co rresponded to α - and γ- form crystals, respectively. This clearly indicated that addition of SiO_2 nanoparticles to PA6 matrix promoted the α- to γ- crystal phase transformation which was already proved by XRD results.

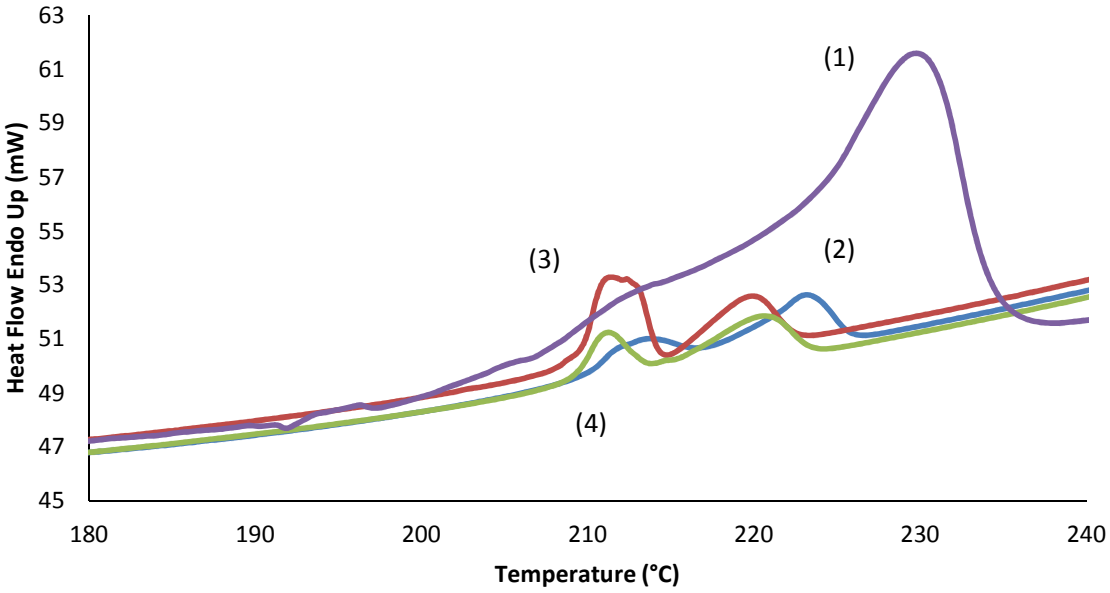

Figure 6.4 DSC heating curve of pure PA6 and nanocomposites at first heating scan as a function of SiO_2, (1): Pure PA6, (2),(3),(4): PSX with 0.05, 0.2, 0.5 wt. % respectively.

In addition, as seen from Figure 6.4 melting peaks of nanocomposite samples shifted to lower temperature in compare to pure PA6 but it seems incorporation of higher concentration has no more effect, and melt temperature of PSX2, PSX5 are almost same.

Figure 6.5 shows two DSC curves for first heating scan and second heating scan of PA6 nanocomposite (PSX05). In first heating scan there are two melting peaks which as mentioned above are α-form and less stable γ-form crystal, but in second heating scan there is one melting peak. The γ-form disappeared during annealing from 30℃ to 250 ℃ with rate of 10 ℃/min and changed to more stable α-form crystal. This phenomenon was observed with all of the nanocomposite samples which were measured in this thesis.

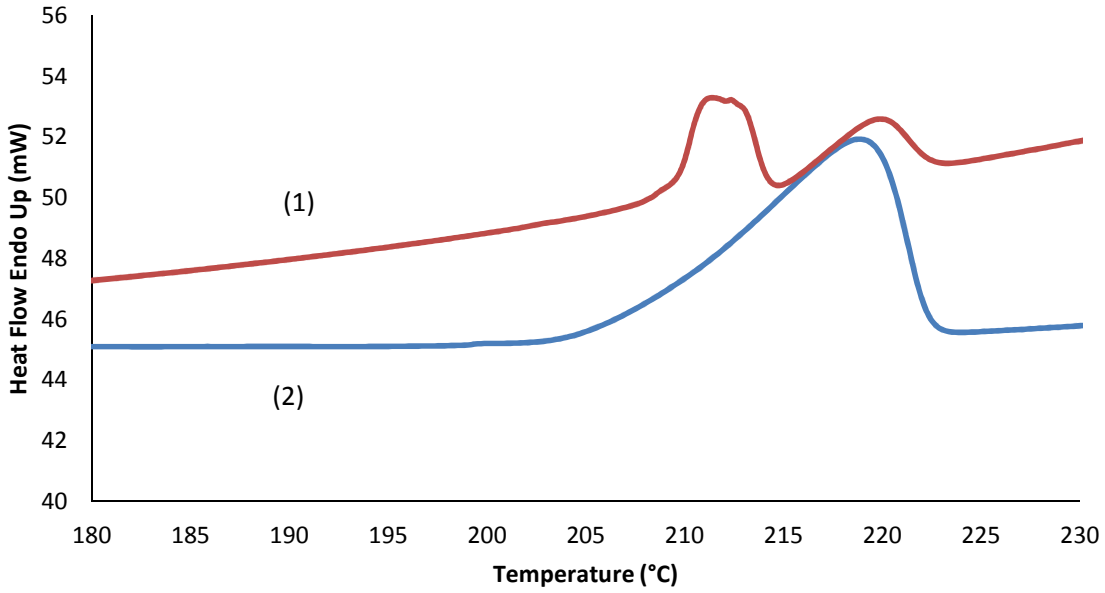

Figure 6.5 DSC heating curve for PSX05 at first heating scan (1) and second heating scan (2)

In most semicrystalline polymers, as well as in copolymers and blends, multiple melting peaks have been observed during DSC scans. Many investigations have been made into the origin of multiple melting behaviors in semicrystalline polymers, copolymers, and polymer blends [261-265]. Various factors such as a change in morphology, orientation effects, the presence of more than one crystal modification, and melting-recrystallization-remelting processes occurring during DCS scans, have influenced multiple melting behaviors.

Figure 6.6 shows that the effect of particle size on endothermic melting peak for PSX05 and PSA05 nanocomposites (same concentration and different particle size) prepared by melt compounding is almost negligible. From these results it can be concluded that crystal size of PA6 crystals in nanocomposites did not change.

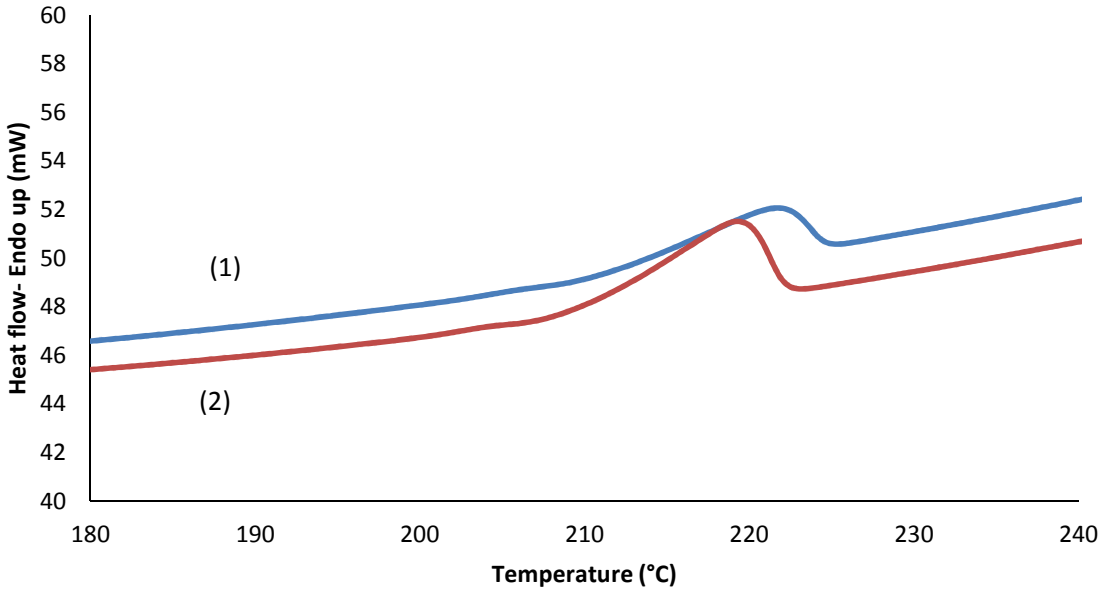

Figure 6.6 DSC heating curve of PA6/SiO_2 nanocomposites fiber as a function of Silica size (1) PSX05 (Aerosil OX50), (2) PSA05 (Aerosil 150)

6.4.2.3. Effect of Silica size and concentration on crystalline temperature

On the cooling curves an exothermic crystallization peak was observed, as shown in Figure 6.7 by incorporation of even low content of SiO_2, crystallization temperature (Tc) shifted toward a higher temperature in compare pure polyamide 6. This indicated that the added SiO_2 acted as effective nucleation sites, and faster crystallization rate. But addition of more silica has no more effect.

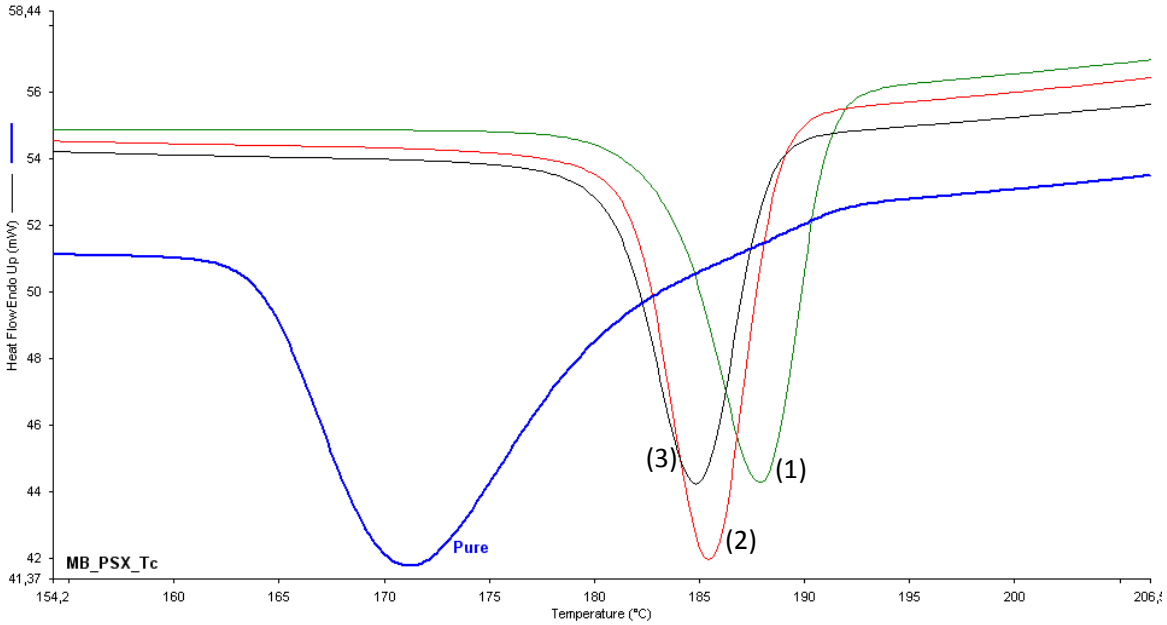

Figure 6.7 DSC cooling curves of PA6 and PA6/SiO_2 nanocomposites fiber as a function of Silica content, (1), (2), (3): PSX 0.05, 0.2, 0.5 wt. %, respectively

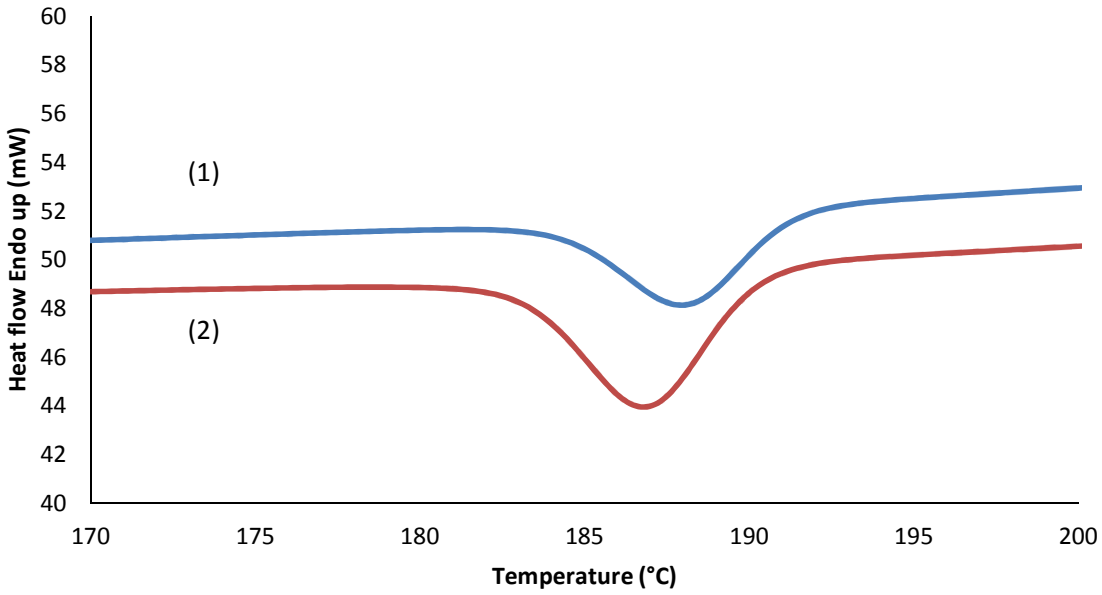

Figure 6.8 DSC cooling curve of PA6 and PA6/SiO_2 nanocomposites fiber as a function of Silica size, (1) PSX05 (Aerosil OX50), (2) PSA05 (Aerosil 150)

6.4.3. Effect of silica nanoparticle on thermal properties of PA6/SiO_2 nanocomposite fibers

As thermal stability of the polymer composites is the most important parameter for their processing and applications, it is very instructive to characterize the thermal degradation behavior. That is, from these data the limiting uppermost temperature for usage and dimensional stability (especially in melt process) can be derived, which are essential for their application in end-uses and the conditions they have to stand there, or for developing polymer composites with better balance in processing and performance [266]. Thermal gravimetric analysis (TGA) involves continuous weighing of a small sample in a controlled atmosphere (e.g., air or nitrogen) as the temperature is increased at a programmed linear rate [8].The analysis of thermal behavior of Polyamide 6 and nanocomposites were performed using the Perkin Elmer TGA7 from 30℃ to 600℃ at a heating rate of 5℃ mi n^{-1} under nitrogen atmosphere and the results are summarized in Table 6.5.

Table 6.5 TGA data of PA6/SiO_2 nanocomposites fibers as a function of silica content

	SiO_2 Wt. %	T_s[1] ℃	T_d[2] ℃
PA 6	0	377.5	434.88
PSX05	0.05	388.86	442.44
PSX2	0.2	389.81	447.02
PSX5	0.5	408.79	465.01
PSA05	0.05	379.93	439.26
PSA2	0.2	384.7	444.06
PSA5	0.5	397.82	448.75
PAL05	0.05	400.79	440.65
PAL2	0.2	401.34	445.82
PAL5	0.5	412.27	447.62
PCe05	0.05	415.75	446.53
PCe2	0.2	396.54	447.81
PCe5	0.5	406.94	469.32

[1] Onset degradation temperature

[2] Degradation temperature

According to Table 6.5 and Figure 6.9 an increase in the thermal stability of nanocomposites as function of silica content was observed in comparison with that of the pure polyamide 6. The enhanced thermal stability of nanocomposite fibers may be attributed to the strong adhesion between SiO_2 and the matrix, which stabilizes the composite against thermal decomposition. The incorporation of silica was beneficial in improving the thermo-oxidative stability of polyamide 6 as can be seen in Table 6.5. All the nanocomposites showen in Figure 6.9 and Figure 6.10 have no weight loss until around 370℃ (onset decom position) and retained 90% of their weight at about 385℃.

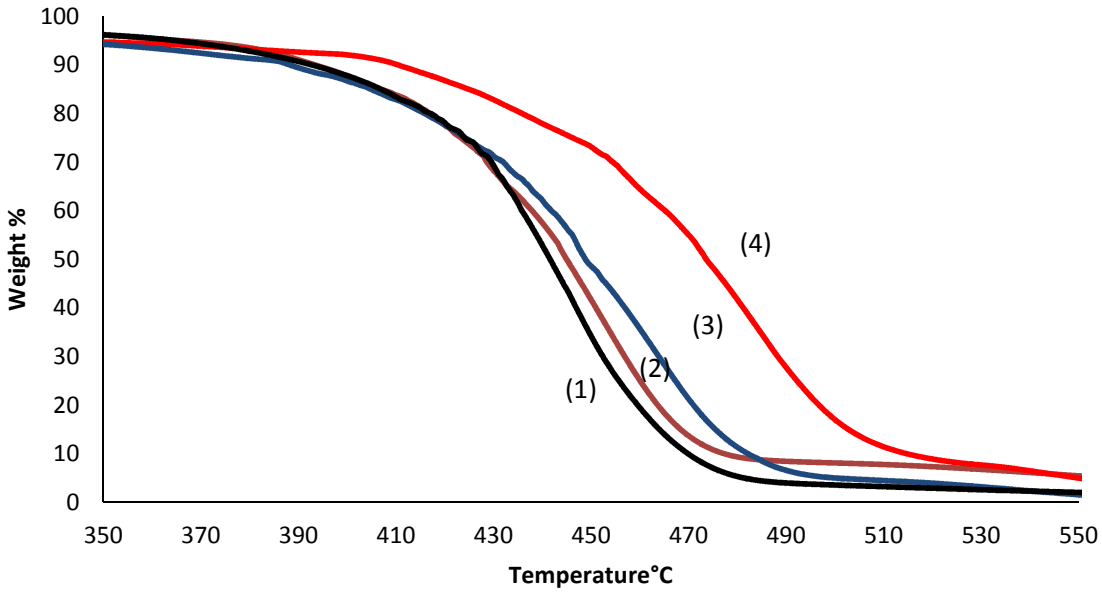

Figure 6.9 TGA analysis of PA6/SiO_2 nanocomposites fibers as a function of SiO_2 content, (1) pure PA6, (2) PSX05, (3) PSX2, (4) PSX5 with 0, 0.05, 0.2, 0.5 wt. % respectively.

The neat fiber starts to decompose at 377.5℃, some what lower than that for the SiO_2 filled fibers, which began to decompose at 388.86℃ (0.05 wt %), 389.81℃ (0.2 wt %), and 408.79℃ (0.5 wt %). The reason for the additional increase in the onset temperature is that extra energy is required to break down the adhesion force at the polymer–SiO_2 particle interface. Therefore, the interfacial interaction plays an important role in the degradation of polymer nanocomposites. In the case of a good interfacial interaction, particles are capable of restricting the movement of a polymer chain, making the scission of polymer chains harder at a given temperatures. As a consequence, the degradation temperature of the nanocomposite shifts to a higher temperature.

Though according to Figure 6.10 the particle size in general has not a significant effect on thermal stability, still a slight increase in the thermal stability caused by finer particle size (Aerosil 150) was observed. In addition, in compare between different particle types, nanocomposites prepared from Ceria have higher thermal stability, which is due to its high thermal properties (melting point 2400℃). (Figure 6.11)

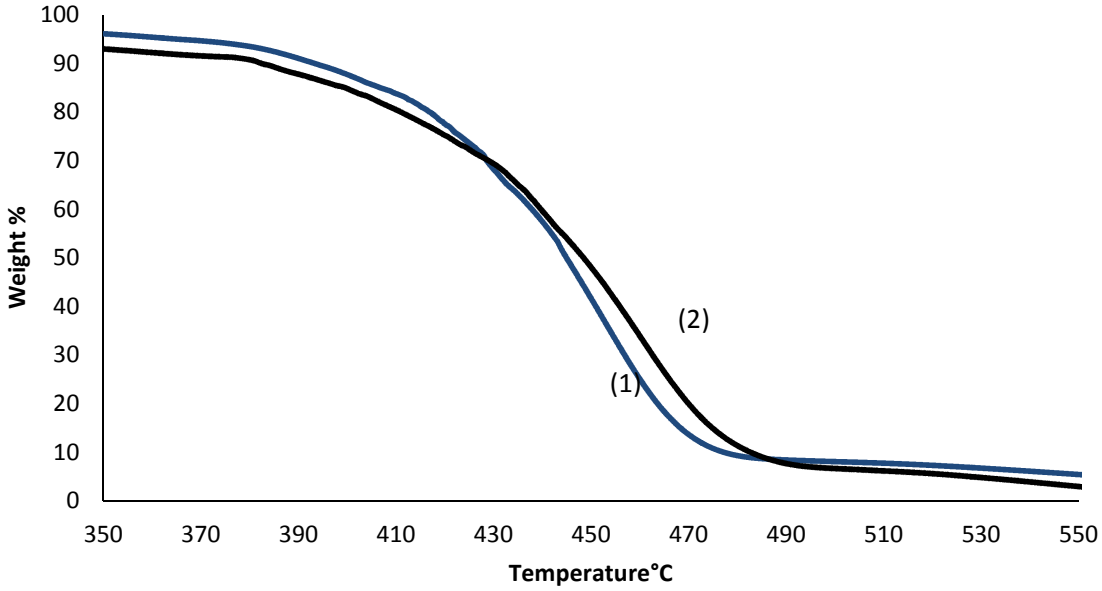

Figure 6.10 TGA analysis of PA6/SiO_2 nanocomposites fibers as a function of SiO_2 size, (1) PSX05 (Aerosil OX50), (2) PSA05 (Aerosil 150),

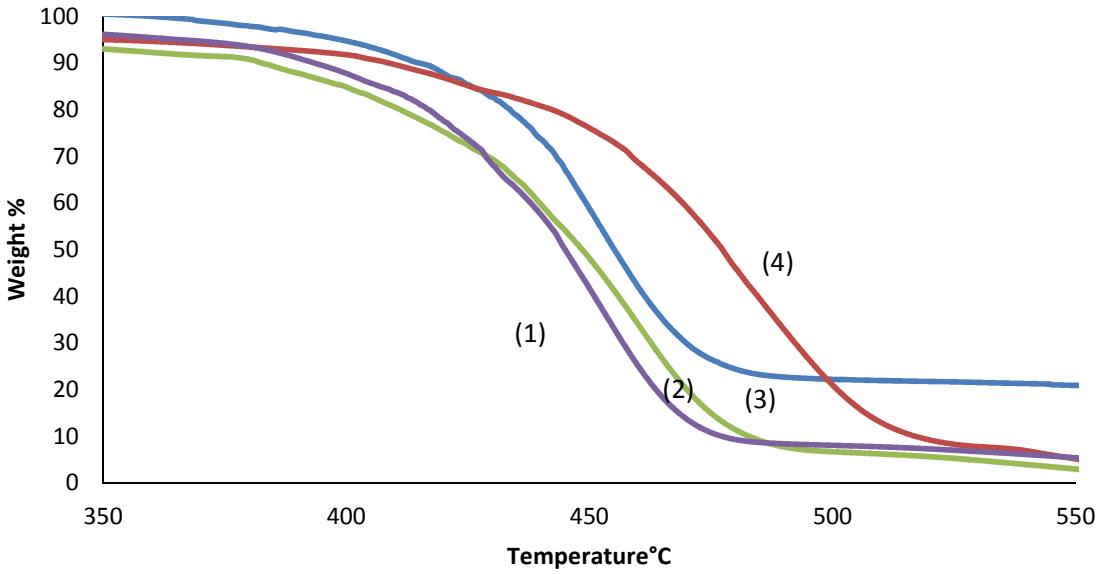

Figure 6.11 TGA curves of PA6 nanocomposite fiber in different nanoparticle type, (1) PA6/SiO_2 (Aerosil OX50), (2) PA6/SiO_2 (Aerosil 150), (3) PA6/Alumina, (4) PA6/Ceria

6.4.4. Mechanical properties of polyamide6/SiO_2 nanocomposite fibers

Tensile properties of nanocomposite fibers such as tenacity, elongation at break (EAB) and modulus were measured to evaluate the effect of nanoparticles on fiber properties. The results are summarized in Table 6.6 The tenacity values of pure polyamide 6 and PA6/SiO_2 (Aerosil OX50) containing 0.05, 0.2 and 0.5 wt % SiO_2 were about 48.68, 39.06, 38.53, and 35.48 cN/tex, respectively (Table 6.6). The elongation at break values also show a similar trend of decreasing with increasing levels of SiO_2, with values of 66.98, 52.81,52.29, 48.3%, respectively.

Table 6.6 Tensile properties of PA 6/SiO_2 nanocomposite fibers as a function of silica content

	SiO_2 wt. %	Tenacity [cN/tex]	Elongation at break [%]	Modulus [cN/tex]
PA 6	0	48.68	66.98	105.84
PSX05	0.05	39.06	52.81	189.01
PSX2	0.2	38.53	52.29	190.44
PSX5	0.5	35.48	48.38	206.01
PSA05	0.05	38.31	48.32	205.35
PSA2	0.2	35.41	45.58	215.11
PSA5	0.5	34.2	44.1	220.30
PAL05	0.05	42.43	51.71	209.35
PAL2	0.2	37.15	50.84	182.77
PAL5	0.5	35.31	48.88	195.54
PCe05	0.05	37.49	49.02	184.58
PCe2	0.2	37.74	50.53	185.43
PCe5	0.5	36.28	48.11	188.69

As seen in Figure 6.12 and Figure 6.13, tenacity and elongation at break of PA6/SiO_2 (Aerosil 150) nanocomposite fibers also decreases as the content of nano-SiO_2 particles increases. Incorporating nanoparticle into the polymer matrix increases the stiffness and makes fibers more brittle. The increase in stiffness is no doubt contributed to the silica reinforcement [107]. Since the fiber containing nano-SiO_2 is brittle, it does not elongate much.

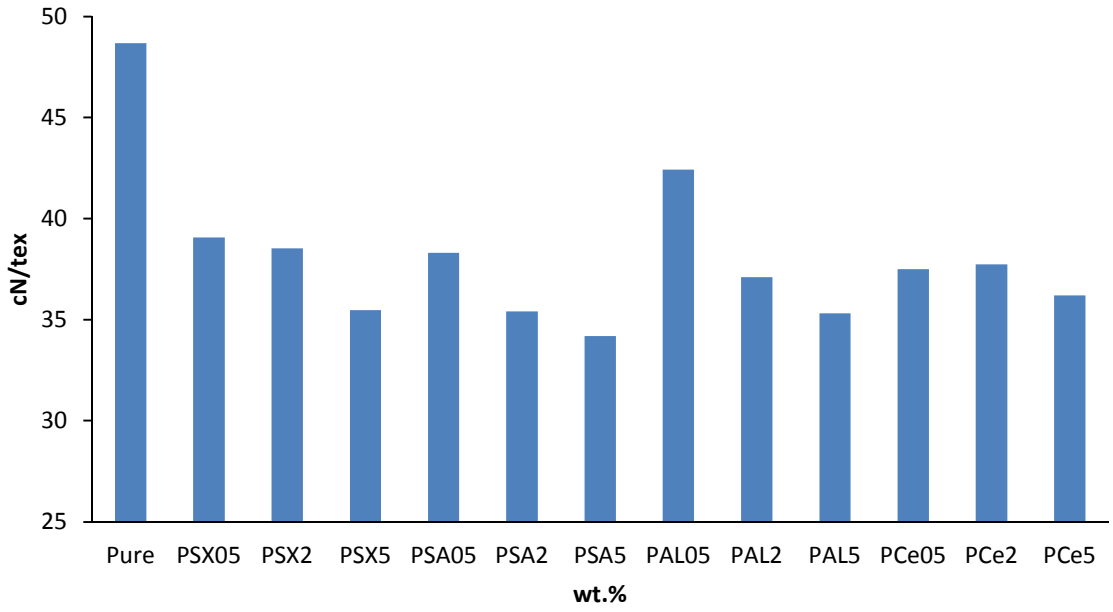

Figure 6.12 Tenacity of PA6 fiber and nanocomposite fibers as a function of silica content

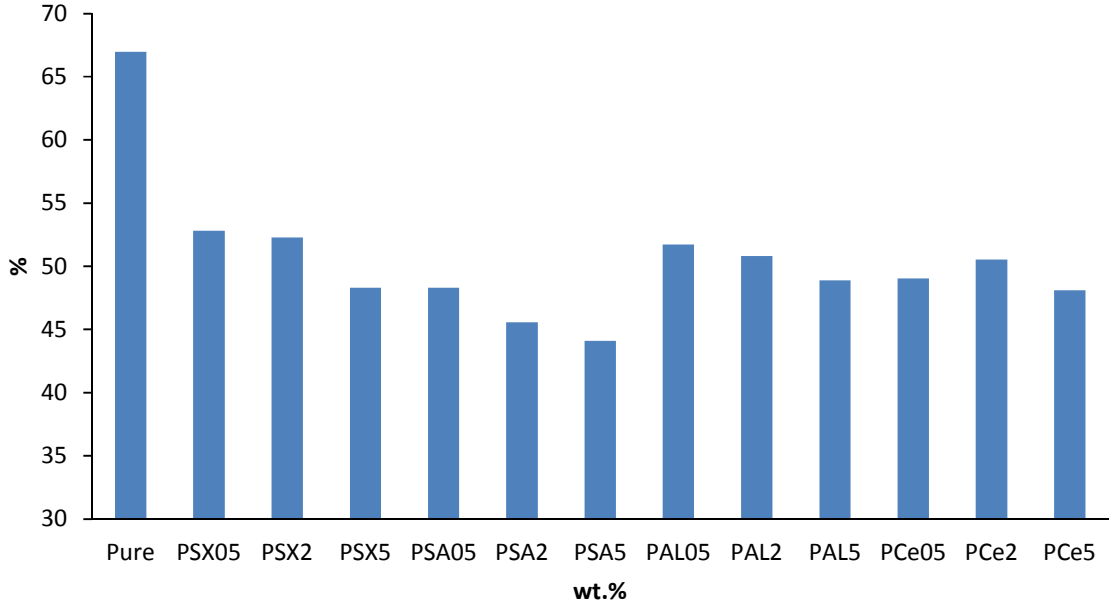

Figure 6.13 Elongation at break of PA6 fiber and nanocomposite fibers as a function of silica content

Figure 6.14 shows that the modulus of the PA6/SiO_2 increased by increasing amounts of SiO_2 (Aerosil OX50). The modulus of the PA6/ SiO_2 containing 0.5, 0.2, 0.5 wt. % SiO_2 were 189.01, 190.4, 206.01 cN/tex, respectively, which was higher than that for the pure polyamide. The similar trend for other silica type (Aerosil 150) was observed. The increased modulus of the nanocomposites can be attributed to the large aspect ratio and high stiffness of the silica particle. Vlasveld and et al. [267] have analyzed the modulus of polyamide 6/silicate nanocomposite and reported despite all the work done on nanocomposites, there is still discussion about the reason of the large modulus increase by using such small amounts of filler. The nature of the mechanism is a subject of debate was various contrasting ideas seem to exist: (a) the increased modulus could be contributed to the reduced mobility of a constrained polymer phase close to the silicate layers. The large surface area of the exfoliated platelets is considered to be responsible for this constrained polymer phase with a higher modulus [268- 270]. (b) The strong ionic bond between the polymer and the silicate platelets is sometimes assumed to be the main reason for the enhanced modulus [271]. (c) The reinforcement mechanism in nanocomposites could be similar to traditional composites. In that case the modulus of the composite is dependent on the modulus of the matrix, the modulus of the filler and the shape and orientation of the filler particles. According to this view traditional composite theories can explain most of the properties of nanocomposites without assuming a change in the polymer properties [272]. In the first two theories the inherent modulus of the silicate particles is considered to be of minor importance, or even completely ignored. As has been shown by Van Es et al. and Fornes et al. [272] the presence of very stiff, high aspect ratio particles is expected to give a large increase in modulus and should not be ignored, as is sometimes done [269]. It is unlikely that the type of bond is very important for the modulus, because the bonding strength is not important for the modulus, although it is important for the strength of the composite. It has been reported that it is possible to make nanocomposites with layered silicates without any surfactant, which can give similar moduli [273], despite the lack of modification on the silicate filler.

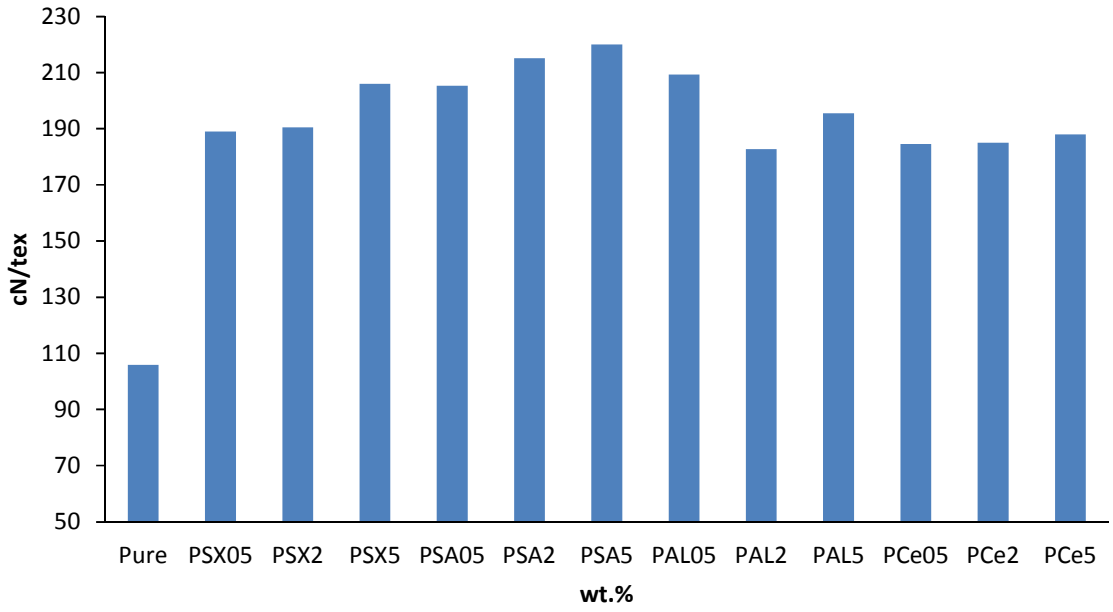

Figure 6.14 Modulus of PA6 fiber and nanocomposite fibers as a function of silica content

6.4.5. Morphology and distribution of particles in polyamide-particle nanocomposites

The dispersion of nanoparticles in the master batches was examined using a scanning electron microscope (SEM). And the results are shown in Figure 6.15 the images show that nanoparticles in PSX (b) and PAL (d) were relatively well-dispersed in polymer matrices, in PSA (c) despite a good and uniform dispersion, there is an agglomeration in the center; however dispersion quality in PCe (e) is not acceptable.

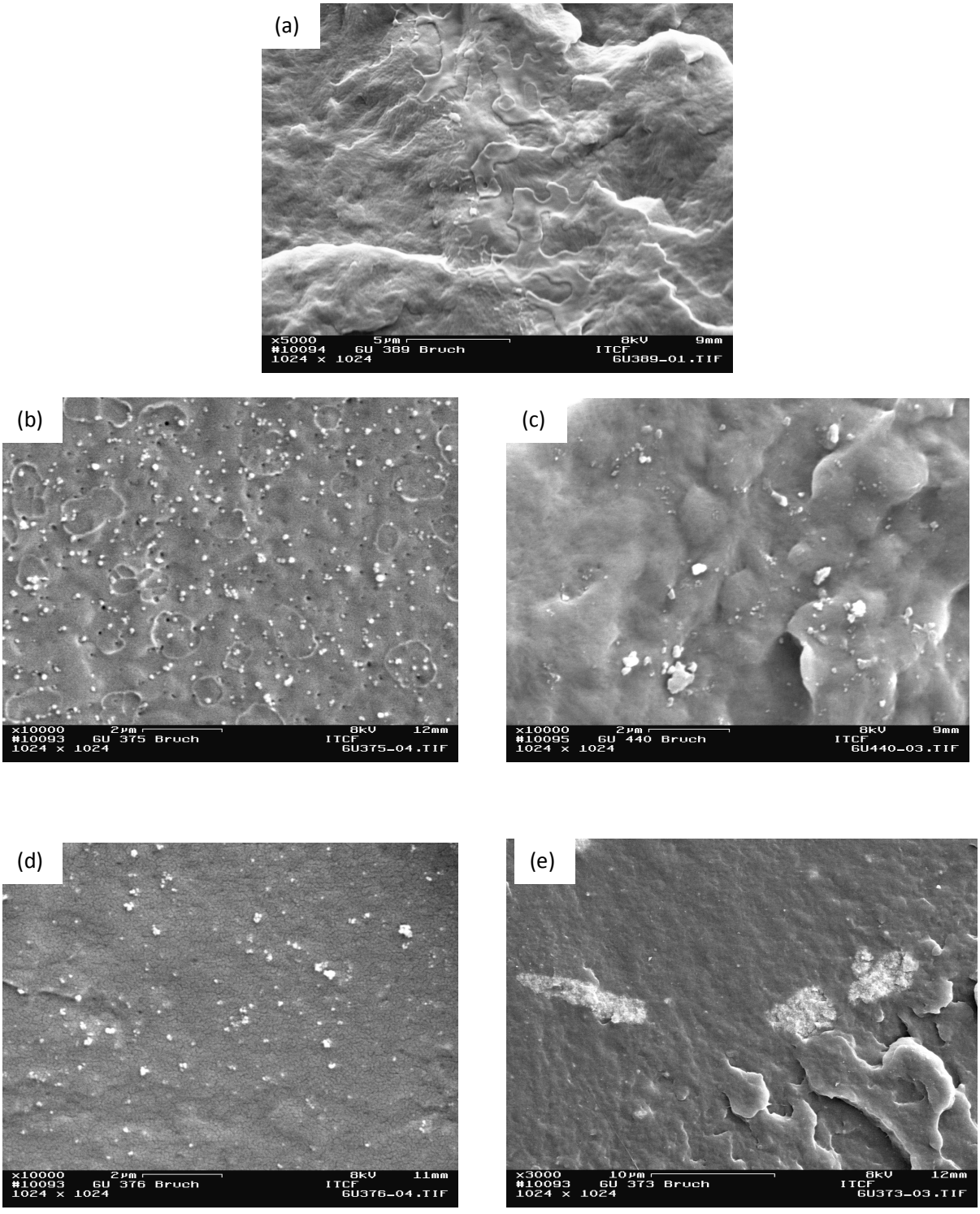

Figure 6.15 SEM picture of 10 wt % master batch samples (a) Pure PA6, (b): PSX, Aerosil OX50, (c): PSA, Aerosil 150, (d):PAL, Aeroxide Alu65 (e):PCe, Ceria

Figure 6.16 shows the SEM pictures of pure polyamide 6 and PA6/SiO_2 nanocomposite fiber containing 0.05, 0.2, 0.5 wt. % of silica (Aerosil OX50). Fiber surfaces were investigated with respect to their shape and uniformity. The neat fibers show a smooth surface along the length of fiber, but fibers filled with nano-SiO_2 particles show some surface irregularities as the content of nanoparticle increases. These surface protrusions of fibers are most probably due to nanoparticle agglomeration. It is also evident from the figures that the agglomerates are discontinuous throughout the fiber.

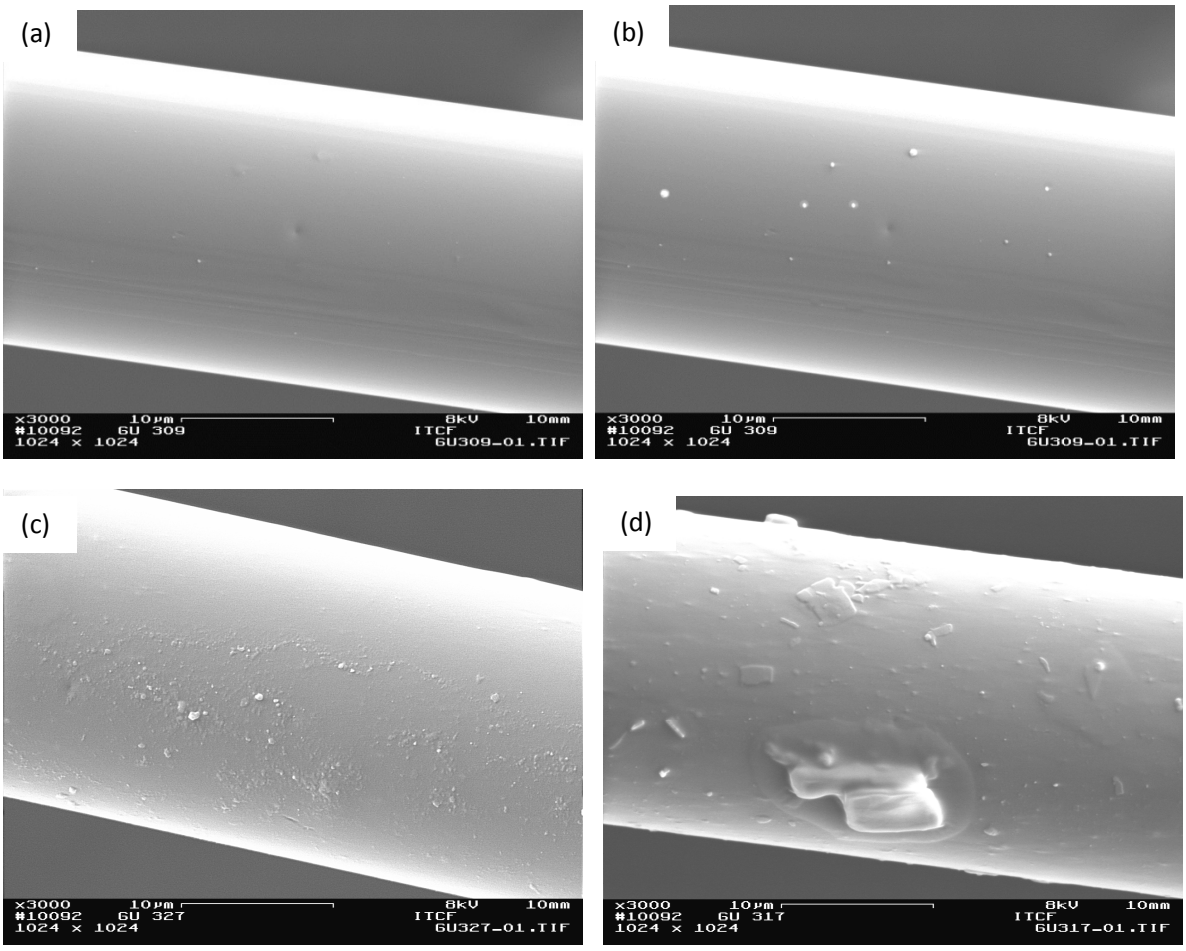

Figure 6.16 SEM pictures of pure PA6 and PA6/SiO_2 nanocomposite fiber as a function of silica content, (a) pure PA6, (b) PSX05, (c) PSX2, (d) PSX5

Chapter 7

Synthesis and characterization of PA6/ SiO_2 nanocomposites by solution intercalation method

7.1. Introduction

Organic-inorganic nanocomposite polymers continue to be an area of great interest due to remarkable improvements in properties that these materials have over conventional composites [274-275]. These show better thermal, mechanical, barrier, and other properties because of excellent dispersion of filler and stronger interfacial force between the well dispersed nanometer-sized domains and a polymer, than the conventional polymer/filler composites [276-281]. Typical preparation methods include in-situ polymerization, solution intercalation, and melt intercalation, among which solution intercalation has been known for over a century and has proved to be one of the most successful methods of incorporating delaminated particle into polymers. Polymer solution intercalation is based on a solvent system in which the polymer is soluble and the particles are swellable [282]. Solution intercalation method has been employed either for water soluble polymers, such as polyvinyl alcohol [283], and poly (ethylene oxide) (PEO) [284], and hydrophobic polymer systems such as high density polyethylene (HDPE) [285]. Despite many laboratory successes with solution intercalation, its application on an industrial scale is still hindered by two major problems: (1) involvement of large quantities of aqueous/organic solvent; (2) a limited number of solvent/polymer pairs available for polymer dissolution and subsequent intercalation. In this study, it was planned to produce nanocomposite fibers by compounding nanoparticles into polymer via solution intercalation technique. Therefore, spherical silica nanoparticles in two different particle sizes were incorporated into polyamide 6 and extruded into filaments through a melt-extrusion process. First, PA6/SiO_2 nanocomposites were prepared by dispersing silica nanoparticle in formic acid and mixing with polyamide 6, then after vigorous stirring the solvent was removed by heating the mixture. Nanoparticles are dispersed in formic acid under vigorous stirring condition as well as using ultrasonic device. And then nanocomposite fibers were prepared with diluting prepared nanocomposites and polyamide 6 in three different weight percent. Filaments with circular cross sections were spun using HAAKE MiniLab pilot melt spinning equipment. The thermal and structural properties of composite fibers were analyzed using differential scanning calorimetry (DSC) and thermal gravimetric analysis

(TGA). The quality of particle dispersion was also studied by scanning electron microscopy (SEM).

7.2. Experimental

7.2.1. Raw material

Same as raw materials mentioned in part 6.2.1 in addition Formic acid 90% which was acquired from Merck.

7.2.2. Sample preparation

Part one: PA6/SiO_2 nanocomposite production

After dissolving polyamide 6 granules in formic acid, silica nanoparticle in 3 different concentrations (10, 20, 30 wt. %) were added to solvent under temperature and stirring for 4 hours, then for another 4 hours and at 80℃ an ultr asonic device is used for better dispersing and deagglomeration of the solid in the solvent. Then the solvent is removed by heating and after several washing with water the obtained nanocomposites were dried in vacuum oven.

Part two: PA6/SiO_2 nanocomposite fibers production

In order to prepare nanocomposite fiber, the prepared nanocomposites were diluted with polyamide 6 in order to reach a concentration of 0.05, 0.2, 0.5 weight percent and were dried at 90℃ for 24 hours in a vacuum oven. Fiber melt spin ning was carried out using a spinning apparatus (HAAKE Minilab twin screw extruder). Filaments extruded through a single-hole spinneret with a diameter of 0.3 mm and at 270℃ we re collected on a reeling device at low speed. Basic characteristics of polymers applied, and the spinning conditions are summarized in Table 7.1.

Table 7.1 Specification of material and fiber melt spinning in chapter 7

Material	Pure Polyamide 6	
	PA6/Aerosil OX50	0.05, 0.2, 0.5 wt. %
	PA6/Aerosil 150	0.05, 0.2, 0.5 wt. %
Spinning Temperature (℃)	270	
Screw speed (rpm)	90	
Spinneret diameter (mm)	0.3	
Winding Speed (m/min)	50	

7.3. Characterization

The crystallization behavior of the PA6/particle hybrid nanocomposites was determined with Perkin Elmer 7 differential scanning calorimetry (DSC) over the temperature range of 30 to 250 °C at a heating rate of 10°C/min under nitrogen atmosphere and hold at that temperature for 2 minutes. Then the samples were cooled down very rapidly to 10 °C. the specimens were heated again to assess the effect of previous cooling scan. Heating scans were analyzed for the crystallization temperature, melting temperature T_m and heat of melt ΔH_f. Finally the samples were cooled down slowly at 10 °C /min to 30℃ to complete crystallization. Crystal linity degree (X_c) of different samples was calculated by the ratio of heat of fusion of the sample to heat of fusion of the purely crystalline polyamide 6, i.e. 240 J/g. The 8 step program for DSC characterization is summarized in Table 7.2. In order to obtain the information on thermal stability, thermogravimetric analysis of PA6/silica nanocomposites was performed using a Perkin Elmer TGA7 under nitrogen atmosphere over the range of 30℃ to 600 ℃ at a heating rate of 5 ℃/min. The morphology of polyamide 6 nanocomposite was investigated by scanning electron microscope analysis using Zeiss DSM 962 microscope.

Table 7.2 DSC Heating and cooling scan

1-	Hold for 2 min. at 30.0 °C
2-	Heat from 30 °C to 250 at 10 °C/min
3-	Hold for 2 min. at 250 °C
4-	Cool from 250 °C to 10 °C at 500 °C/min
5-	Hold for 2 min. at 10 °C
6-	Heat from 10 °C to 250 °C at 10°C/min.
7-	Hold for 2 min. at 250 °C
8-	Cool from 250 °C to 30 °C at 10°C/min.

7.4. Results and discussion

7.4.1. Differential Scanning Calorimetry of PA6/SiO_2 nanocomposite fibers

Crystallization kinetics and the morphology of crystallized products are strongly influenced by cooling rate, system pressure and the presence of particles. Melting and crystallization of crystalline polymers generally occurs over a range of temperature, because of the presence of a distribution of molecular weights and the mixed crystalline/amorphous phase in the sample. Polymer crystals occur in a variety of crystallite sizes and phases (e.g. α, β, γ, etc.). These phases may exhibit different melting/crystallization temperature. The preparation method of polymer composites involves complex deformation behaviors which may affect the nucleation and crystallization behavior of polymer composites. It is known that polyamide 6 is semicrystalline and generally exhibits two kinds of crystal forms (α and γ) depending on the preparation method and particle percentage. The α- phase consists of fully extended planar zigzag chains, in which adjacent anti-parallel chains are joined by the hydrogen bonds. Therefore, it is the thermodynamically most stable crystalline form, and can be obtained by slowly cooling from the melt. The γ phase is composed of pleated sheets of parallel chains joined by the hydrogen bond. It is less stable and can be obtained by fiber spinning at a high speed or by fast cooling from the melt; in addition, the γ–crystalline form is enhanced by the addition of particle. The γ form can be converted into α form by melting followed by recrystallization. Also annealing treatment not only promotes the transformation from amorphous

to crystal phase, improves the γ form crystalline structure and increases the crystal degree, but also resultes in γ→α crystal-phase transformation.

Figure 7.1 shows the melting peak of PA6/SiO_2 nanocomposites as a function of silica content which were prepared by solution intercalation technique. From literature it is well known that formation of γ-form in polyamide 6 depends on the rate of cooling and the presence of particles. Thus a higher cooling rate and presence higher concentration of particles result a higher amount of γ-form [8]. Observed melting peaks are 217.03, 214.03 and 210.7℃ for PSX10, PSX20, PSX30, respectively. Thus, it is obvious that by addition of nanoparticle as well as preparation method the crystal phase shifted to γ-phase as indicated in melting point range. But Figure 7.2 shows that during fiber formation process and melt spinning, the melting peaks are shifted to higher temperature range due to the thermal treatment. The melting peaks of nanocomposite fiber PSX05, PSX2 and PSX5 are 220.5, 221.0 and 221.1 respectively, which prove the formation of α- crystals during extrusion process.

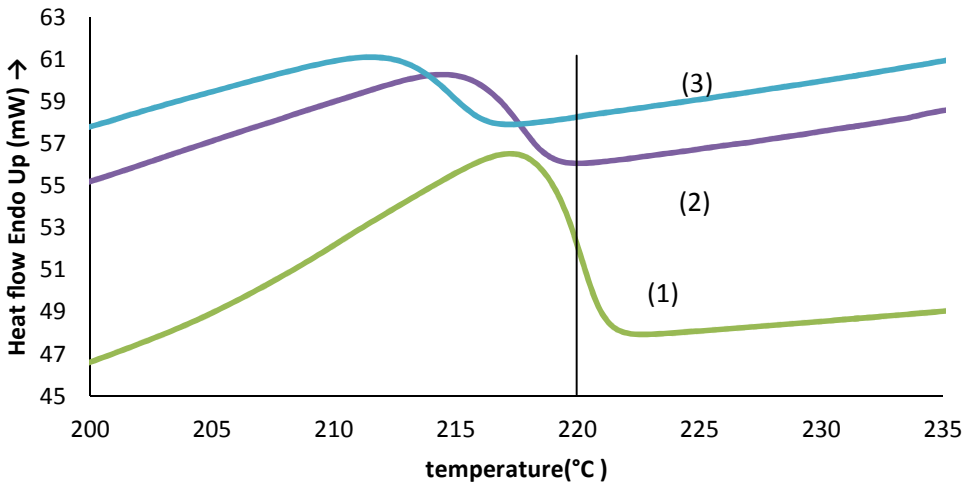

Figure 7.1 DSC heating curve of PA6/SiO_2 nanocomposite as a function of SiO_2, (1): PSX10, (2) PSX20,(3) PSX30 with 10, 20, 30 wt. % respectively.

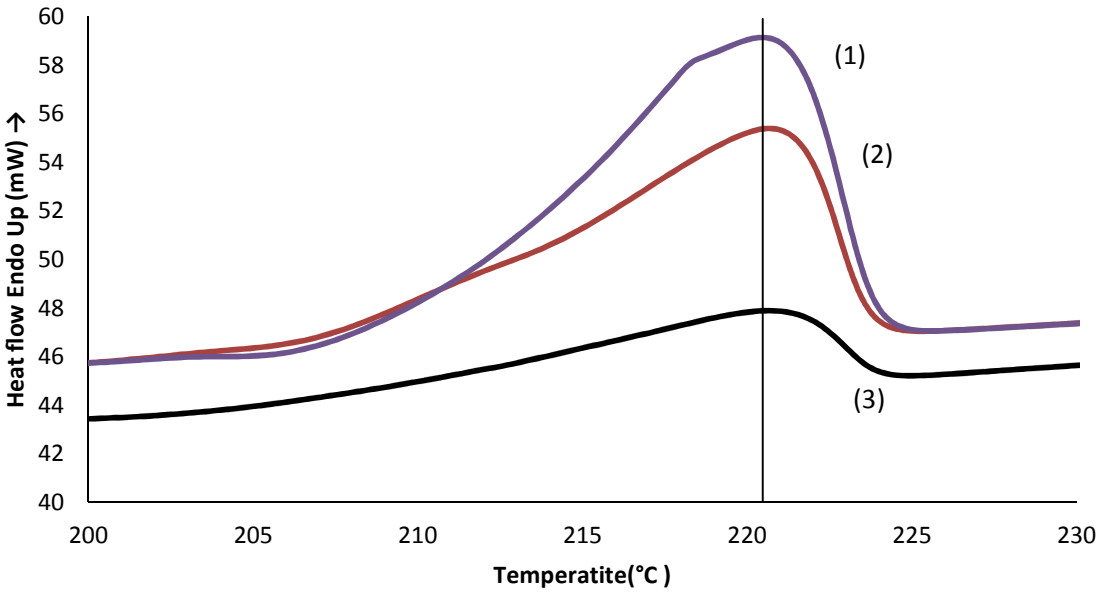

Figure 7.2 DSC heating curve of PA6/SiO_2 nanocomposite fiber as a function of SiO_2, (1): PSX05, (2) PSX2,(3) PSX5 with 0.05, 0.2, 0.5 wt. % respectively.

The preparation method of polymer composites involves complex deformation behaviors which may affect the nucleation and crystallization behavior of polymer composites. The DSC results of PA6, PA6/Aerosil OX50, and PA6/Aerosil 150 nanocomposites in different silica concentrations prepared by solution intercalation method are summarized in Table 7.3.

Table 7.3 DSC data of PA6/SiO_2 nanocomposite prepared as function of silica content

		heating scan			cooling scan	
	SiO_2	T_g	T_m	ΔH	T_c	X_c
	wt. %	℃	℃	J/g	℃	%
PA6	0	26.9	227.3	70.1	171.3	29.2
PSX05	0.05	32.6	220.5	46.3	186.2	20.3
PSX2	0.2	33.0	221.0	47.9	185.4	24.9
PSX5	0.5	33.9	221.1	53.8	184.6	44.8
PSA05	0.05	33.0	219.9	51.1	185.3	22.4
PSA2	0.2	33.1	219.7	49.7	184.6	25.9
PSA5	0.5	32.9	220.2	46.1	184.1	38.4

As seen from Table 7.3 by addition of silica nanoparticle (Aerosil OX 50), melting peak of nanocomposite fibers shifted to lower temperature in compare to pure PA6 due to formation of γ-phase, but it seems in addition that higher concentration has not a significant effect, and melt temperatures of PSX2, PSX5 are almost same. Figure 7.3 shows similar trend for the other nanoparticle (Aerosil 150).

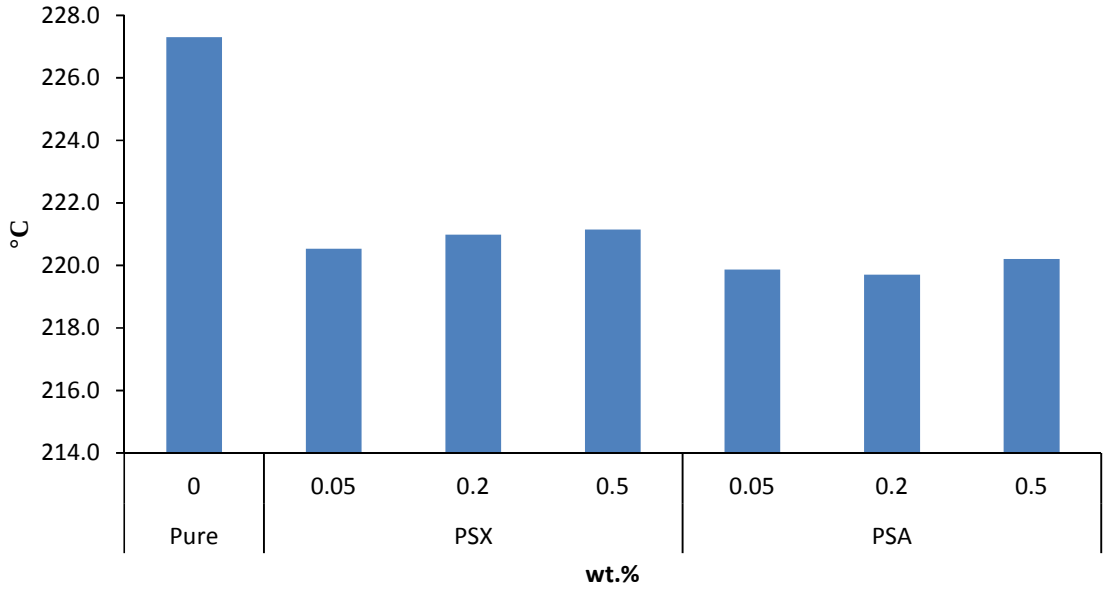

Figure 7.3 Melting temperatures of PSX and PSA fibers as a function of silica content and size

Figure 7.3 shows the effect of silica size on melt temperature of PSX and PSA nanocomposite fibers prepared by solution intercalation technique. As can be seen from Table 7.3 and Figure 7.3 melt temperature of PSX05 (220.5℃) is slightly higher than PSA05 (219.9℃). By figures given in Table 7.3 this trend is also proved for other concentrations, but in general the effect of particle size on melt temperature for PSX and PSA nanocomposites fiber (same concentration and different particle size) is almost negligible.

The crystallization peak temperature of the PSX nanocomposite fibers as a function of SiO_2 content is shown in Figure 7.4. The result clearly indicates that addition of silica nanoparticles to PA6 shifts crystallization peak to higher temperature range. The increase in crystallization temperature of the PA6/SiO_2 nanocomposites with increasing silica content, together with the fact that PA6/SiO_2 nanocomposites have a lower degree of supercooling ($\Delta T = Tm - Tc$) for

crystallization with increasing silica content in compare to pure PA6, suggests that the silica nanoparticles can effectively act as nucleating agents in the PA6/SiO_2 nanocomposites. Therefore, it can be stated that the incorporation of silica nanoparticles by solution intercalation effectively enhances the crystallization of the PA6 matrix by heterogeneous nucleation. The temperatures of crystallization of PSA samples are also higher than of pure PA6 (Table 7.3). Figure 7.4 and Table 7.3 show that a higher silica concentration actually retards the rate of crystallization and crystallization temperature decreased which might be caused by reduced chain mobility due to the presence of the nanoparticles. Generally, there are two effects of the silica on the crystallization of PA6: on the one hand, the silica nanoparticles - serving as nucleation sites – allow crystallization of PA at a higher temperature; on the other hand these particles impede the motion of the PA6 molecular chain [286]. Many other papers [287-292] also reported that different kinds of nanoparticles are able to shift the crystallization temperature. That means nanoparticles can effectively act as a nucleation agent in the hybrid nanocomposites. But similar to melt peaks, incorporation of higher concentration has no major visible effect.

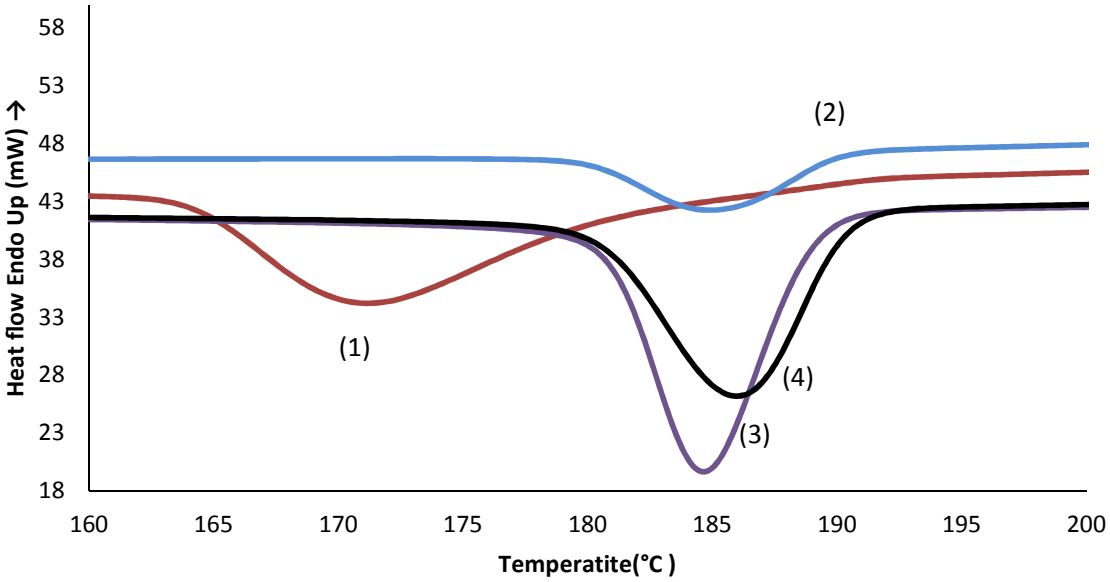

Figure 7.4 DSC crystallization curve of pure PA6 and PA6/SiO_2 nanocomposites as a function of Silica content, (1): Pure PA6, (2),(3),(4): PSX with 0.05, 0.2, 0.5 wt. % respectively.

Figure 7.5 shows that regarding crystallization temperature of PSX05 and PSA05 nanocomposites prepared by solution intercalation process the bigger particle size is responsible for shifting the crystallization peak to higher temperature range. And, as well, according to Table 7.3 crystallization temperature of the PSX2 nanocomposite is slightly higher than for the PSA2 nanocomposite prepared from the smaller sized silica.

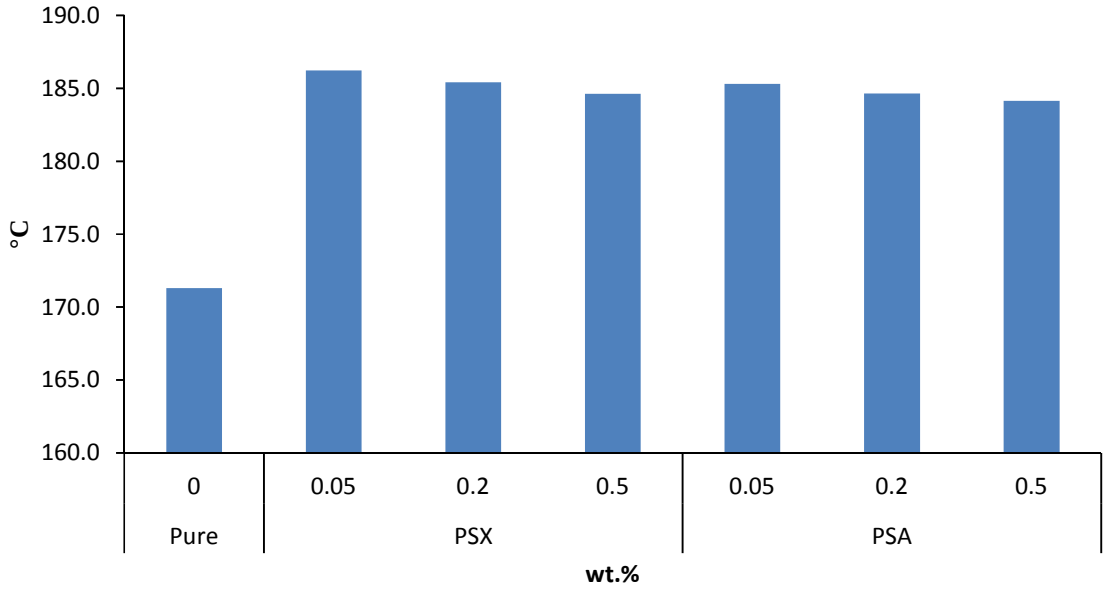

Figure 7.5 Crystallization temperature of PSX and PSA fibers as a function of silica content and silica size

7.4.2. Thermal Gravimetric Analysis of PA6/SiO_2 nanocomposite fibers

As thermal stability of the polymer composites is the most important parameter for their processing and applications, it is very instructive to characterize the thermal degradation behavior. That is, from these data the limiting uppermost temperature for usage and dimensional stability (especially in melt process) can be derived, which are essential for their application in end-uses and the conditions they have to stand there, or for developing polymer composites with better balance in processing and performance [266]. Thermal gravimetric analysis (TGA) involves continuous weighing of a small sample in a controlled atmosphere (e.g., air or nitrogen) as the temperature is increased at a programmed linear rate [8].The analysis of thermal behavior of Polyamide 6 and nanocomposites were performed using the Perkin Elmer TGA7 from 30℃ to

600℃ at a heating rate of 5℃ min^{-1} under nitrogen atmosphere. TGA results of PA6/SiO_2 nanocomposites fibers are summarized in Table 7.4

Table 7.4 TGA characteristic data of Polyamide 6/SiO_2 nanocomposite fiber

	SiO_2	T_{25}[1]	T_{50}[1]	T_{75}[1]	T_s[2]	T_d[3]
	Wt. %	℃	℃	℃	℃	℃
PA6	0	362.3	379.1	388.7	330.1	380.0
PSX05	0.05	368.1	382.6	393.5	347.25	387.25
PSX2	0.2	368.8	384.1	396.2	342.16	390.00
PSX5	0.5	374.1	386.2	400.1	349.50	393.90
PSA05	0.05	364.6	381.1	390.4	337.8	384.6
PSA2	0.2	364.5	383.2	396.1	334.1	388.3
PSA5	0.5	369.2	387.4	398.8	340.9	392.2

[1] Decomposition temperature at 25, 50, 75% weight loss, respectively

[2] Onset degradation temperature

[3] Degradation temperature

Table 7.4 shows the TGA data of the PSX and PSA nanocomposites fibers prepared by solution compounding as a function of SiO_2. By incorporating nanoparticles into PA6 both onset of degradation temperature and temperature at the maximum rate of degradation is increased in comparison with pure PA6, which means the thermal stability of PA6/SiO_2 nanocomposites is improved by addition of silica nanoparticles. This is confirmed by the fact that silica nanoparticles themselves exhibit good thermal stability. On the other hand polymer chain mobility is restricted due to polymer-particle interactions [293, 294]. Also according to data in Table 7.4 and figure 7.6 and 7.7 it can be seen that by increasing silica content in both types of nanoparticles the thermal stability at 25, 50, 75 percentage of weight loss is increased. According to literature [294-297] it is understood that during TGA the crystal structure would disappear at the melting point (~222 ℃) and is replaced by an unordered molecular arran gement in the melt. Beyond the melting temperature, the first sign of weight loss is seen at around 330 ℃ in the TGA curve, signaling

the beginning breakdown of the polymer-backbone. At 380 ℃, the material looses about 50% of its weight and the major weight loss occurs at about 385-395℃ which indicates the bond break of the amide group. It is clear that, in the breakdown process of the polymer, when the crystals have melted, the covalent bonds such as C—O, N–H, may still interact with the nanoparticles which obviously have an influence. i.e. retards, on the final decomposition of the material. Thus, the decomposition of the nanocomposites is prolonged by about 10 ℃ and the reason for this higher thermal stability of the nanocomposites is hence traced to the interaction of nanoparticles and the polymer in the molten state.

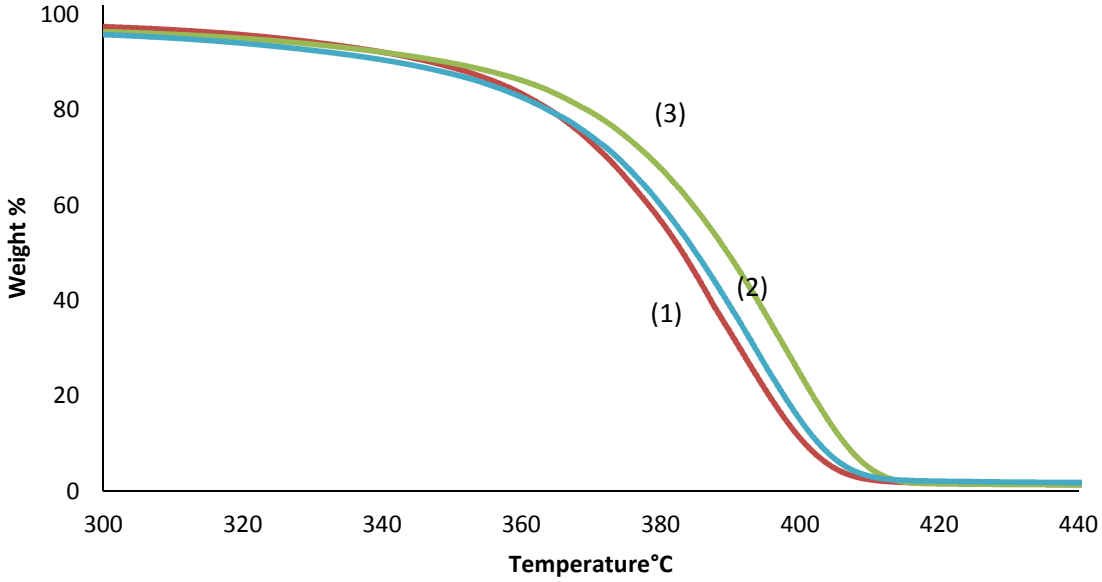

Figure 7.6 TGA thermogram of PA6/SiO_2 nanocomposites fiber as a function of Silica content (Aerosil OX50), (1):PSX05, (2): PSX2, (3): PSX5, 0.05, 0.2, 0.5 wt. % respectively.

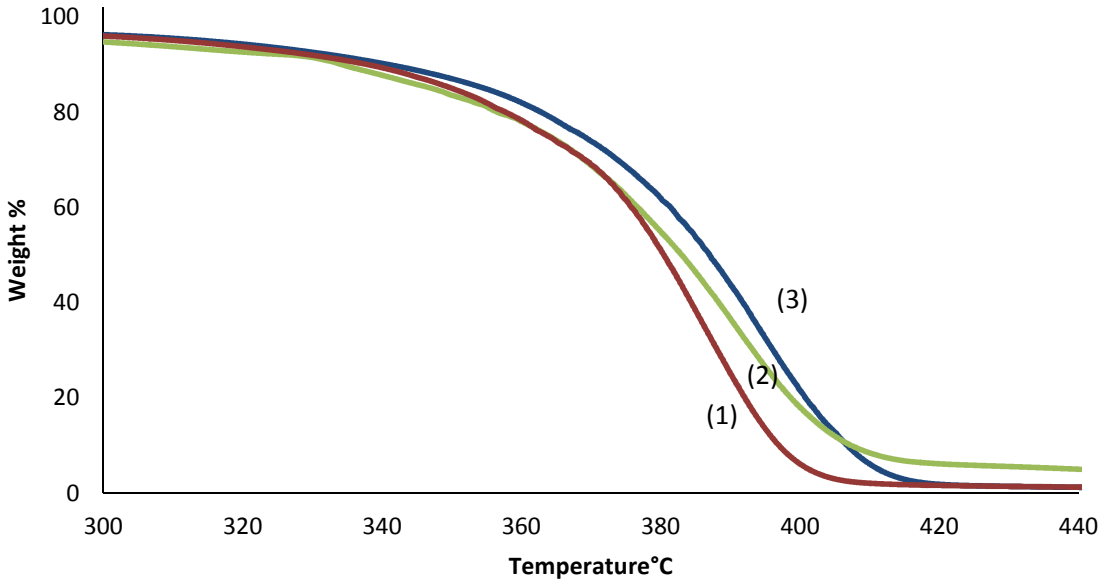

Figure 7.7 TGA thermogram of PA6/SiO_2 nanocomposites as a function of Silica content (Aerosil 150), (1): PSA05, (2):PSA2, (3):PSA5, 0.05, 0.2, 0.5 wt. % respectively.

In addition from Table 7.4 and Figure 7.8 the effect of nanoparticle size on thermal stability is also clearly to be seen. Figure 7.8 shows the TGA thermogram of PSX5 and PSA5 from which it can be observed that the thermal stability of PSX5 nanocomposite fiber (bigger particle size) is higher than of PSA5 nanocomposite fiber, this hold for the entire range of scanned temperature, which can be cause of more even distribution of Aerosil OX (bigger particle size) in composite and high risk of agglomeration for finer particle size. From Table 7.4 the same trend can be derived for the over investigated nanocomposite fibers of different particle size but same weight percentage.

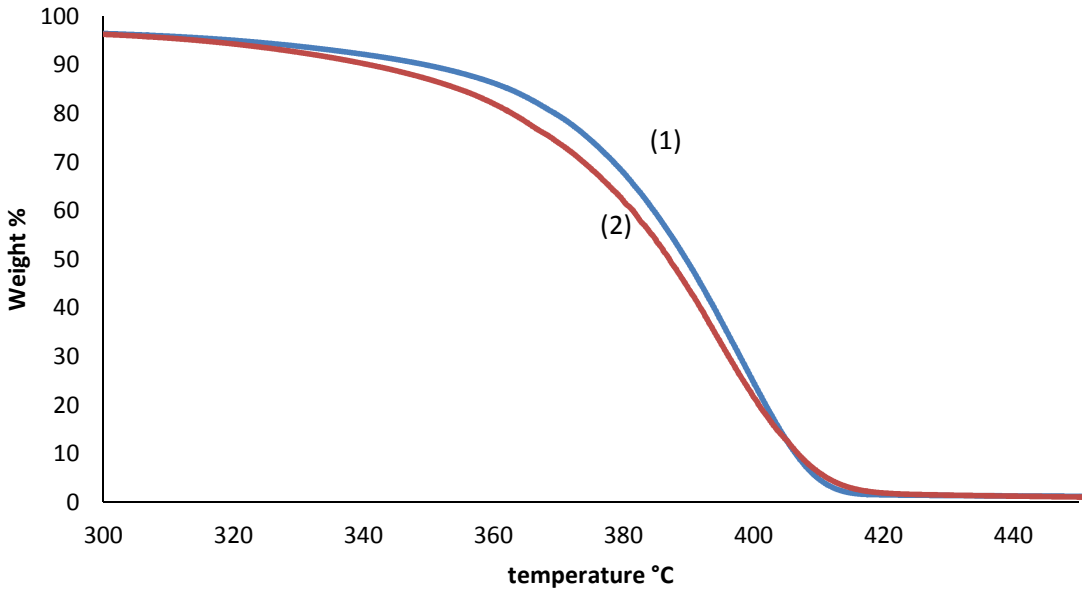

Figure 7.8 TGA thermogram of different silica size (1) PSX5 versus (2) PSA5

7.4.3. Morphology of PA6/SiO_2 nanocomposite and nanocomposite fibers

To investigate the dispersion quality of silica particles, the morphology of PA 6/silica composites as well as nanocomposite fibers were studied and the results are shown in Figure 7.9, 7.10 and 7.11. The SEM images of the nanocomposites prepared, show that the fillers are reasonably well dispersed in the polymeric matrix. Nevertheless, some aggregates at the surface of the polymer were also identified. Figure 7.9 shows a very good quality and uniform distribution of silica Aerosil OX 50 in polymeric matrix for the three silica content levels of 10, 20, and 30 weight percent. In contrast to that, as can be seen from Figure 7.10, distribution of silica Aerosil 150 in polymer is not as good and by increasing the silica content the agglomeration of particle is increased. Which shows vice versa that by decreasing the particle size the risk of agglomeration will be increased.

In addition, Figure 7.11 shows the SEM picture of pure PA6 fiber and PA6/SiO_2 nanocomposite fibers in 0.05, 0.2 and 0.5 weight percent. Particle distribution is almost uniform and by increasing the weight percent partly agglomeration is observed.

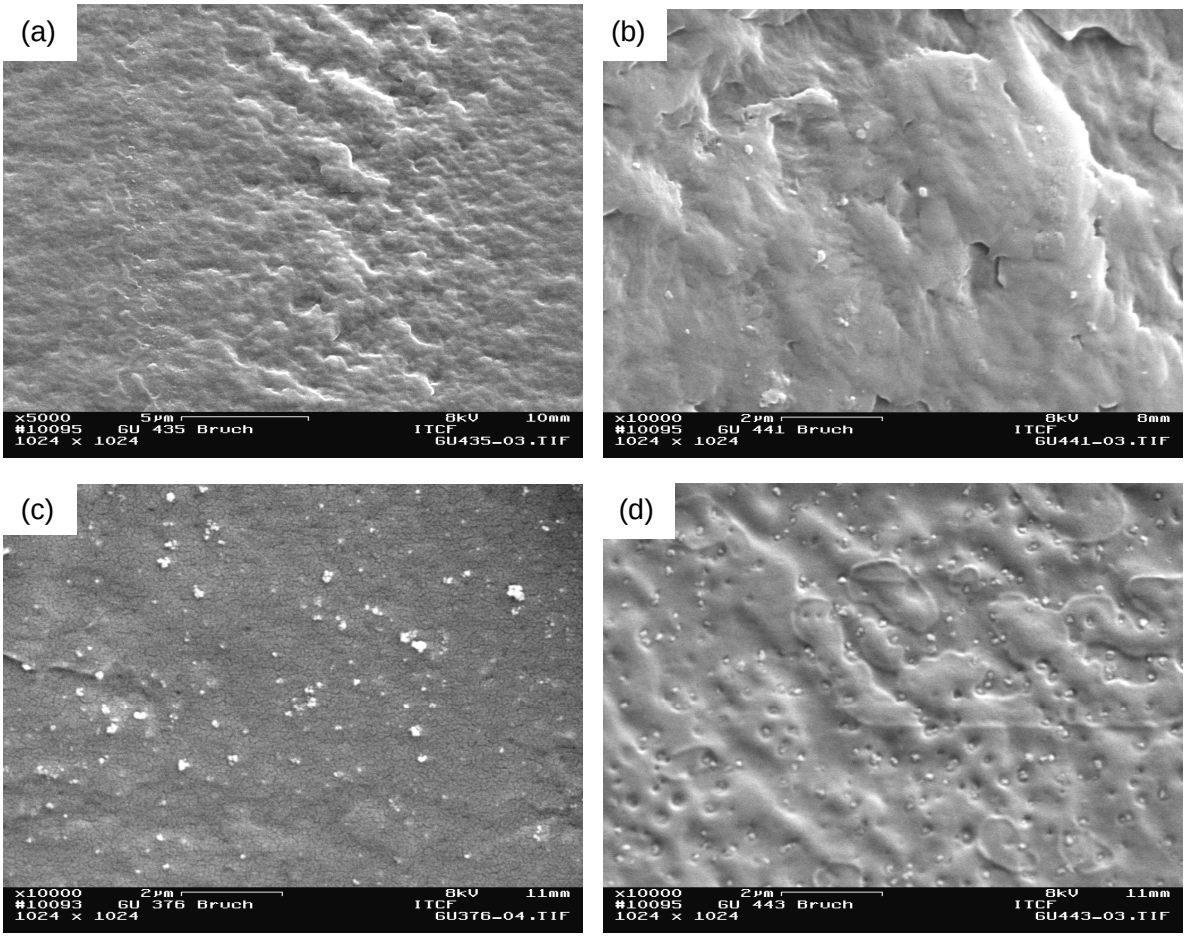

Figure 7.9 SEM picture of pure PA6 and PA6/SiO_2 nanocomposites (a): pure PA6, (b): PSX10, (c): PSX20, (d): PSX30 with 10, 20, 30 wt. %, respectively. (Silica Aerosil OX50)

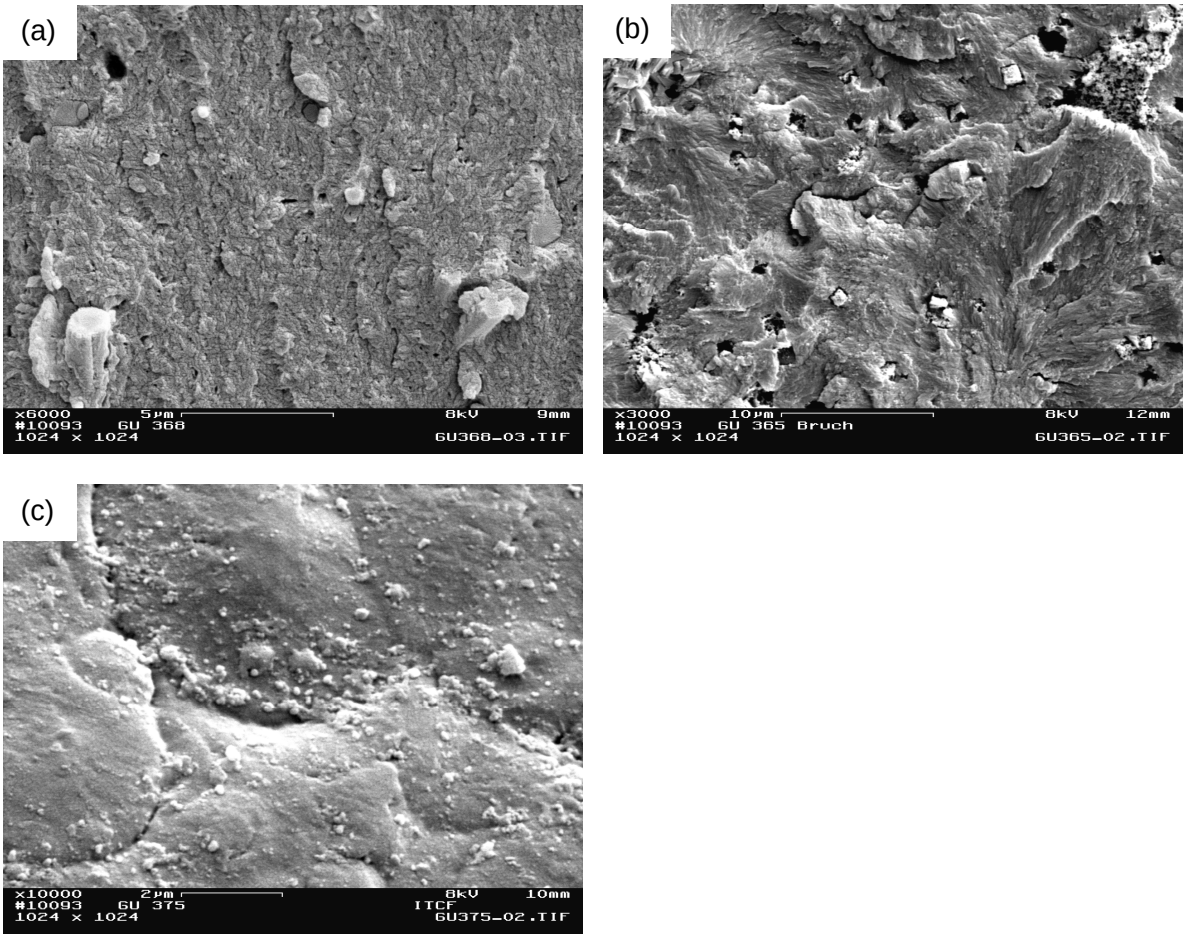

Figure 7.10 SEM picture PA6/SiO_2 nanocomposites (a): PSA10, (b): PSA20, (c): PSA30 with 10, 20, 30 wt. %, respectively. (Silica Aerosil 150)

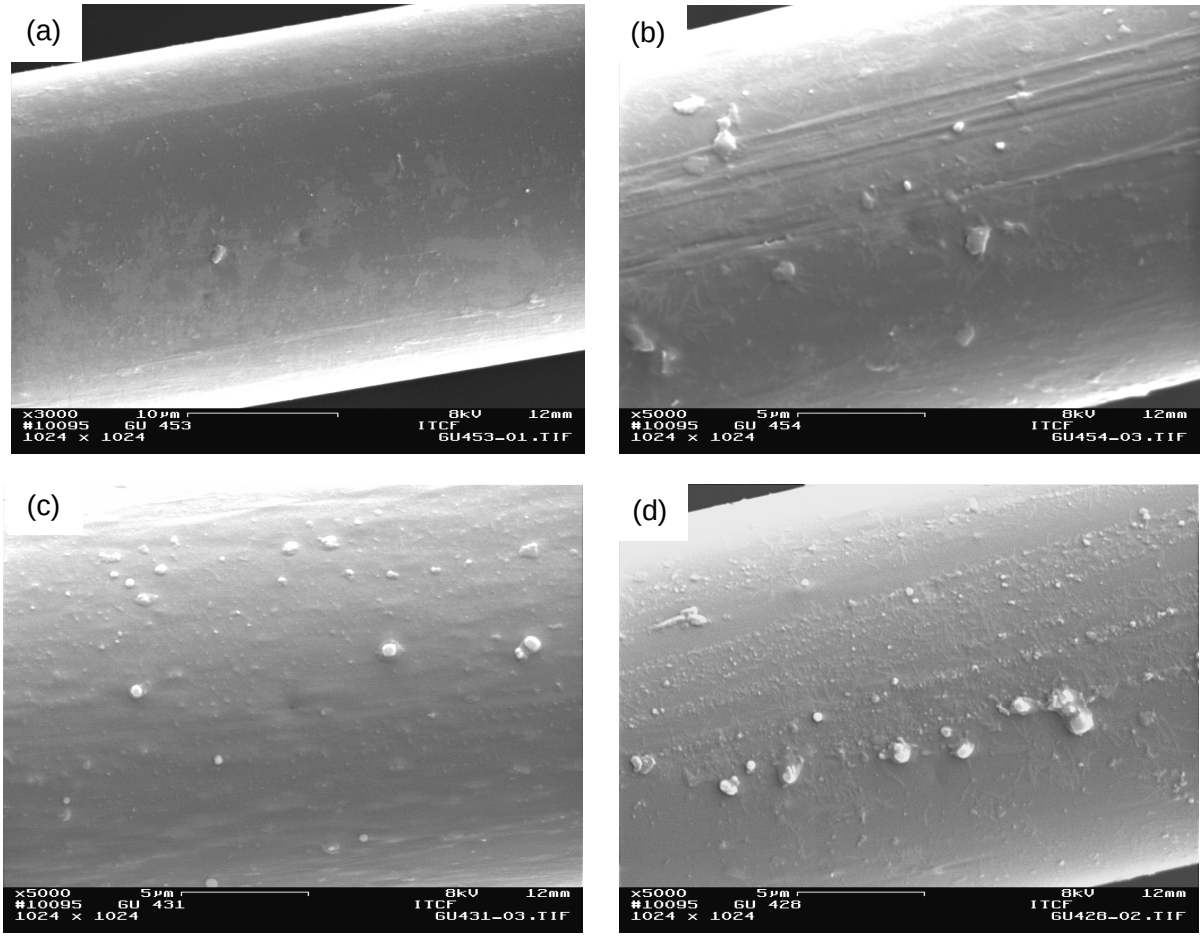

Figure 7.11 SEM picture of pure PA6 and PA6/SiO_2 nanocomposite fibers (a): pure PA6 fiber, (b): PSX05, (c): PSX2, (d): PSX5 with 0.05, 0.2, 0.5 wt. %, respectively. (Silica Aerosil OX50)

Chapter 8

Synthesis and characterization of PA6/ SiO_2 nanocomposites by In-situ polymerization method

8.1. Introduction

Nanocomposites present exciting opportunities for manipulating structure and properties, they are mostly influenced by the composition, method of preparation (in-situ polymerization [298, 299], solution intercalation [300] or melt compounding [301-303]), polymer matrix characteristics, size, shape, microstructure and state of agglomeration of the dispersed phase and degree of matrix–filler adhesion [304-305]. Due to the strong tendency of nanoparticles to agglomerate, manufacturing composites with uniformly distributed nanoparticles becomes a challenging task [306]. To break down these nanoparticles aggregates and manufacture nano-structural composites, in-situ polymerization with the presence of nanoparticles seems to be rather facile. In this method, first, nanoparticles are dispersed in monomer, and then the mixture is polymerized using a technology similar to bulk polymerization. It is obvious that the most important factor that affects the properties of composites is the dispersion of nanoparticles.

According to Tadros [307], the dispersion of ultrafine particles in medium can be divided into three steps:

1. Wetting of particles by dispersion medium;

2. Breaking of aggregates into dispersed primary particles or smaller aggregates;

3. Stabilization of dispersed primary particles or smaller aggregates against re-agglomeration.

Referring to these three mentioned points; preparation of nanocomposites by silica/caprolactam in-situ polymerization reaction was aimed according to the following procedure: nano-silica was dispersed in a medium (water or ethanol) with the assistance of ultrasonic, then added to melted caprolactam and polymerization was initiated to form the resulting nanocomposites. Such plan was designed according to the following information gained from literature: (i) it was reported that particles with polar surface can be easily wetted by polar liquid [308]. Accordingly, nano-silica with polar silanol groups on the surface can be easily wetted by polar melted caprolactam containing amide group, (ii) The preparation of the polyamide 6/silica nanocomposites using in-

situ polymerization was also recently reported by Rusu [294]. It is found that nano-silica was simply dispersed in the melted caprolactam by ordinary stirrer. Hence, although some of the nano-silica was homogeneously dispersed, there were still some bigger aggregates (ca. 200 nm in diameter) within the polyamide 6 matrix. Considering that the tremendous energy offered by ultrasonic is likely to break the nanoparticles aggregates into smaller ones or even mono molecular dispersed particles [309], in the present work, ultrasonic was employed to disperse nanosilica in melted caprolactam. Thus, the agglomerated nanoparticles would be separated and coated with caprolactam, leading to the improved stability of smaller aggregates or mono-molecular dispersed nanoparticles against re-agglomeration [210].

The present chapter consist two parts, the first part aims to obtain PA6/Silica nanocomposites in granule form via ring-opening polymerization of ε-caprolactam in the presence of untreated silica and surface modified silica, whereas in the second part, PA6/Silica nanocomposite fibers were produced from the thus prepared granules by extrusion process.

Before adding to polymerization reactor, silica nanoparticles were dispersed in water or ethanol. To promote dispersion of nano-silica in caprolactam, nano-silica was dispersed with the assistance of ultrasonic. According to Cai [310], it was found that hydrogen bonds were formed between nano-silica and caprolactam and ultrasonic helped to break the nanoparticles aggregates into smaller ones leading to the uniform distribution of nanoparticles in the polymer matrix.

The influence of the particle content, particle size, dispersion medium and surface modification are examined on structure, physical and mechanical properties of nanocomposites (granules form) and nanocomposite fibers.

8.2. Experimental

8.2.1. Raw materials

ε-caprolactam, aminocaproic acid and terephthalic acid (TPA) from MERCK were used to prepare polyamide 6. The different types of nanosilica(SiO_2 , Aerosil OX50, Aerosil 150) in spherical shape which were used as filler being characterized by mean particle size of 40 nm , 14 nm and a specific surface area of 50 $m^2 g^{-1}$ and 150 $m^2 g^{-1}$, respectively, were supplied by EVONIK Company and used as received. While BYK 3650 a silica nanoparticle surface modified with linear non-polar polysiloxane with a mean particle size of 20 nm and 25% nanoparticle content in methoxypropylacetate/methoxypropanol solvent was supplied by BYK Company.

8.2.2. Sample preparation

8.2.2.1. Part one: Preparation of PA6/ SiO_2 nanocomposites (granule)

The pure polyamide 6 was synthesized by ring opening polymerization of ε-caprolactam using 6-aminocaproic acid as initiator in a 5L-reactor according to the following steps:

1- caprolactam melting
2- adding reactant
3- heating and pressurizing under Nitrogen
4- pressure release
5- pelletizing
6- extraction

At the first step 1000 gr. caprolactam was added to a 5L reactor and stirred under nitrogen atmosphere at 90℃ until all the caprolactam had me lted. Then 30 gr. water as ring opening agent, 10 gr. aminocaproic acids as an initiator and 4 gr. TPA as a chain regulator was added. Reactor temperature was increased to 130℃, 170℃, 210℃ stepwise in intervals of 30 minutes and finally to 245℃. The mixture was maintained un der stirring and nitrogen atmosphere for about 90 minute. After reaction completion, pressure was released and the melt polymer transferred through die plate which was preheated at 285 ℃ to a water bath and finally cut in pelletizing machine to granules. The granules were extracted in boiling water before used in extrusion process. Polyamide 6/ silica nanocomposite obtained according to the above procedure by adding nanoparticle dispersion in second steps along with reactant. PA6/SiO_2 nanocomposites were prepared from two different particle sizes (Aerosil OX50, Aerosil 150) and each one in 3 different silica percentage, 0.05, 0.15 and 0.5 weight per cent. Silica

nanoparticle-water dispersion as well as silica-ethanol dispersion were prepared by ultrasonic method and then added to reactor.

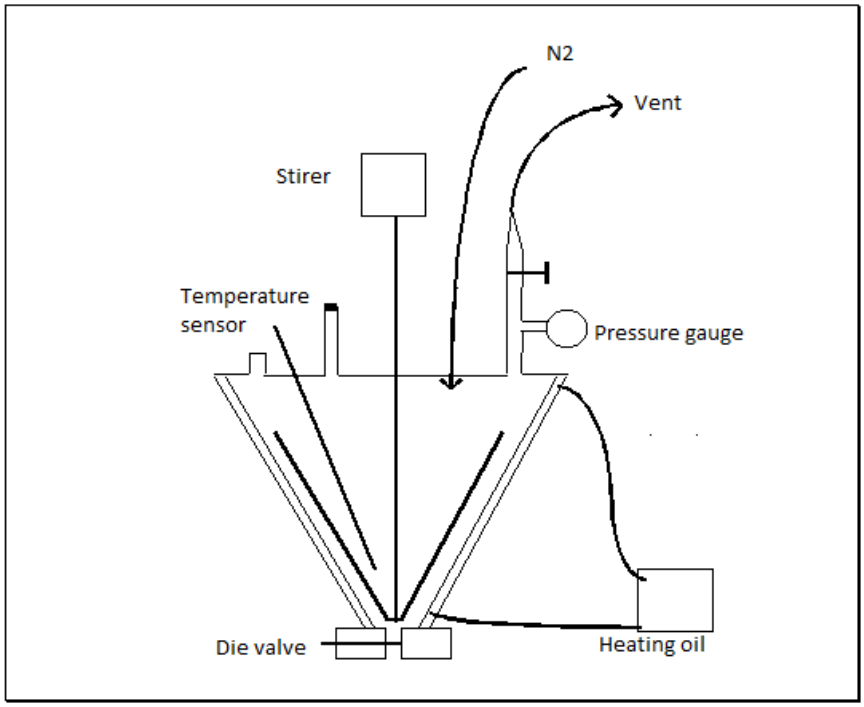

8.2.2.2. Part two: Preparation of PA6/ SiO_2 nanocomposites fibers

Nanocomposite fibers were prepared from nanocomposite granules with melt spinning process. Melt spinning was carried out using a spinning apparatus HAAKE consisting of an extruder and a gear pump to control precisely the throughput rate, which was kept at 40 g/min for all polymers. Filaments extruded from the spinneret through a multi-hole nozzle with a diameter of 0.3 mm and at 270℃ were taken up by the high-speed winder.

8.3. Characterization

The crystal structures of the polyamide 6 and polyamide 6/nanocomposites was followed by X-ray diffraction analysis (XRD), using a PW 1050 Philips diffractometer (Ni—filtered Cu-K_α radiation of wavelength 0.1542 nm) in the reflection mode over the range of diffraction angles (2θ) from 5 to 35°, at room temperature. The voltage a nd tube current were 40 kV and 30 mA, respectively. The Fourier transfer infrared (FTIR) spectra were scanned using Bruker IFS 28

spectrometer. Molecular weight of samples were determined by gel chromatography permeation (GPC) method using high temperature chromatograph PL-GPC 220.The crystallization behavior of the PA6/particle hybrid nanocomposites was determined with Perkin Elmer 7 differential scanning calorimetry (DSC) over the temperature range of 30 to 250 °C at a heating rate of 10°C/min under nitrogen atmosphere and hold at that temperature for 2 minutes. Then the samples were cooled down very rapidly to 10 °C. The specimens were heated again to assess the effect of previous cooling scan. Heating scans were analyzed for the crystallization temperature, melting temperature T_m and heat of melt ΔH_f. Finally were cooled down slowly at 10 °C /min to 30℃ to complete crystallization. Crystal linity degree (X_c) of different samples was calculated by the ratio of heat of fusion of the sample to heat of fusion of the purely crystalline polyamide 6, i.e. 240 J/g. In order to obtain the information on thermal stability, thermogravimetric analysis of PA6/silica nanocomposites was performed using a Perkin Elmer TGA7 under nitrogen atmosphere over the range of 30℃ to 600 ℃ at a heating rate of 5 ℃/min. The morphology of polyamide 6 nanocomposite was investigated by Scanning Electron microscope analysis using Zeiss DSM 962 microscope. Tensile properties of fibers were measured at standard climate conditions using STATIMAT M automatic tensile testing machine equipped with a 10N cell according to ASTM D-3822-07. The gauge length was 200 mm and the crosshead speed was 200 mm/min. An average of 25 reading for each fiber sample is reported.

8.4. Results and discussion

8.4.1. Part one: nanocomposite (granule form)

8.4.1.1. Molecular weight and Amino end Group of Polyamide 6/SiO_2 nanocomposites

Molecular weight and its distribution are important factors with respects to properties and processing of polymers. And for examples many influence on mechanical properties such as stiffness, strength, viscoelasticity, toughness, and viscosity. If molecular weight is too low, the transition temperatures and the mechanical properties will generally be too low for the polymer material to have any useful commercial applications. For a polymer to be useful it must have transition temperatures above room temperatures and it must have mechanical properties sufficient to bear design loads.

Table 8.1 Amino end groups and molecular weight of Polyamide 6 and PA6/SiO_2 nanocomposites

Sample	SiO_2 wt. %	$[NH_2]$ mmol/kg	Number average molecular weight M_n
PA6	0	27.8	34501
PSX05-W	0.05	34	29479
PSX5-W	0.5	38.8	28093
PSA05-W	0.05	33.1	34282
PSA5-W	0.5	38.4	32940
PSX05-E	0.05	29.8	24633
PSX1.5-E	0.15	32.2	22830
PSX5-E	0.5	38.9	21027
PSA05-E	0.05	38.3	25445
PSA1.5-E	0.15	41	26584
PSA5-E	0.5	45.7	26809
PA/Mod. Silica	0.5	29	20646

Control and determination of molecular weight are common problems in polymer science and are important for processing behavior. For linear polyamides, the average molecular weight can be determined by end-group analysis as well as by size-exclusion/gel permeation chromatography (SEC/GPC) [142]. In the polymerization of ε-caprolactam, the reactive groups should correspond to a 1: 1 mole ratio; any increase of the content of NH_2 groups can be related to a decrease in polymer molecular weight. Comparative examination of the data presented in Table 8.1 revealed that the number average molecular weight of polyamide 6 nanocomposites prepared in the presence of the silica nanoparticle decreased as the amount of filler increased.

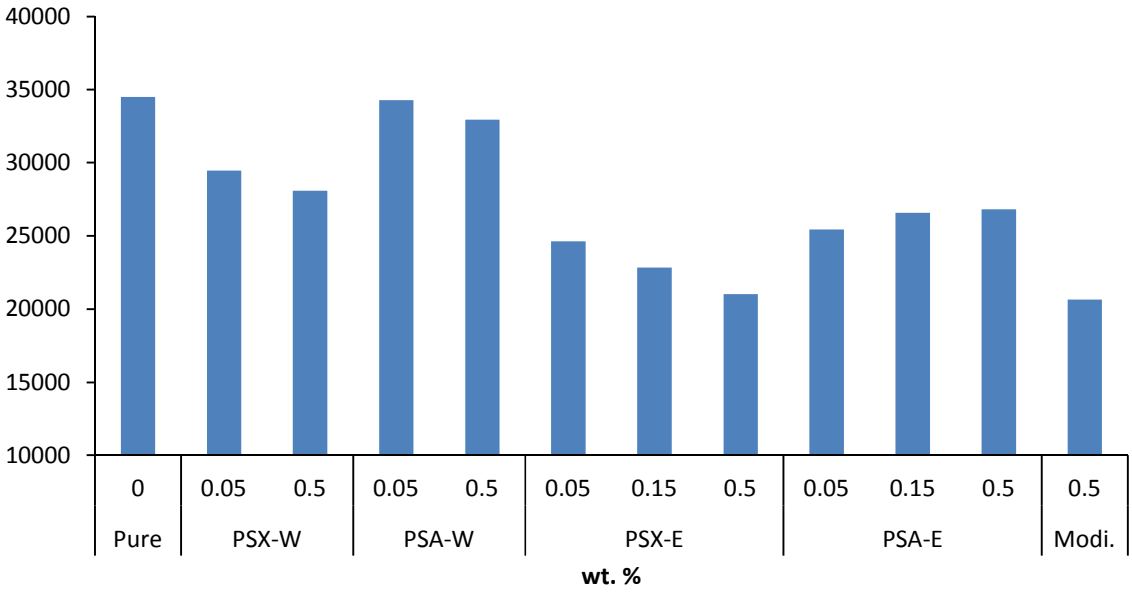

Figure 8.1 Number average molecular weight of polyamide 6 and nanocomposite as a function of silica content

Also, as seen from Table 8.1 and Figure 8.2, the addition of nanometer silicas (pretreated or not) resulted in an increase in amino content in compare to pure polyamide 6, indicating a decrease in the molecular weight of polyamide 6 formed. It is reasonable that the reaction between silica and polyamide 6 would alter the proportion of the two end groups (COOH and NH_2) [311]. The results from Figure 8.1 show the effect of particle size and dispersion medium on molecular weight. On the one hand nanocomposites prepared from silica particles dispersed in ethanol exhibit better dispersion in compare to same particles dispersed in water and in addition show less agglomeration, hence the probability of bond formation between silica particle and NH_2 groups must be higher and thus will cause decrease in molecular weight. On the other hand, the finer particle size, the higher probability of agglomeration which reduce the chance of less bond formation between silica and NH_2 and finally results in higher molecular weight. Moreover in Figure 8.3 this assumption is confirmed by the result found with the surface modified silica. There the chance of bond formation between Si-OH and NH_2 is higher than for untreated silica. Hence the 1:1 stoichiometric ratio between NH_2 and COOH is changed and a molecular weight reduction is caused.

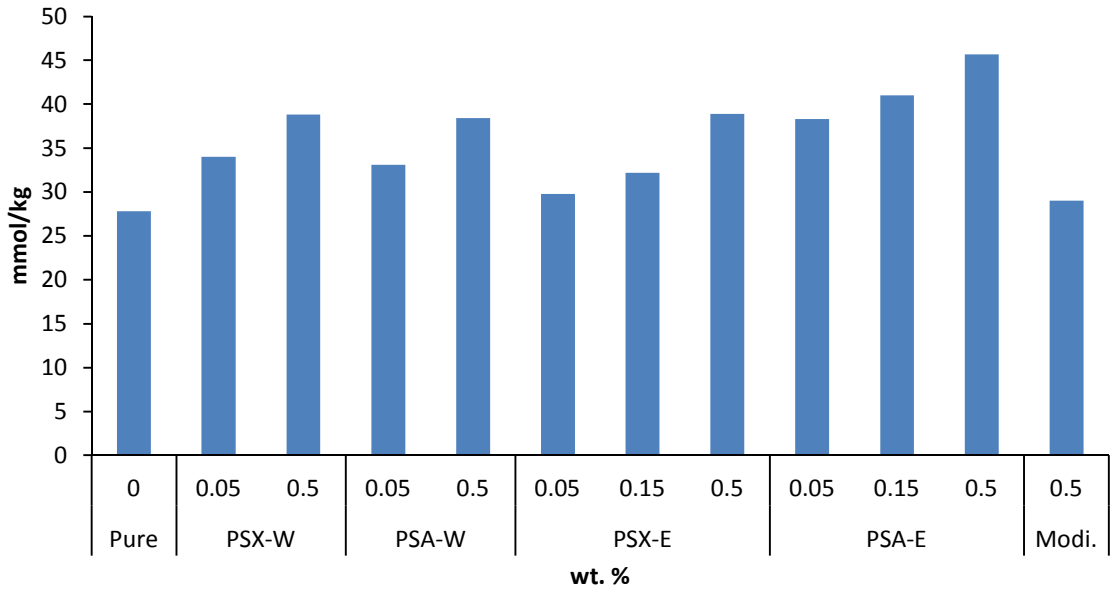

Figure 8.2 Amino end group of polyamide 6 and nanocomposite as a function of silica content

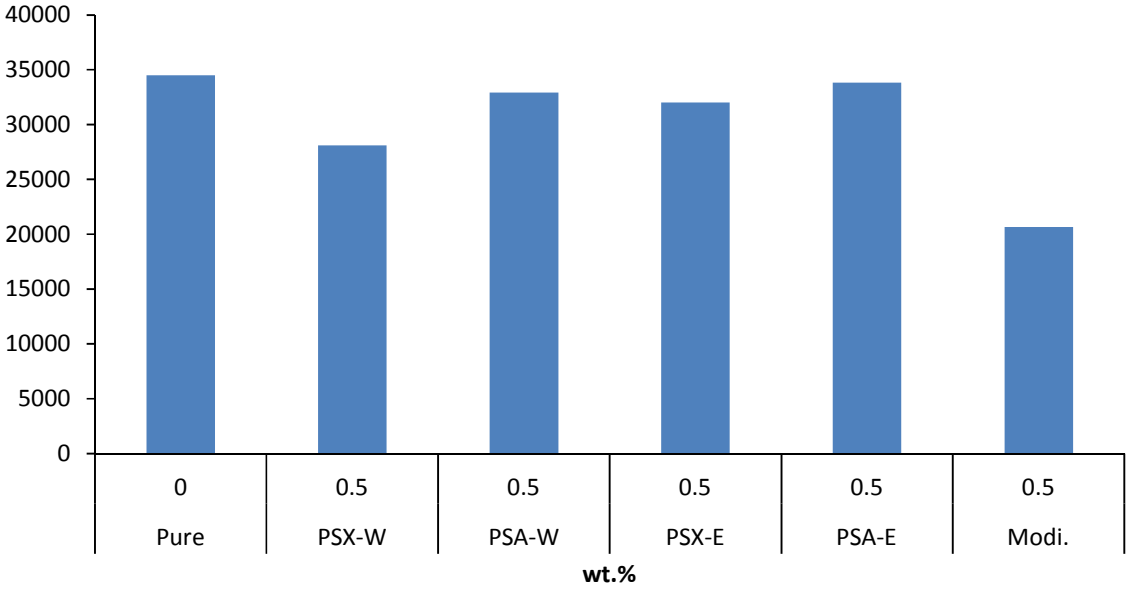

Figure 8.3 Number average molecular weight (M_n) of untreated and modified silica nanocomposite. (all samples 0.5 wt. %)

8.4.1.2. Relative viscosity of nanocomposite

One of the most important factors in polymer processing is viscosity which is a good indication for molecular weight; viscosity of a polymer solution depends on concentration and molecular weight of the dissolved polymer. By determination of solution viscosity it is possible to get an indirect measure of molecular weight.

Table 8.2 Relative viscosity of Polyamide 6 and PA6/SiO_2 nanocomposites

Sample	SiO_2 wt. %	Relative viscosity
PA6	0	2.9538
PSX05-W	0.05	2.742
PSX5-W	0.5	2.6076
PSA05-W	0.05	2.9595
PSA5-W	0.5	2.8977
PSX05-E	0.05	2.651
PSX1.5-E	0.15	2.489
PSX5-E	0.5	2.4054
PSA05-E	0.05	2.7296
PSA1.5-E	0.15	2.69
PSA5-E	0.5	2.5491
PA/Mod.Silica	0.5	1.703

The results of relative viscosity measurement in formic acid are presented in Table 8.2. As seen in Figure 8.4 the presence of silica in the nanocomposites resulted in the decrease of the relative viscosity of nanocomposites in compare to pure polyamide 6 which confirm the reduction of molecular weight by incorporation of silica nanoparticle.

One of the reasons of viscosity reduction could be changing in proportion of the two end groups of polyamide by incorporation of silica particle. Other possibility is a reduced molecular weight of nanocomposite due to degradation (e.g. hydrolysis) in the presence of SiO_2. [256, 319]

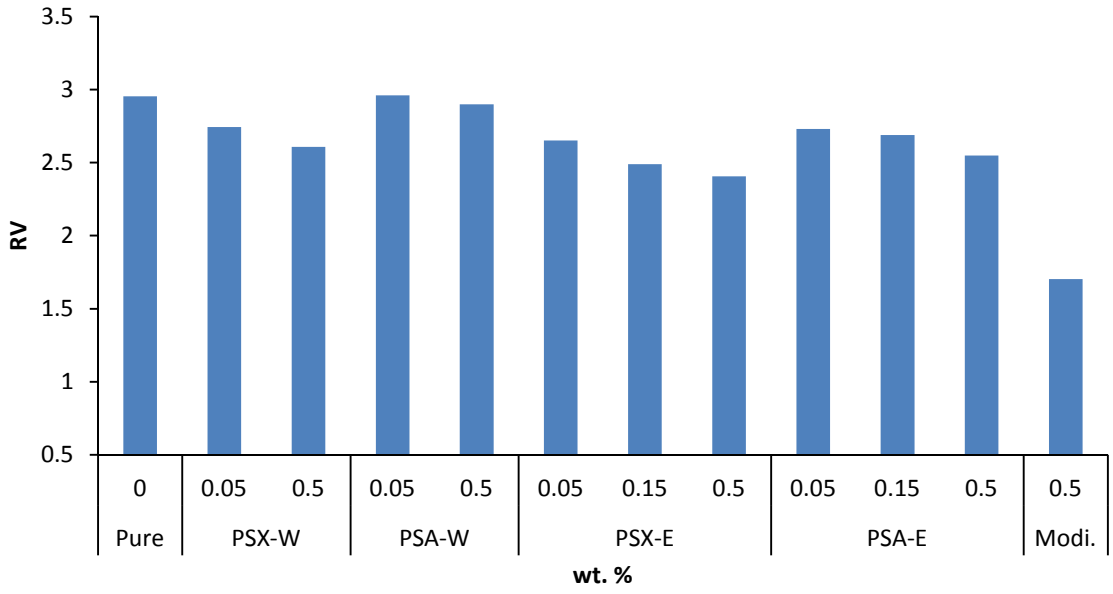

Figure 8.4 Relative viscosity of polyamide 6 and nanocomposites as a function of silica

Structure and thermal behavior of polyamide6/SiO_2 nanocomposites

8.4.1.3. Differential Scanning Calorimetry of polyamide6/SiO_2 nanocomposites

The melting temperatures Tm_1, Tm_2, degree of crystallinity, non-isothermal crystallization temperature Tc, and the heats of fusion ΔHm_1 and ΔHm_2 of polyamide 6 and polyamide 6/nanocomposites were evaluated by differential scanning calorimetry (DSC). Parameters such as heat of fusion (ΔHm) and heat of crystallization (ΔHc) were used to determine the melting and crystallization behavior of the polyamide 6 and prepared nanocomposites. The results related to the melting and crystallization behavior of nanocomposites, observed during the first and second heating and during cooling, together with data for polyamide 6 are presented in Table 8.3.

Table 8.3 DSC data of PA6/SiO_2 nanocomposite prepared as function of silica content (in-situ polymerization)

		1st heating		2nd heating		cooling		
	SiO_2	Tm_1	ΔH_1	Tm_2	ΔH_2	Tc	ΔH	Xc
	Wt. %	℃	J/g	℃	J/g	℃	J/g	%
PA6	0	227.37	86.403	224.53	76.76	171.63	79.74	31.98
PSX05W	0.05	226.370	67.277	223.53	60.20	182.30	63.75	25.21
PSX5W	0.5	224.700	63.690	221.53	60.52	182.13	62.53	25.34
PSA05W	0.05	224.700	70.429	221.87	58.66	182.63	65.61	24.57
PSA5W	0.5	223.530	71.273	220.87	61.05	181.97	70.65	27.24
PSX05E	0.05	225.200	67.730	222.70	60.92	181.30	64.17	25.51
PSX1.5E	0.15	226.100	63.680	221.53	52.16	187.30	60.23	21.84
PSX5E	0.5	226.030	65.177	220.37	59.11	180.63	59.17	24.75
PSA05E	0.05	223.370	69.867	220.03	61.05	181.13	62.42	25.56
PSA1.5E	0.15	226.530	66.374	218.53	58.64	183.30	60.18	24.55
PSA5E	0.5	226.200	68.003	218.70	59.65	181.80	58.78	24.98
Modif.	0.5	224.700	72.432	217.03	63.87	184.63	68.48	26.75

DSC thermograms of nanocomposites with untreated SiO_2 and modified SiO_2 nanoparticles recorded on the first heating displayed the endothermic melting peak (noted as Tm_1), associated with the α-form crystals of polyamide 6 matrix [313, 315, 316] in the 223–227℃ temperature range. On the second heating scan, the melting peaks (Tm_2) of *α*-form crystals slightly shifted to lower temperature values (see Table 8.3). The melting point of pure PA6 decreased slightly by increasing the silica nanoparticle. Similarly, the melting enthalpy decreased significantly by the presence of nanoparticle. This shift can also be attributed to the fact that the polyamide chains are anchored to the silica surface thus reducing the PA6 chains mobility. The obtained results show changes in the structure of nanocomposites due to the incorporation of SiO_2, different thermal history, and also imperfect re-crystallization of each sample under the DSC measurement conditions. The degree of crystallinity of polyamides was calculated from the ratio of the measured enthalpy of fusion of the sample and the enthalpy of fusion of a completely crystalline polymer by using the following equation:

$$X(\%) = \frac{\Delta Hm}{(1-\varphi)\Delta Hm^{\circ}} \times 100$$

Where ΔHm is the enthalpy of fusion of the sample, ΔHm° is the enthalpy of fusion of 100% crystalline sample of the same polymer which is the average of ΔHm° (α) and ΔHm° (γ) i.e. 240 jg^{-1} [183] and φ is the weight fraction of the filler in the nanocomposite. Increasing the filler concentration in the nanocomposites decreased the degree of crystallinity.

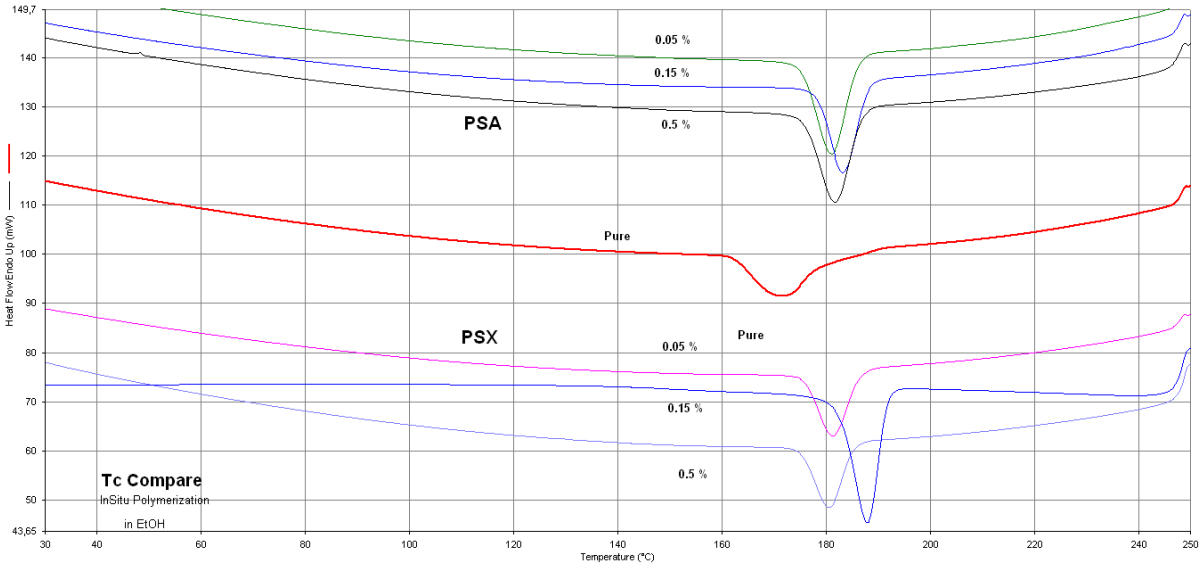

Figure 8.5 DSC cooling scans of samples as function of SiO_2 content: pure PA 6, PSX-E (0.05, 0.15, 0.5 wt. %) and PSA-E (0.05, 0.15, 0.5 wt. %)

Moreover as is shown in Table 8.3 and Figure 8.5 the presence of both SiO_2 and modified SiO_2 affects the crystallization temperature and causes an increase in the crystallization temperature (T_c) of nanocomposites relative to pure polyamide 6 due to the increase of the nucleation. The crystallization temperature increases from 171°C in pure PA6 to about 187℃ in the nanocomposites. This rise in temperature is due to the formation of more perfect crystals generated by the presents of nanoparticles that act as nucleation agents. When the nanoparticles are functionalized, ΔH_m of nanocomposites increases since there is a better interaction with the polymeric matrix and the polymer chains are immobilized.

According to Wunderlich [191], decreasing the polyamide molecular weight results in faster crystallization and higher crystalline temperature which has a very good agreement with the result reported in Table 8.1 and Table 8.3.

XRD was used as an alternative method to investigate the crystal structure of polyamide 6 nanocomposites

8.4.1.4. X-Ray Diffraction (XRD)

The crystallinity of the prepared nanocomposites was followed with X-ray diffraction (XRD) as a function of wt. % filler added. As described in chapter 4 that two crystalline forms α and γ can be observed in PA6 from XRD pattern.

Figure 8.6 illustrates the X-ray diffraction pattern of the pure polyamide 6 and nanocomposites with 0.05, 0.15, 0.5 silica nanoparticle content and Figure 8.7 shows nanocomposites with treated and untreated silica. It can be seen that the pure polyamide 6 displayed peaks at the Bragg's angles (2θ) of about 20.5° and 24° corresponding to the reflections of the crystalline planes (200) and combined (002)/ (202) (labeled α_1 and α_2), respectively, indicative of a monoclinic α-phase morphology, α_1 originates from the distance between hydrogen-bonded chains, whereas α_2 comes from the distance between hydrogen-bonded sheets [294, 312, 313]. This indicates that the α-phase is the dominant crystalline phase for pure polyamide 6. X-ray spectra of the nanocomposites in different silica percentages presented in addition to the two reflections of pure polyamide 6, another reflection which is detected at $2\theta = 22°$, and is related to γ-crystal planes of polyamide 6, The γ-form is characterized by a parallel arrangement of the chains with hydrogen bonds in which the amide groups are twisted out of the zig–zag plane of the methylene groups, leading to a shorter repeat distance than the α-form. Both spectra of α- and γ- phase exhibit the same shape but a decreasing order of the intensity of α_1 and α_2 peaks, and this behavior indicates that the presence of silica nanparticle disturbs the perfect arrangement of hydrogen bonded sheets of the α-phase.

It appeared that even at very low (0.05 wt. %) silica additions, a slight decrease in the degree of polyamide crystallinity was caused, and XRD result shows that, the addition of silica nanoparticle in both treated and untreated form into polymer matrix favored the formation of γ-phase crystal. The γ-phase is an unstable form, and as explained in chapter 4 it can be transformed into the α-form by annealing or by treatment with a phenol aqueous solution.

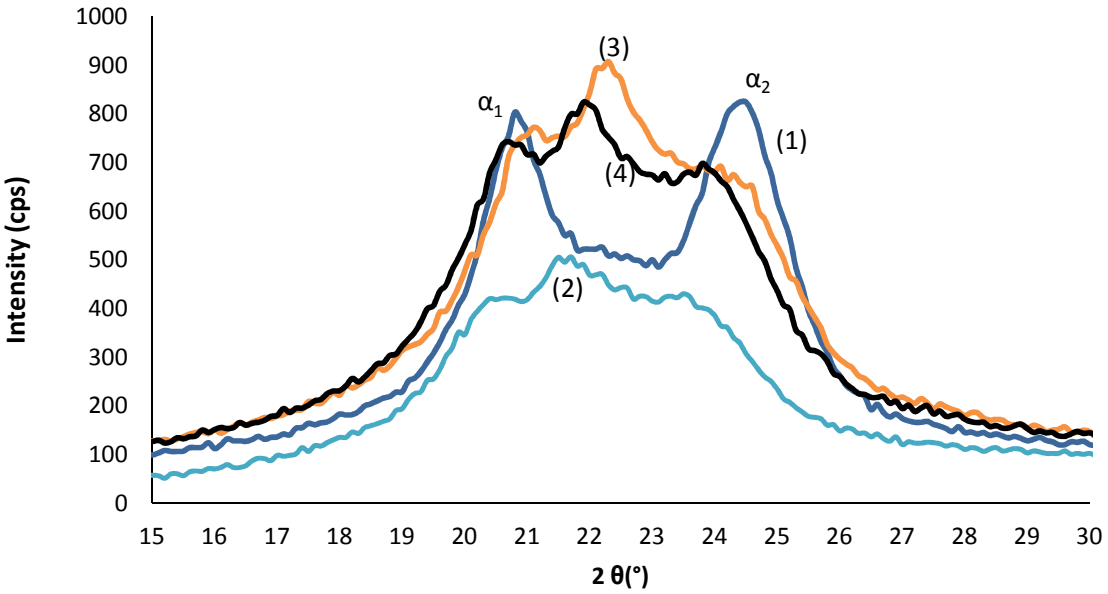

Figure 8.6 X-ray diffraction patterns of pure polyamide 6 and PA6/SiO_2 nanocomposites as function of silica content. (1): pure PA6, (2), (3), (4): PSA with 0.05, 0.15, 0.5 wt. %, respectively

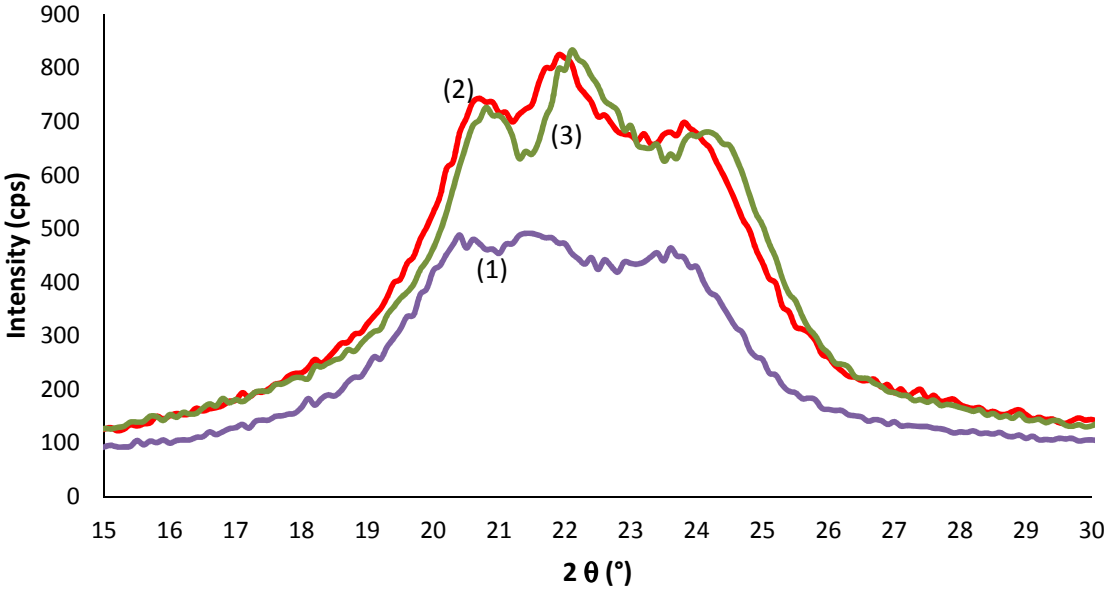

Figure 8.7 X-ray diffraction patterns of treated and untreated silica nanocomposites (1): PSX5, (2): PSA5, (3): Modified Silica

8.4.1.5. Thermal Gravimetric Analysis of polyamide 6/SiO_2 nanocomposites

The thermal stability of polymeric materials is usually studied by thermogravimetric analysis (TGA). The weight loss due to the formation of volatile products after degradation at high temperature is monitored as a function of temperature. The evaluation of the thermal behavior of polyamide 6 and nanocomposites was performed using the data obtained from measurements by thermogravimetry analysis. Table 8.4 provides a summary of the results. According to the data in Table 8.4 which shows the results from TGA experiments, carried out under nitrogen at a temperature range from 30℃ to 600℃. By incorpora tion of silica nanoparticle to polymer matrix a slight increase in the thermal stability of nanocomposites in comparison to pure PA6 was observed. This is justified by the fact that inorganic components of nanocomposites themselves possess good thermal stability and the polymer chain mobility was restricted due to polymer–filler interactions [316].

Table 8.4 TGA data of polyamide 6 and polyamide 6/SiO_2 nanocomposites

	SiO_2 wt. %	T_s[1] ℃	T_d[2] ℃
PA6	0	368.8	401.5
PSX05W	0.05	371.5	413.8
PSX5W	0.5	371.3	417.1
PSA05W	0.05	364.4	408.1
PSA5W	0.5	371.7	416.9
PSX05E	0.05	374.1	405.0
PSX1.5E	0.15	360.7	407.9
PSX5E	0.5	367.4	408.8
PSA05E	0.05	365.9	405.0
PSA1.5E	0.15	368.7	406.3
PSA5E	0.5	369.6	406.4
PA6/Modi. Silica	0.5	347.7	406.3

[1] Onset degradation temperature

[2] Degradation temperature

It is known from the literature data related to the thermal degradation of the polyamides, that chain scission takes place at the –NH–CO– bonds in the neighborhood of the carbonyl group [295, 317, 318]. All the nanocomposites showed no weight loss until around 330℃ (onset decomposition) and retained 90% of their weight at about 350℃.

Figure 8.9 shows that the major stage of weight loss occurs in the range of 400–420℃, and should be associated to the break of amide groups.

Moreover, the temperatures corresponding to 10% weight-loss of the nanocomposites were also increased in comparison to the pure polyamide 6, which had a T_s of 368℃.

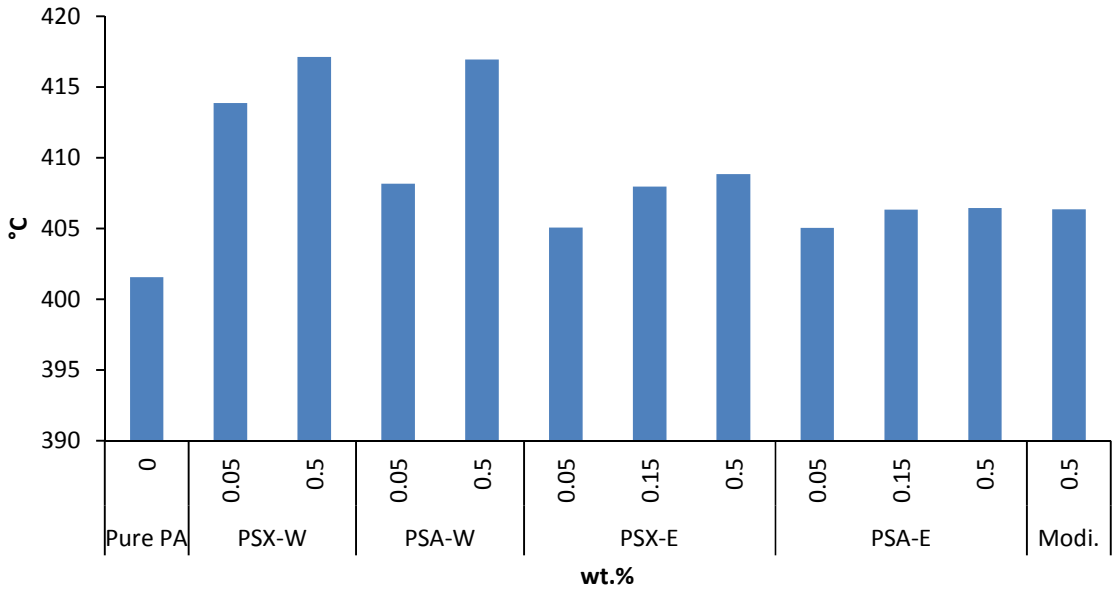

Figure 8.8 Thermal degradation of PA6/SiO_2 as a function of Silica content

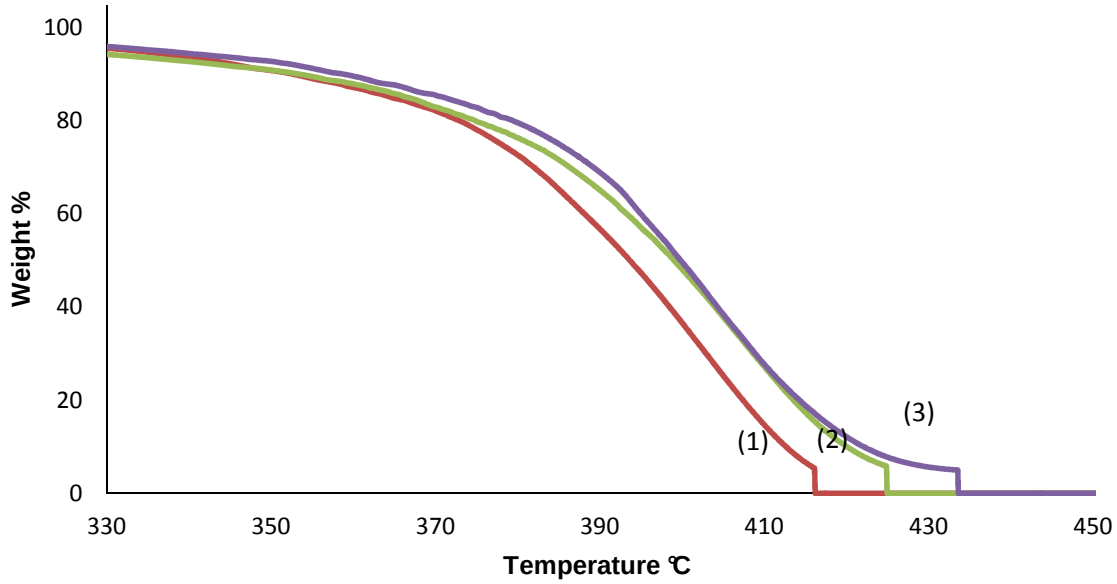

Figure 8.9 TGA graph of PA6/SiO_2 nanocomposites as a function of Silica content. (1), (2), (3): PSX with 0.05, 0.15, 0.5 wt. %, respectively.

8.4.1.6. SEM observation of polyamide 6/SiO_2 nanocomposites

To investigate the dispersion quality of silica particles, the morphology of PA 6/silica composites was studied and the results are shown in Figure 8.10. It is evident that the modified silicas have a more homogenous dispersion in the polyamide matrix compared with the unmodified silica. It can also be seen from Figure 8.10 that the size of both the modified and unmodified silica particle are mostly in the range of 20 – 200 nm except the aggregated silica in unmodified silica.

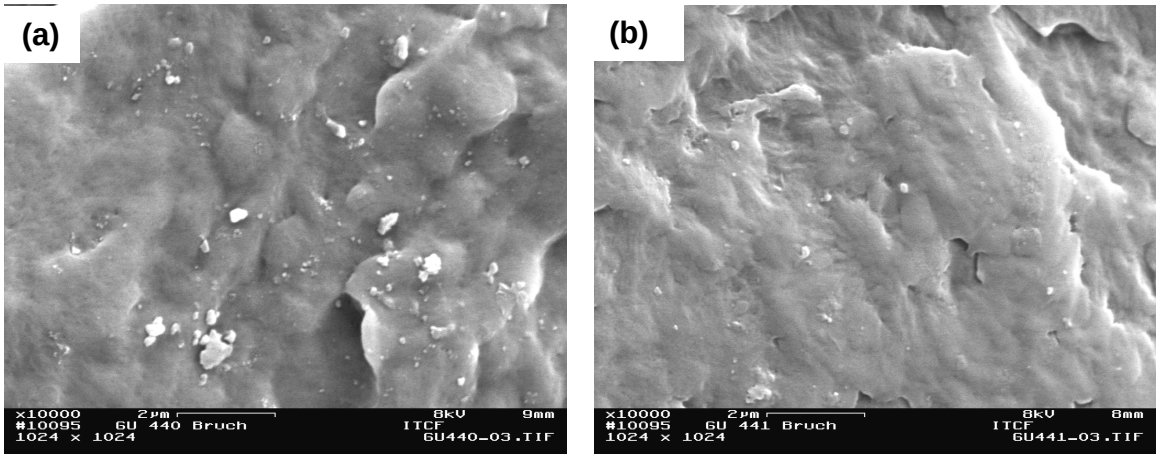

Figure 8.10 SEM image of (a) PA6/ unmodified silica nanocomposite and (b) PA6/ modified silica nanocomposite. (0.5 wt. %)

8.4.2. Results and discussion Part 2: nanocomposite fiber

8.4.2.1. FTIR characterization of nanocomposite fibers

In order to determine the development of various functional bonds during polymerization, FTIR spectroscopy was performed. An FTIR experiment with polyamide 6 and with functionalized silica nanoparticles is shown in Figure 8.11. Three curves are shown in Figure 8.11; (a) pure polyamide, (b) polyamide with 0.5 wt. % untreated SiO_2, and (c) polyamide with 0.5 wt. % functionalized SiO_2. Three basic bonds of polyamide 6, i.e. amide N–H at 3297 cm^{-1}, hydroxyl O–H at 2800–3000 cm^{-1}, and carbonyl C=O at 1637 cm^{-1} were of primary interest. It is seen in Figure 8.11(b) that IR absorbance for each of the three basic bonds has increased significantly, characterized by their sharper and higher peaks. Higher peak and larger area under the curve corresponds to higher absorption of light energy of the chemical bond concerned. In other words, the IR absorbance is a direct measure of the interaction with the molecular environment, indicating that SiO_2 reinforcement into polyamide was responsible for such an increase. On the other hand, after functionalization of SiO_2 particles, i.e. in Figure 8.11(c), it is seen that the wave number of the three basic bond are maintained, while in addition, a siloxane Si–O–Si bond at 1090 cm^{-1} is formed which was not seen with Figures 8.11(a). This is what was expected from functionalization; establishing a continuous covalent linkage across the particle (silica) and polymer (polyamide 6) interface [107].

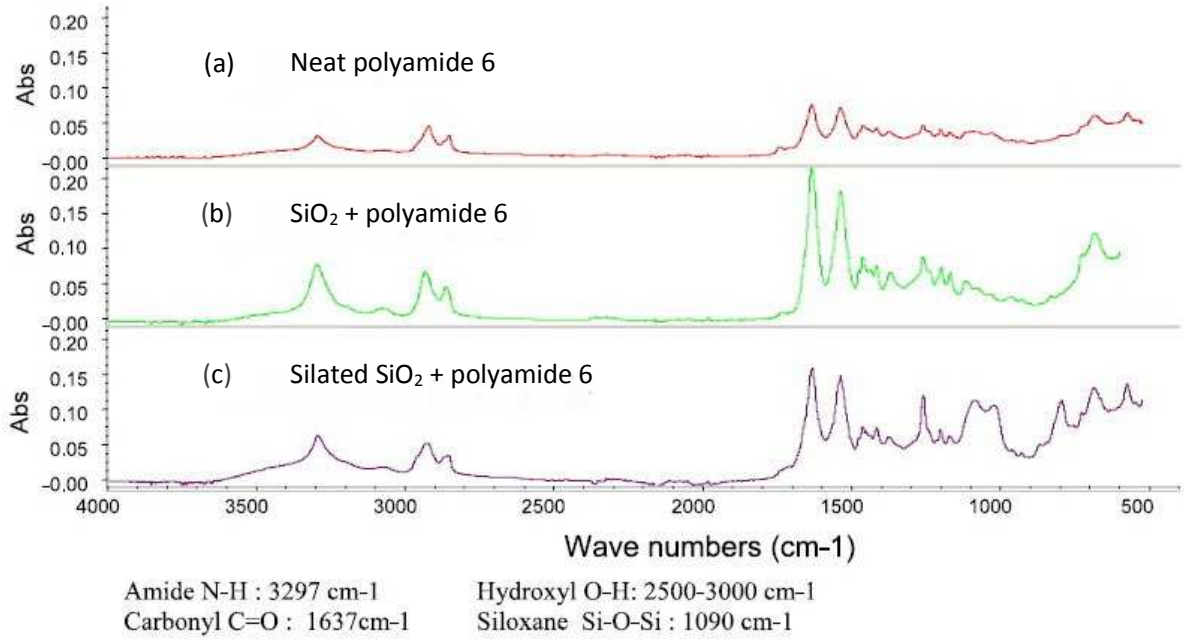

Figure 8.11 FTIR spectra (a) pure PA6 fiber, (b) PA6 fiber with 0.5% silica, (c) PA6 fiber with 0.5 % modified silica.

8.4.2.2. Differential Scanning Calorimetry of polyamide6/SiO_2 nanocomposites fibers

The endothermic melting peaks and corresponded heat of fusion as well as crystalline temperature of virgin PA6 fiber, pure PA6 fiber and nanocomposite fibers as a function of silica content are summarized in Table 8.5. It is observed that melting endotherm of nanocomposite fibers has lower melting temperature in compare to virgin polyamide and somewhat to pure polyamide 6. This suggests that the enthalpy calculated from the area under the melting endotherm would be higher in the case of polyamide 6/SiO_2. A reduction of the melting temperature is an indication of an increase in crystallinity. It is understood that the polymer would be more crystalline if the amount of ordered chains were more. As the temperature reaches the melting point, these chains would tend to get out of their ordered arrangements and begin to move freely. The polymer crystals will begin to fall apart at an earlier stage than their highly-entangled counterparts, meaning that the melting temperature of the crystalline polymer will be lower.

Table 8.5 DSC results of pure PA6 fiber and PA6/SiO_2 fiber nanocomposite as a function of silica content

	SiO_2	Tm	ΔH_m	Tc	Xc
	wt. %	℃	J/g	℃	%
PA6-virgin	0	225.36	47.55	171.3	19.81
Pure PA6	0	222.03	48.87	186.47	20.3
PSX05-W	0.05	222.87	50.44	186.47	22.12
PSX5-W	0.5	222.53	42.61	186.3	35.51
PSA05-W	0.05	223.3	52.46	186.8	23.00
PSA5-W	0.5	224.0	43.73	186.9	36.44
PSX05-E[1]	0.05	220.03	55.26	186.3	24.24
PSX1.5E	0.15	222.3	55.60	186.9	27.25
PSX5-E	0.5	222.7	54.32	187.6	45.26
PSA05-E	0.05	224.8	46.36	188.4	20.33
PSA1.5-E	0.15	221.8	47.33	186.3	23.20
PSA5-E[2]	0.5	223.7	48.94	188.1	40.78
PA6/Modif. silica	0.5	225.0	56.47	190.3	47.06

[1] PSX05-E i.e. PA6/Silica(Aerosil OX50), 0.05 wt. %,

[2] PSA5E i.e. PA6/Silica(Aerosil 150), 0.5 wt. %

Non-Isothermal crystallization of polyamide 6 nanocomposites fibers

An extensive analysis of non-isothermal crystallization behavior was carried out on pure polyamide 6 and its nanocomposites. To rightfully compare pure polyamide 6 materials with its nanocomposites, it was necessary to extrude the pure polyamide under the same processing conditions used to form the nanocomposites. Regardless of the molecular weight, the extruded materials exhibit faster crystallization than the virgin samples (Figure 8.12 labeled as (1)). There are several possible reasons why such behavior is observed. Faster crystallization may arise from increased nucleation due to the presence of impurities incorporated in the matrix during processing. Memory effects associated with thermal and stress histories that remain present in the sample after annealing in the melt may also lead to an increased rate of crystallization.

Numerous studies have shown that the processing history of the polymer, e.g. melting, mixing, cooling, pelletizing, etc. is often not fully erased when the polymer is annealed at high melt temperatures [289,–320-325].

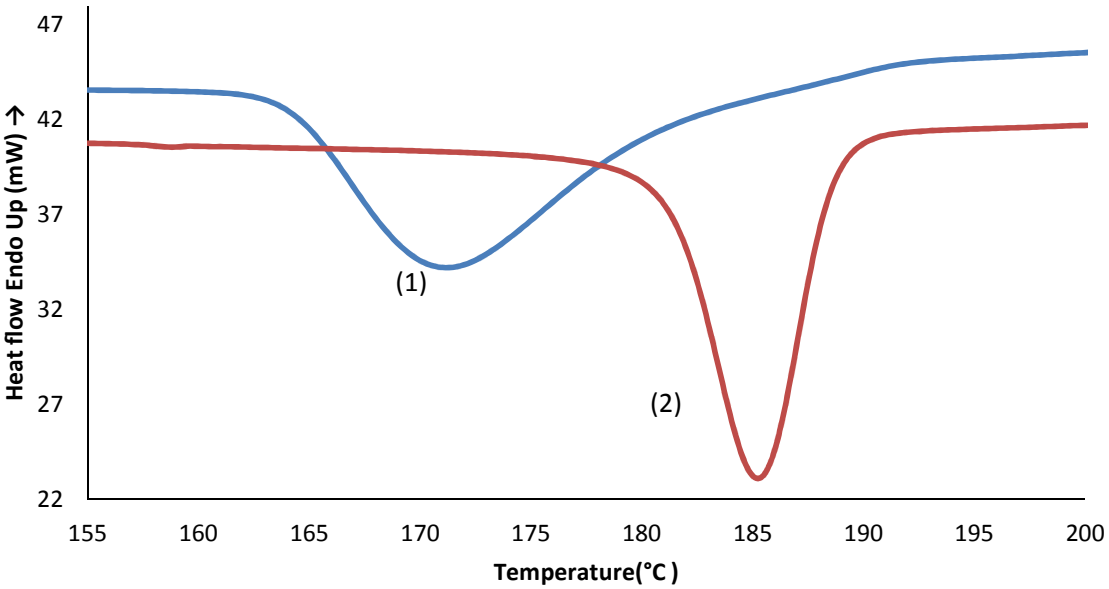

Figure 8.12 Crystalline temperature of virgin PA6 (1) and pure extruded PA6 (2). Faster crystallization may arise from increased nucleation due to the presence of impurities incorporated in the matrix during processing.

Aharoni [173] reports that any shearing imposed on the polymer during melt processing may facilitate the production of aligned arrays of bridged H-bonded sections that act as stable nuclei, capable of remaining intact in the melt state for long periods of time. These arrays ultimately act as crystallization sites upon cooling from the melt. Indeed, Khanna et al. [321] showed that extruded polyamide 6 leads to faster crystallization than virgin polyamide 6 under both isothermal and non-isothermal conditions. The temperature of melting and the length of time held in the molten state will also determine the amount of stable nuclei remaining prior to recrystallization; this issue has been the topic of many investigations [325-330]. The above demonstrates that processing alone significantly affects the crystallization behavior of polyamide 6; therefore, for proper comparison between pure polyamide 6 and the nanocomposites, the 0 wt. % SiO_2 data presented in the remaining plots represent the extruded version of polyamide 6.

The DSC results of PA6 and PA6/SiO_2 nanocomposites fibers with different silica concentrations are given in Table 8.5. Figure 8.13 shows the cooling scan of PA6/SiO_2 nanocomposite(PSX) as a function of silica content. Addition of small amounts of silica nanoparticle to polyamide matrix results in a significant increase in crystalline temperature from 171℃ to about 186℃; however, further addition of silica has no more further effect.

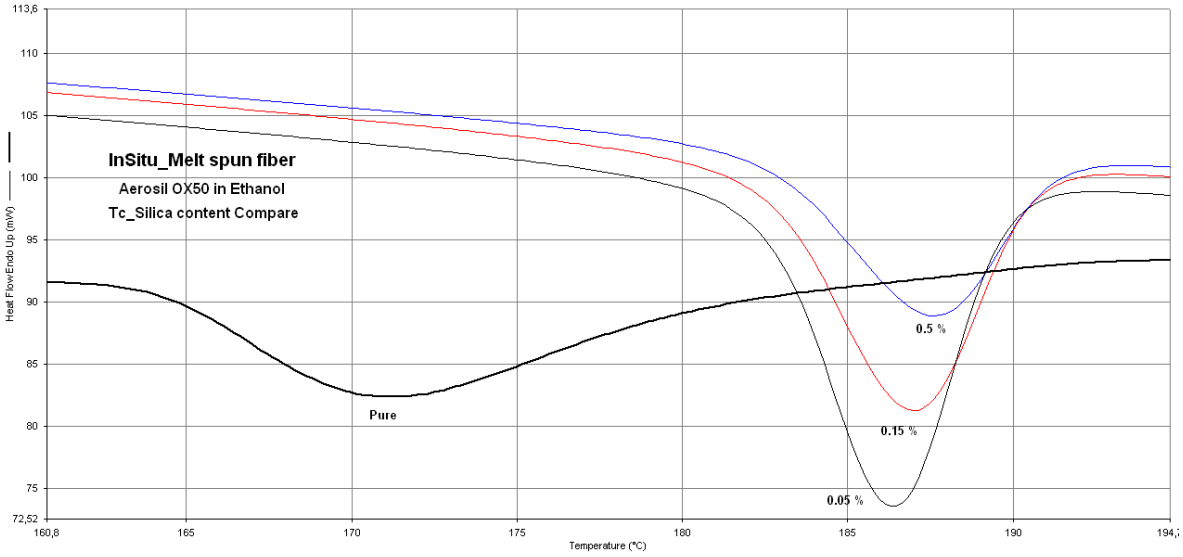

Figure 8.13 crystalline temperatures (T_c) of PA6 fiber and PA6/SiO_2 (Aerosil OX50) nanocomposite fibers as a function of silica content

According Table 8.5 samples prepared by modified surface silica has higher crystalline temperature (190.3℃) in compare to untreated sampl es (186.5℃) due to more silica-polymer interactions cause by improved compatibility of organic silica and polyamide. Similar behavior is observed in the case of modified silica nanocomposite as well as samples prepared in two different silica dispersion mediums. Figure 8.14 shows comparison between nanocomposites at 0.05 and 0.5 wt. % prepared from silica-water dispersion and silica-ethanol dispersion in 0.05 and 0.5 wt. %. Samples prepared in silica-ethanol system have slightly higher crystalline temperatures, which indicate earlier crystallization at cooling down from the melt stage cause by better distribution and more effective nucleation of these silica particles.

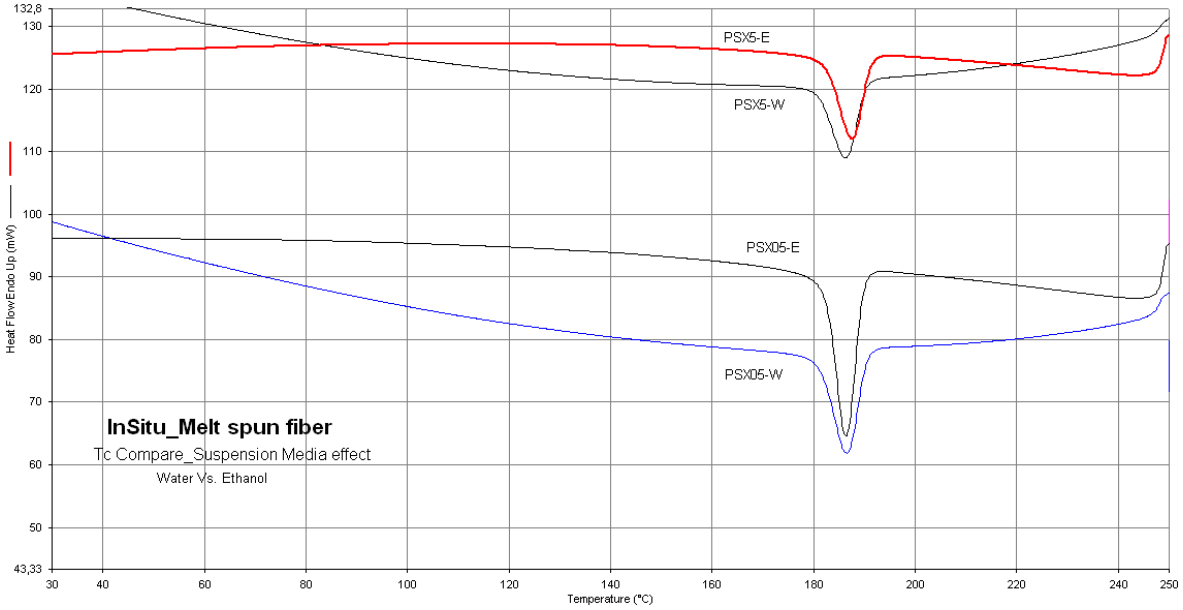

Figure 8.14 Effect of silica dispersion medium on crystalline temperature (T_c) of nanocomposite fiber

Also Table 8.5 and Figure 8.15 show that the crystalline temperature of samples made from both silica particle sizes are almost same and all higher than pure polyamide.

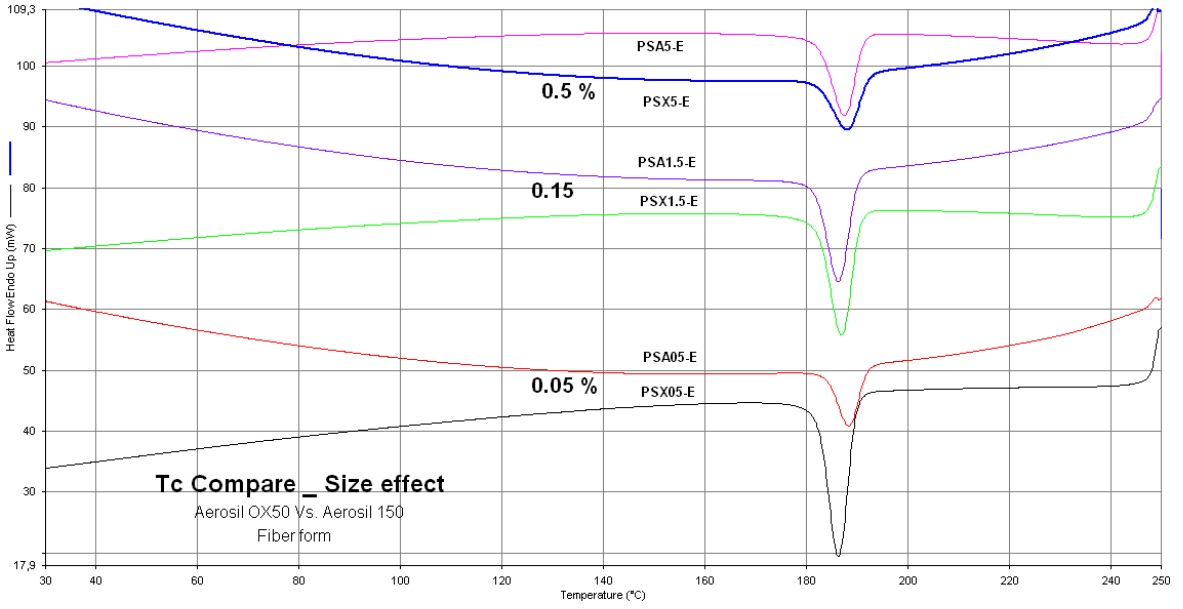

Figure 8.15 Effect of particle size on crystalline temperature

8.4.2.3. Thermal Gravimetric Analysis of PA6/SiO_2 nanocomposite fibers

The thermal stability of the pure polyamide fiber and nanocomposite fibers were characterized by Thermo gravimetric analysis (TGA). Results of thermal stability at onset degradation temperature and degradation temperature as a function of silica content and modification are summarized in Table 8.6.

Table 8.6 TGA results of PA6 fiber and PA6/SiO_2 nanocomposite fibers as a function of silica content

	SiO_2 wt. %	T_s[1] ℃	T_d[2] ℃
PA6	0	340.7	390.0
PSX05-W	0.05	352.4	402.2
PSX5-W	0.5	366.9	409.0
PSA05-W	0.05	349.4	398.6
PSA5-W	0.5	361.9	394.8
PSX05-E[3]	0.05	338.7	394.2
PSX1.5-E	0.15	342.9	396.0
PSX5-E	0.5	355.8	401.3
PSA05-E	0.05	361.1	416.9
PSA1.5-E	0.15	357.8	397.9
PSA5-E[3]	0.5	361.9	394.6
PA6/Modi. silica	0.5	348.6	398.9

[1] Onset degradation temperature

[2] Degradation temperature

As seen from Table 8.6 both, degradation temperatures, (T_d) and start of degradation temperature (T_s) of nanocomposites are higher than observed with pure PA6 which indicates the successful incorporation of silica in fiber.

All the nanocomposites showed in Figure 8.16 have no weight loss until around 300℃ (onset decomposition) and still retained 90% of their weight at about 340℃.

Figure 8.16 shows that the major stage of weight loss occurs in the range of 385–405℃, and should be associated to the break of amide bonds. It is understood that during TGA the crystal structure would disappear at the melting point and be replaced by an unordered molecular arrangement in the melt. Beyond the melting temperature, the first sign of weight loss is seen at around 395℃ in the TGA curve, signaling the breakd own of the polymer-backbone.

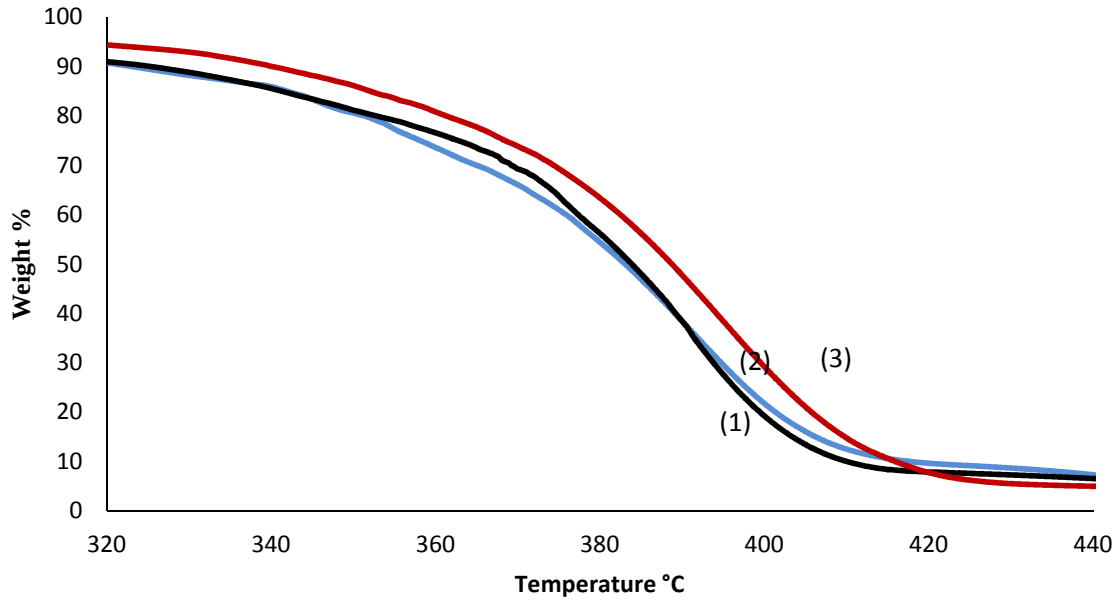

Figure 8.16 TGA thermograms of PA6/Silica nanocomposites fiber (Aerosil OX50) as function of silica content. (1), (2), (3): PSX with 0.05, 0.15, 0.5 wt. %, respectively.

In the breakdown process of the polymer, after the crystals have melted, the covalent bonds such as C–O, N–H, and O–H formed during polymerization will get decisive influence in the final decomposition of the material. Due to their ability to interact with the polar sites on the nanoparticle surface energy dissipation is facilitated and stability increased. By increasing the particle content, thermal stability also increased as shown in Figure 8.16 and also Figure 8.17 showed that thermal stability of samples with bigger primary particle size (PSX, Aerosil OX50) is higher than the other particle(PSA, Aerosil 150), it must be concluded that this behavior most likely is caused by agglomeration of the smaller particles.

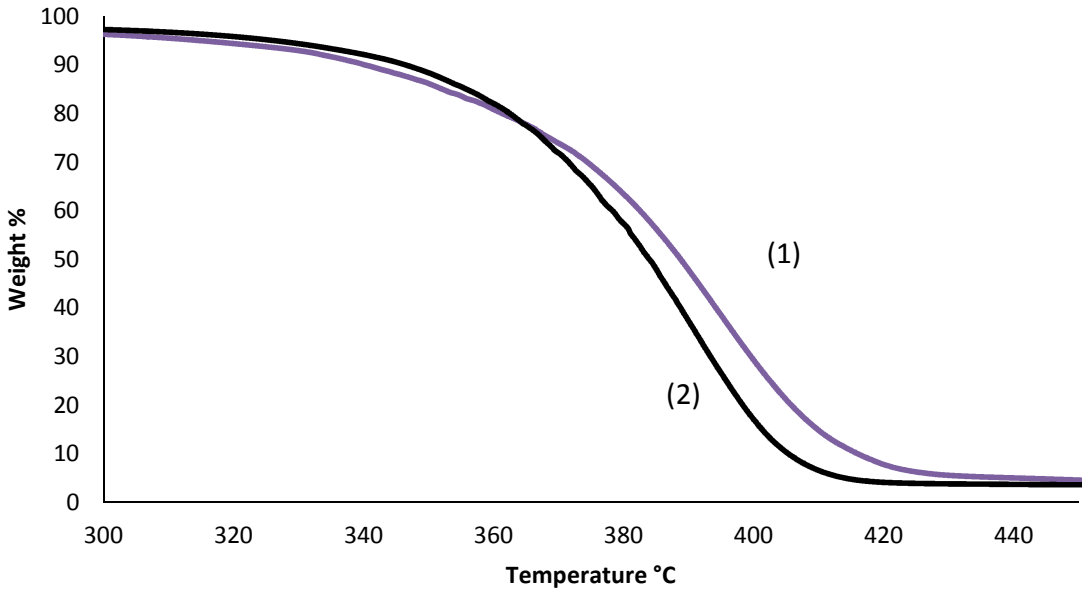

Figure 8.17 TGA thermograms of PA6/nanocomposite fiber with different particle size, (1) PSX5E, (2) PSA5E

The effect of dispersion medium is shown in Figure 8.18. The decomposition of the nanocomposites seems to have been retarded by dispersion in ethanol. This can be assumed from the fact that the silica-ethanol system results a finer and more even distribution than silica-water system.

Also, as seen in Figure 8.19, nanocomposite prepared from surface modified silica has higher thermal stability than the untreated silica due to the same reason as indicated above: more sites of interaction and finer dispersion of the modified nanoparticles.

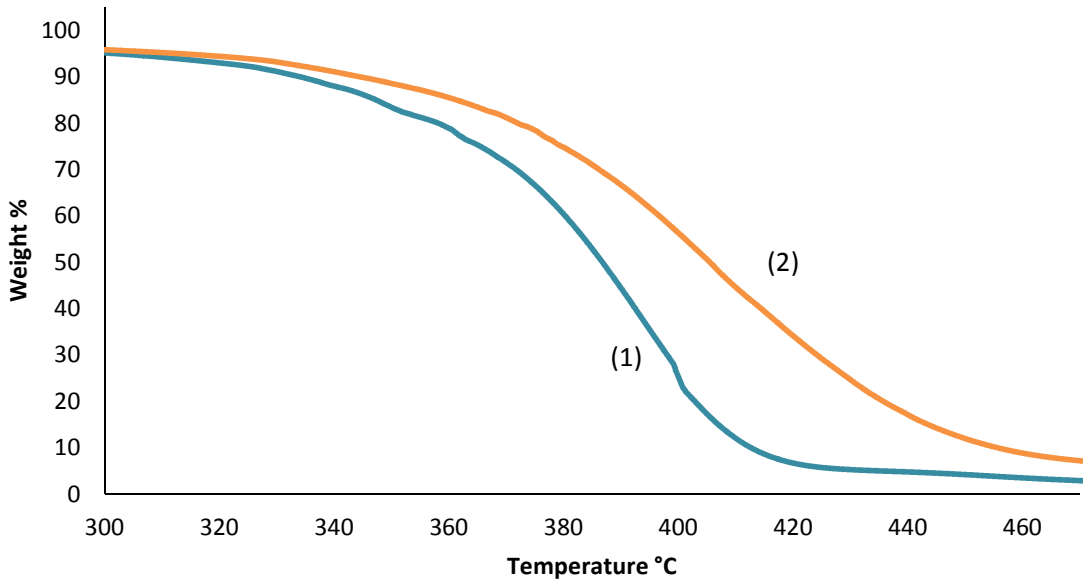

Figure 8.18 TGA thermograms of nanocomposites fiber: compare of dispersion medium between (1) silica-water system and (2) silica-ethanol system

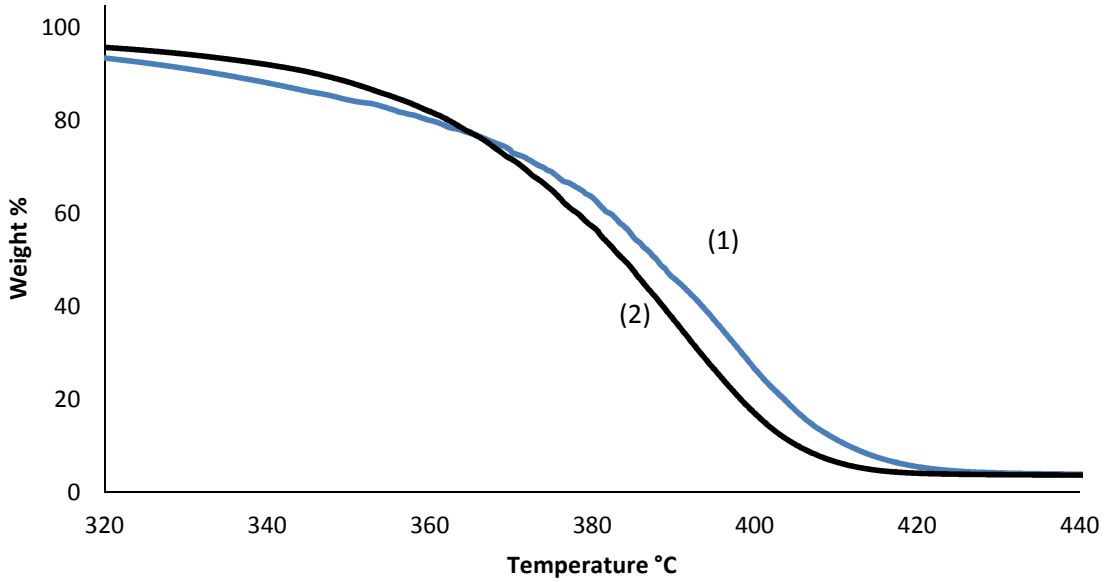

Figure 8.19 TGA thermograms nanocomposites fiber: (1) modified silica, (2) untreated silica

8.4.2.4. Tensile properties of PA6/SiO_2 nanocomposite fibers

Tensile properties of fibers such as initial Young's modulus, tenacity, and elongation at break (EAB) were measured to evaluate the effect of nanoparticles on fiber properties. The results are summarized in Table 8.7.

Table 8.7 Tensile properties of PA6 fiber and PA6/SiO_2 nanocomposite fibers as a function of silica content

	SiO_2	Tenacity	Elongation at break	Modulus
	wt. %	[cN/tex]	[%]	[cN/tex]
PA6	0	47.5	71.36	102.46
PSX05-W	0.05	41.4	61.93	243.65
PSX5-W	0.5	32.14	52.45	257.12
PSA05-W	0.05	37.45	60.81	275.9
PSA5-W	0.5	36.92	57.43	277.06
PSX05-E	0.05	36.46	68.01	206.99
PSX1.5-E	0.15	35.31	54.81	255.88
PSX5-E	0.5	35.28	58.96	240.58
PSA05-E	0.05	37.95	65.2	264.09
PSA1.5-E	0.15	34.17	64.03	212.35
PSA5-E	0.5	31.64	62.03	185.98
PA6/Modif. SiO_2	0.5	27.33	53.75	322.95

Figure 8.20 shows that by incorporating silica nanoparticle in polymer matrix, the modulus of nanocomposite fibers increased in compare to pure PA6 fiber and by increasing the silica content, the modulus is increased too.

The tensile properties of fibers reflect their structure. It is well known that the modulus of fibers depends strongly on the crystallinity and amorphous orientation in the fiber and, as well, on the denseness of the crystalline-amorphous network established at fiber formation.

The modulus of fibers is determined by the taut polymer chains of the intercrystalline region, which is reinforced in addition by hydrogen bond of SiO_2 particles in nanocomposite [322]. Thus, the nanocomposite fibers with higher silica content show a higher modulus.

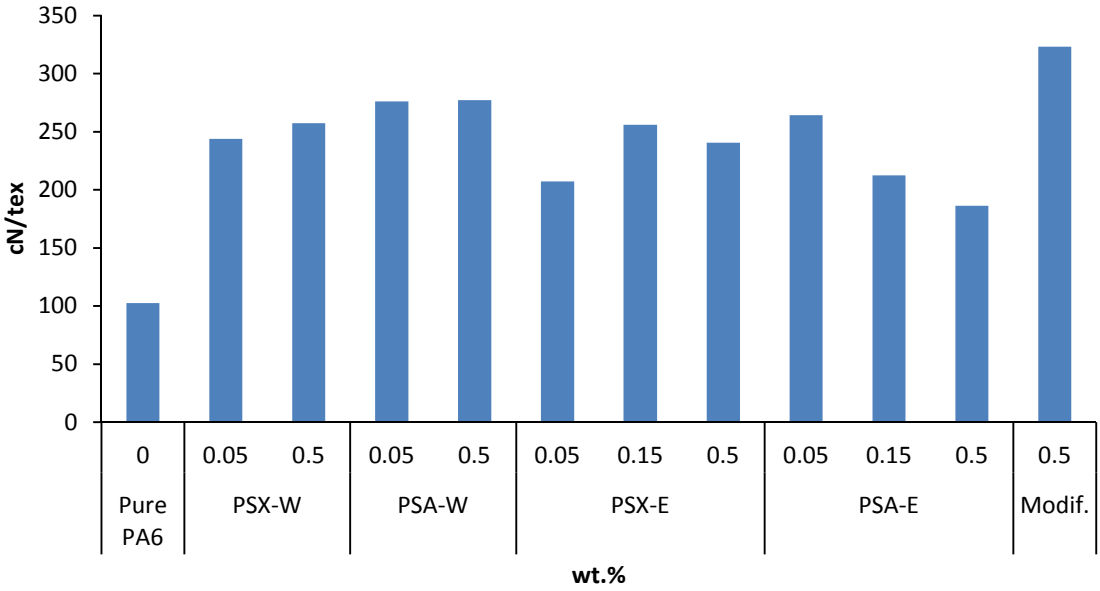

Figure 8.20 Modulus of PA6 fiber and nanocomposite fibers as a function of silica content

In addition, Ito et al. [213] investigated the deformation behavior of solid-state co-extrusion-drawn PA 6 films of solution and melt-grown aggregates of α- and γ-form crystals and reported higher ductility and efficiency of draw for samples with γ-crystalline phase. They concluded that the density of hydrogen bonding, which is higher in more densely packed α-form crystals, severely restricts the chain sliding, and thus the modulus of highly crystalline PA 6 is sensitive to the α-crystalline phase content. However, in moderately crystallized melt-spun fibers, the intercrystalline structure is likely to play a fundamental role in stress transmission, and the considerations that focus the rigidity of crystalline phases are less applicable. Therefore, the inter-chain interaction in the amorphous region (i.e., molecular entanglement and physical cross-linkage) should be regarded as crucial factors in the determination of the ductility of semicrystalline polymeric materials. From this point of view, the SiO_2 particles connected with the macromolecules by hydrogen bonds reinforce the intercrystalline network in nanocomposite,

which results in the higher modulus of fibers. It is then obvious that the modulus is higher for nanocomposite fibers with higher SiO_2 content.

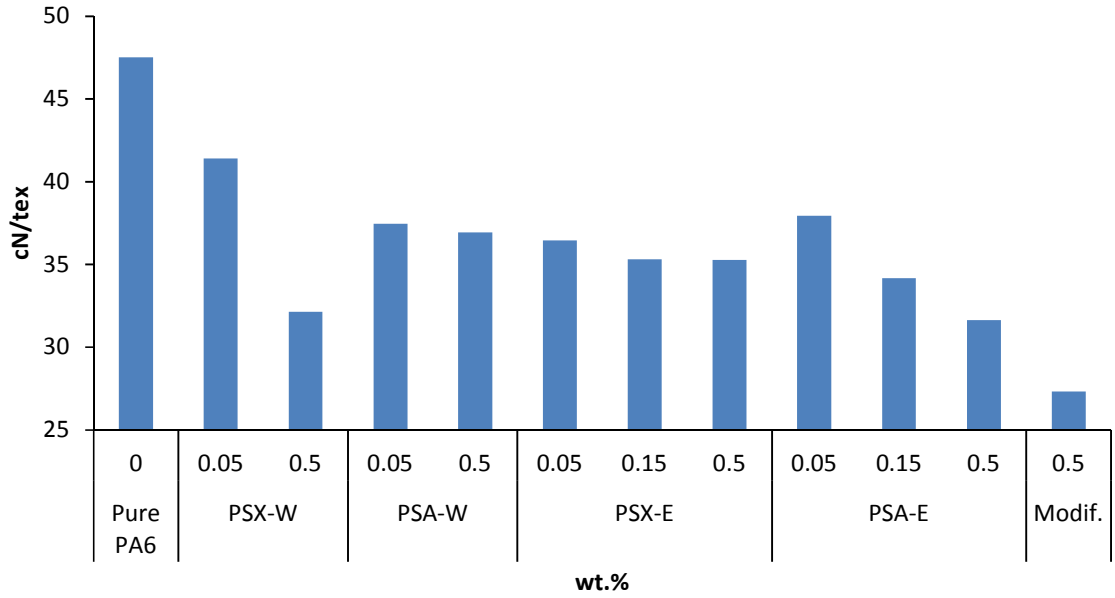

Figure 8.21 Tenacity of PA6 fiber and PA6/SiO_2 nanocomposite fibers as a function of silica content

Tenacity of fiber depends strongly on molecular weight, i.e. relative viscosity of granules, and take-up velocity. The higher relative viscosity (RV) the higher is tenacity. As take-up velocity for all of the samples was same, dependence of tenacity on molecular weight follows the same trend as is valid for molecular weight (Table 8.1 and Table 8.3), i.e. by increasing the silica content the tenacity of nanocomposite fibers decrease which could be seen in Figure 8.21.

Elongation at break (EAB) is also directly related to molecular weight and take-up velocity, that means the same explanation which holds for tenacity is also valid for elongation at break as can be seen in Figure 8.22.

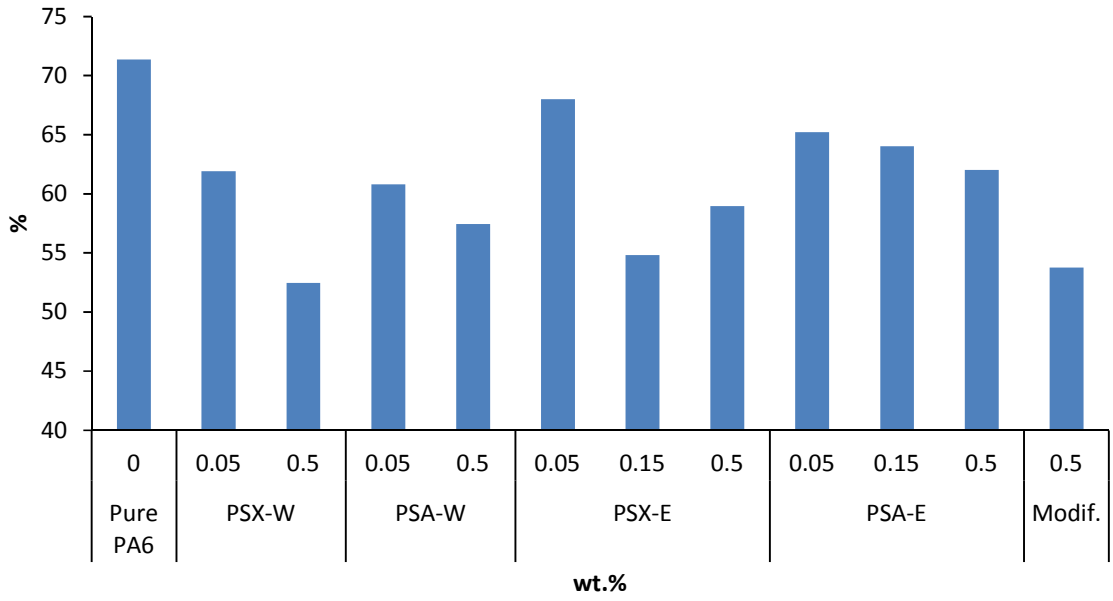

Figure 8.22 Elongation at break (EAB) of PA6 fibers and PA6/SiO_2 nanocomposite fiber as a function of silica content

8.4.2.5. SEM observation of polyamide6/SiO_2 nanocomposites fibers

To investigate the dispersion quality of silica particles, the morphology of PA 6/silica nanocomposites fibers were studied and the results are shown in Figure 8.23. It is evident that the modified silica labeled (a) have a more homogeneous dispersion in the fiber matrix compared with the unmodified silica labeled (b). Figure 8.23 also shows the effect of silica dispersion medium on dispersion quality in fiber matrix. Picture labeled (c) shows nanocomposite fiber prepared by silica-ethanol system and picture labeled (d) is a nanocomposite fiber prepared by silica-water system, the latter is showing more agglomerated particles in the surface of fiber prepared by silica-water system. The silica-water system presumably led to more aggregation and probably some degree of degradation, while in the case of silica-ethanol system, these obstacles were either minimized or not encountered.

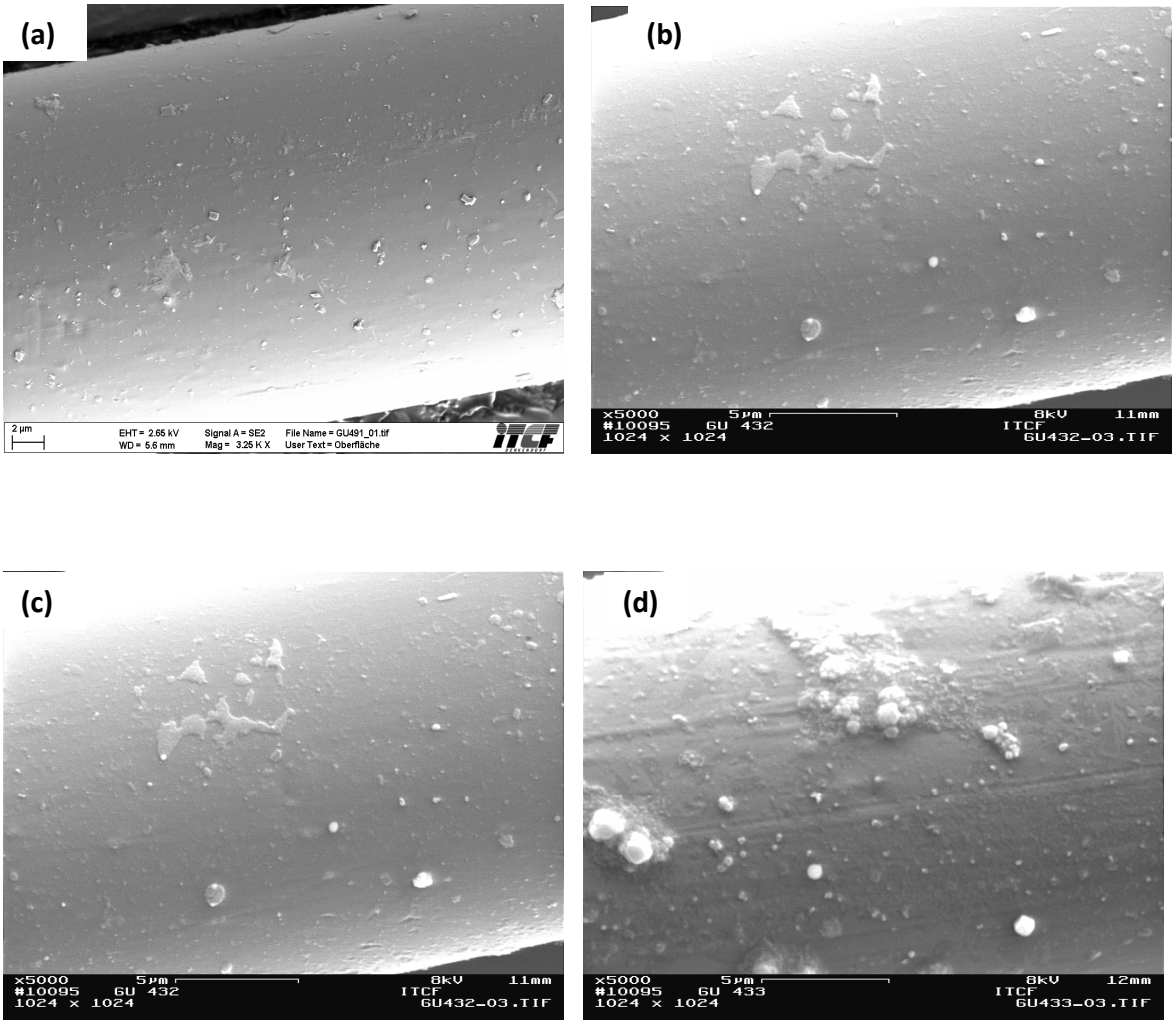

Figure 8.23 SEM pictures (a) PA6 / 0.5% modified silica nanocomposite fiber, (b) unmodified silica nanocomposite fiber, (c) PSX5 in silica-ethanol system, (d) PSX5 in silica-water system

Chapter 9

General conclusion

The main targets of this study were to produce PA6/SiO_2 nanocomposites and nanocomposites fibers according to three different methods of composite preparation. In addition the effect of preparation method as well as particle content, size and surface modification on the thermal, structural, tensile and morphological properties of nanocomposites was investigated.

On the basis of the above discussion, the following conclusions can be drawn:

By this study it was shown that PA6/SiO_2 hybrid nanocomposites can be prepared by melt compounding, solution intercalation and in-situ polymerization and by applying these compounds nanocomposites fibers were prepared successfully by melt spinning process. The only limitation which has to be stated is for spinnability of nanocomposite fibers with high silica content (more than 0.5 wt. %) which was limited and in some cases not possible.

The crystalline structure of PA6/silica was studied by DSC and X-ray diffraction methods and XRD results show an evident phase transformation from α-form to γ-form crystals, This polymorphic behavior indicates that with the introduction of nano-silica particles into the polymer matrix as well as with the preparation method the growth of α-form crystal is suppressed and the formation of γ-form crystals is promoted. And this phase transformation is more evident in solution intercalation than other two methods.

The DSC results show that the polyamide 6 matrix has one melting peak corresponding to α - form, while the nanocomposites system have two melting peaks, in which the high-temperature peak corresponds to the α-form and the low-temperature peak corresponds to the γ crystalline form. Further thermal after-treatment (melt spinning or second heating scan in DSC measurement) promotes the α-form crystallites and after annealing, only the relatively sharp α-form crystalline peaks are present.

Investigations on polymer crystallization behavior were carried out on polyamide 6/SiO_2 nanocomposites prepared with all three preparation techniques. Thus the effect of silica nanoparticles on the crystallization and melting characteristics of the PA6/silica hybrid nanocomposites was investigated. The incorporation of nanoparticles, even very low concentration, effectively enhanced crystallization of PA6, i.e. crystallization temperature shifted to higher temperature range in compare to pure PA6.

DSC results show that by incorporation of silica nanoparticles the melting peak of nanocomposites decreased in compare to pure polyamide 6 due to the presence of silica particles which disturb the perfect arrangement of hydrogen bonded sheets structure of the α-phase, hence the melt temperature of nanocomposites decreased in compare to pure PA6. Moreover a comparison study between melt temperatures of nanocomposites prepared by different techniques shows the effect of preparation method on melt temperature that, although at nanocomposite preparation, melting peaks of samples prepared by solution intercalation were lower than samples prepared by melt intercalation, after fiber formation process, melt temperatures of the nanocomposite fibers of both methods were almost same.
TGA results show that by incorporation of silica nanoparticles into a polyamide 6 matrix, for all three preparation methods, both onset temperature and degradation temperature increased in compare to pure PA6, and in addition, the higher the silica content was the higher was thermal stability. This means inorganic silica particles improve the thermal stability of PA6 polymer. According the results of TGA the nanocomposites prepared by melt intercalation are more thermally stable than the nanocomposites prepared by the other two methods.
The molecular weight of nancomposite prepared by in situ intercalation were determined by gel permeation chromatography (GPC), also relative viscosity and end groups were measured with capillary viscometer and end groups titration method, respectively.
Using different dispersion media in in-situ polymerization techniques shows that the silica-water system presumably led to more aggregation and probably some degree of degradation, while in the case of silica-ethanol system, these obstacles were either minimized or not encountered. The number average molecular weight of PA6/SiO_2 nanocomposites in the presence of silica nanoparticles decreased in the same way the amount of filler increased. Moreover by addition of nano-silica the relative viscosity of nanocomposites decreased in compare to pure polyamide 6. Finally, tensile tests were conducted on SiO_2 nanoparticle filled polyamide 6. Based on the experimental results, introduction of the nanoparticles into polyamide 6 increases the modulus and decreases the tenacity due to reduction of molecular weight. In addition by increasing silica content elongation at break of nanocomposites fibers decreased because polymer chain mobility is restricted due to polymer-particle interactions. The effect of preparation technique was investigated and the results showed that modulus of samples prepared by in-situ polymerization were higher than the samples prepared in the other techniques. This demonstrates that particle dispersion is of great importance for the physical behaviors of polymer composites.
In- situ polymerization and solution intercalation are good methods for the preparation of inorganic/organic nanocomposites and both are able to avoid the agglomeration of inorganic

particles in polymer matrices and hence improve the interfacial interaction between an inorganic component and the polymeric matrix. SEM observation shows that the modified silicas disperse more homogeneously in the PA 6 matrix in comparison to the unmodified silicas.

Zusammenfassung

Eine gerade in jüngster Vergangenheit stark gestiegene Zahl an Untersuchungen zum Thema: Eingenschaftsverbesserungen von Polymerfasern durch Zusatz organischer und anorganischer Partikel, belegt das zunehmende Interesse an high-tech Fasern und deren Anwendungen. Im Rahmen dieser Versuche spielen auch die Innovationen im Bereich der Nanotechnologie eine wichtige Rolle, die zur Entwicklung spezieller Nanopartikel für verschiedene Endanwendungen – wie beispielsweise von Nanokompositfasern – führten. In dieser Studie wurden sphärische Siliziumdioxid-Nanopartikel mit zwei unterschiedlichen Partikeldurchmessern in Polyamid 6 eingearbeitet und daraus über ein Schmelzextrusionsverfahren verstreckte Filamentgarne hergestellt. Weitere, untersuchte Prozessvariable waren dabei der Füllstoffgehalt und die Oberflächenmodifizierung der Siliziumdioxid-Partikel. Die Herstellung von Polyamid 6 / SiO_2 Nanokompositen erfolgte nach drei unterschiedlichen Methoden: (a) Schmelzeinterkalation,(b) Lösungsinterkalation und (c) in-situ-Polymerisation. . Als Referenz wurde reines Polyamid 6 unter gleichen Bedingungen gesponnen. Die Untersuchung der Nanokomposit fasern bzw. die Wirkung der darin enthaltenen SiO_2-Nanopartikel auf dere thermische, strukturelle, morphologische sowie Zugeigenschaften wurde mittels Thermogravimetrie (TGA), Differential Scanning Kalorimetrie (DSC), Röntgenbeugung (XRD), Fourier-Transform-Infrarotspektroskopie (FTIR), Rasterelektronenmikroskopie (REM) und Zugversuchen erfasst. Die TGA Ergebnisse zeigten, dass die thermische Stabilität von Nanokompositen verglichen mit reinen Polyamid 6 besser ist. Aufgrund der DSC und XRD-Ergebnisse führt die Einführung von Siliziumdioxid-Nanopartikeln in die Polymermatrix bei Abkühlung und Kristallisation in der Schmelze zu einer Phasenumwandlung der gebildeten Kristallite von der α-Form in die γ-Form. Die SEM-Aufnahmen zeigen, dass In-situ-Polymerisation und LösungsiInterkalation geeignete Methoden für die Herstellung von anorganisch-organische Nanokompositen sind, da sie die Agglomeration von anorganischen Partikeln in den Polymermatrices vermeiden, außerdem sind modifizierte Siliziumdioxidpartikel homogener in der PA 6-Matrix dispergiert als im Vergleich dazu unmodifizierte Siliziumdioxidpartikel. GPC Analysen und Messungen der relativen Viskosität weisen darauf hin, dass durch Erhöhung des Siliziumdioxidanteils eine Abnahme des Molekulargewichts der Nanokomposite im Vergleich zu reinem Polyamid 6 erfolgt. Durch die Wirkung des Siliziumdioxids auf das Polyamid 6 wird der Gehalt an Amino-und Carbonsäure-Endgruppen erhöht, dies ist gleichbedeutend mit einer Molekulargewichtsreduktion, woraus seinerseits ein Verlust an Faserfestigkeit bei den Nanokompositfasern resultiert.

Die Erhöhung des Siliziumdioxid-Anteils zeigt sich für den Modul im Gegensatz zur Festigkeit ein Trend zu zunehmenden Werten.

Schlüsselwörter: Nanokomposite, PA6/SiO_2 , In-situ-Polymerisation, Schmelzeinterkalation, Lösungsinterkalation, Schmelzspinnen

References

[1] C. P. Poole, Jr., Frank J. Owens, Introduction to nanotechnology, John Wilez & Sons,Inc., Hoboken, New Jersey (2003)

[2] D.B. Porter, Conference Proceedings from Organic-Inorganic hybrids conference Guildford, U.K. June (2000).

[3] J.G. Winiarz, L.M. Zhang, M. Lal, Friend, Journal of the American Chemical Society, 121, 5287 (1999).

[4] S.N. Sidorov, et al. Journal of the American Chemical Society, 123, 10502 (2001).

[5] T.C. Merkel, B.D. Freeman, R.J. Spontak, American Journal of Science 296, 519 (2002).

[6] C. Joly, M. Smaihi, L. Porcar, Chemistry of Materials, 11, 2331 (1999).

[7] G. Wypych, Handbook of fillers 2nd Ed. New York (1999).

[8] S. N.Bhattacharya, Rahul K. Gupta, Polymeric Nanocomposites Theory and Practice, Hanser 2008

[9] D.R. Paul, L.M. Robeson, Polymer 49 (2008) 3187–3204

[10] J.E.Mark, CY. Jiang, MY. Tang, Macromolecules 1984; 17:2613–6.

[11] S.P. Gubin, Yu A Koksharov, G B Khomutov, G Yu Yurkov, Russian Chemical Reviews 74 (6) 489, 520 (2005)

[12] M. Sezen, Chemical Fibers International ,vol.58 no.4, 2008, pp 112-115

[13] N. Erdem, A. Aysun,H. Umit Erdogan, Journal of Applied Polymer Science,Vol. 111, 2085–2091 (2009)

[14] J. Jordana, K. Jacobb, R. Tannenbaumc, Materials Science and Engineering A 393 (2005) 1–11

[15] G.L. Wilkes, B. Orler, H. Huang, Polymer Preparation 1985; 26:300–1.

[16] H. Mahfuz, M. M. Hasan, Macromolecular Materrial Eng. 2007, 292, 437–444

[17] H. Schmidt, Non-crystal Solids 73 (1985) 681.

[18] E.P. Giannelis, Advanced Material. 8 (1993) 29.

[19] J.Y. Wen, G.L. Wilkes, Chemestry of Materials 8 (1996) 1667.

[20] K.G. Sharp, Advanced Material 10 (1998) 1243.

[21] A.C. Balazs, C. Singh, E. Zhulina, Macromolecules 31 (1998) 8370.

[22] P. Hajji, L. David, J.F. Gerard, C. Paul, Journal of Polymer Science B 37 (1999) 3172.

[23] A. Kelly, Concise Encyclopedia of Composite Materials, Academic Press, New York, 1994, p. 201.

[24] C. Zhaoa,b, P. Zhanga , Polymer Testing 27 (2008) 412–419

[25] H. LU, X. XU, X. LI and Z. ZHANG, Bulletin of Materials Science, Vol. 29, No. 5, October 2006, pp. 485–490

[26] R. Sengupta, A. Bandyopadhyay, Polymer 46 (2005) 3343–3354

[27] H.Sertchook, Hi. Elimelech, C. Makarov, R. Khalfin, Journal of the American Chemical Society. 2007, 129, 98-108

[28] Ch. Yao and G. Yang, Polymer Inernationalt 2010; 59: 492–500

[29] Z.Wang, T.J. Pinnavaia, Chemical Materials 10 (7), 1998, 3769- 3771

[30] P.B., Messersmith, E.P. Giannelies, Chemical Matterial 6, (1994), 1719-1725

[31] T. Lan, T.J. Pinnavaia, Chemical Materials, 6, 1994, 2216- 2219

[32] S.D., Burnside, E.P. Giannelis, Chemical Materials, 7, (1995), 1597-1600

[33] A. Okada, K. Fujumori, A. Usuki, Polymer Chemistry, 32,(2), 540-541, 1991

[34] S. Sinha Ray, M. Bousmina, Progress in Material Science, 50, 962-1079, 2005

[35] S. Sinha Ray, M. Okamoto, Macromolecule Rapid Communication,24 (14), 815- 840, 2003

[36] N. Ogata, G. jimentz, Journal of polymer science Part B, 35 (2), 389- 396, 1997

[37] WULFHORST, B., KOCH, P. A.: Fiber Table, Polyamide Fibers: 4th edition 1997, and references therein.

[38] ISO 2076, AUSG. 12.89: Generic names for man-made fibers. International Organization for Standardization

[39] WULFHORST, B., BÜSGEN, A.: Fiber Table, Aramid Fibers: 1st issue Chem. Fasern /Tex.ind. 39/91 (1989), 1271-1276

[40] W.H., Carothers, journal of American chemical science 51 (1929), 2548-2559

[41] W.H., Carothers, journal of American chemical science 52 (1930), 5289-5291

[42] W.H., Carothers, journal of American chemical science 54 (1932), 1566-1569

[43] O. Wichterle, Makromolekulare Chemie 35 (1960), 174- 182

[44] V.B.Gupta and V.K.Kothart , Manufactured fiber technology, 1997 Chapman and Hall

[45] B.L. Deopura , Polyesters and polyamides, 2008 Woodhead Publishing Limited

[46] Caprolactam, product Data sheet, Allied Chemical Corpn., Morristown, New Jersy, June, 1980;

[47] Bonfield, J.H. and Northcott, J. (1969) Encyclopedia of industrial chemical Analysis, Vol.8 (ed. L.S.Ettre), Wiley-Interscience, New York, P. 114.

[48] Hermans, P.H. (1955) International Journal of Applied Chemistry., 5, 493

[49] Wiloth, F., Makromolekular Chemie., 15, 106. (1995)

[50] Reimschuessel, H.K. (1985) Handbook of Fiber Science and Technology- Fiber Chemistry, Vol. IV (eds M. Lewin and E.M.Pearce), Marcel Dekker, New York, pp. 146,147.

[51] Fukumoto, O. (1956) Journal of Polymer. Science., 22, 263

[52] Reimschuessel, H.K. (1985) Handbook of Fiber Science and Technology- Fiber Chemistry, Vol. IV (eds M. Lewin and E.M.Pearce), Marcel Dekker, New York, pp. 76.

[53] Callister, W.D. Materials Science and Engineering. An Introduction. 5th Ed. John Wiley & Sons, Inc. (1999).

[54] Wypych, G. Handbook of fillers. 2nd Edition. New York (1999).

[55] M.Garcia, G.van Vliet, S.Jain, Review on Advanced Materials Science 6 (2004) 169- 175 PP

[56] Wan-Gyu Hahn, Hee-Soo Myung, Macromulecular Research, vol. 12, No.1, pp 85-93 (2004) PET

[57] H:sertchook, H.Elimelech, C.Makarov, Journal of the American Chemical Society, 2007, 129, 98-108

[58] G. Yao, G. Yang, Polymer International,2010, vol. 59, issue 4, pp 492-500

[59] Seon Hoon Ahn, Seong Hun Kim, Seung Goo Lee, Journal of Applied Polymer Science, Vol. 94, 812–818 (2004) PEN

[60] Igor V. Khudyakov, R. David Zopf, Designed Monomers and Polymers 12(2009) 279-290

[61] M.M. Hasan, Y. Zhou, H. Mahfuz, Materials Science and Engineering A 429 (2006) 181–188

[62] F.Hussain, M.Hojjati, M.Okamoto, Journal of COMPOSITE MATERIALS, Vol. 40, No. 17/2006, and references therein.

[63] Zheng, Y.P., Zheng Y. and Ning, R.C. (2003, Materials Letters, 57(19): 2940–2944.

[64] Tang, J., Wang, Y., Liu, H., Xia, Y. and Schneider, B. (2003), J. of Applied Polymer Science, 90: 1053–1057.

[65] M.W.L. Wilbrink, A.S. Argon, R.E. Cohen, M. Weinberg, Polymer 42 (26) (2001) 10155–10180.

[66] H. Mahfuz, V.K. Rangari, M.S. Islam, S. Jeelani, Compos. Part A: Appl. Sci. Manuf. 35 (4) (2004) 453–460.

[67] G. Chen, G. Luo, X. Yang, Y. Sun, J. Wang, Mater. Sci. Eng. A 380 (1–2) (2004) 320–325.

[68] N. Chisholm, H. Mahfuz, V.K. Rangari, A. Ashfaq, S. Jeelani, Compos. Struct. 67 (1) (2005) 115–124.

[69] M.Z. Rong, M.Q. Zhang, Y.X. Zheng, H.M. Zeng, K. Friedrich, Polymer 42 (7) (2001) 3001–3004, 3001.98

[70] X. Li, G. Wang, X. Li, Surf. Coatings Technol. 197 (1) (2005) 56–60.

[71] G. Vigier, J. Pascualt, J. Gerard, L. David, and Haiji, Journal of Polymer Science. 37, 3172 (1999)

[72] Ch. Landry, and B. Coltrain, Polymer 33, 7 (1992).

[73] Y. Yang, J. Yin, Z. Qi, and Z. Zhu, Journal of Applied Polymer Science 73, 2977 (1999).

[74] F. Yang, Y.Ou, and Z. Yu, Journal of Applied Polymer Science 69, 355 (1998).

[75] J. Kolarik, O. Dukh, L. Matejka, Polymer 41, 1449 (2000).

[76] K. Qiu, and Z. Huang, Polymer 38, 521 (1997).

[77] E. Werner, van Zyl, G. Monserrat, Macromolecular Materials and Engineering, 2002, 287, 106-110, and references therein.

[78] E. P. Giannelis, Advanced Materials 1996, 8, 29.

[79] P. C. le Baron, Z. Wang, T. J. Pinnavaia, Applied Clay Science 1999, 15, 11

[80] W. Helbert, J. Y. Cavaille, A. Dufresne, Polymer Composites 1996, 17, 604.

[81] D. W. Clegg, A. A. Collyer, ªMechanical Properties of Reinforced Thermoplasticsº, Elsevier 1986.

[82] J. Choi, J. Harcup, A. F. Yee, Q. Zhu, R. M. Laine, Journal of the American Chemical Society. 2001, 123, 11420,

[83] Y.C. Chen, S.X. Zhou, H.H. Yang, and L.M. Wu, Journal of Applied Polymer Science, 95(5): 1032–1039. . (2005)

[84] C.L. Wu, Zhang, M.Q., Rong, M.Z. and Friedrich, K., Composite Science and Technology, 62: 1327–1340.2002

[85] Z. Zhang, and J.L. Yang, Polymer, 45: 3481–3485. 2004

[86] Y.C. Chen, S.X. Zhou, and L.M. Wu, (2005). European Polymer Journal (submitted 2005).

[87] J. Rottstegge, X. Zhang, Y. Zhou, D. Xu, C. C. Han, D. Wang, Journal of Applied Polymer Science, Vol. 103, 218–227 (2007), and references therein

[88] F. Schultze-Gebhardt, K.H. Herlinger, In Ullmann's Encyclopedia of Industrial Chemistry; Wiley-VCH: Weinheim, 2002; p 10.

[89] W. Stibal, R. Schwarz, U. Kemp, K. Bender, In Ullmann's Encyclopedia of Industrial Chemistry; Wiley-VCH: Weinheim, 2002; p 3.

[90] Estes, L. L.; Sattler, H.; Berg, H.; Wolf, K. H.; Kausch, M.; Schro¨ er, H.; Pellegrini, A.;

Olivieri, P.; Schoene, W.; Nogaj, A.; Sling, C.; Menault, J.; Osugi, T.; Morimoto, O.; Frankenburg, P. E. In Ullmann's Encyclopedia of Industrial Chemistry; Wiley-VCH: Weinheim, 2002; p 6.

[91] H.G. Elias, An Introduction to Polymer Science; Wiley-VCH: Weinheim, 1997.

[92] J. Rottstegge, C.C. Han, W.D. Hergeth, Macromolecular Material Engineering 2006, 291, 345.

[93] S. Ran, X. Zong, D. Fang, B.S. Hsiao, Macromolecules 2001, 34, 2569.

[94] L.A. Utracki, Commercial Polymer Blends; Chapman & Hall: London, 1998.

[95] A. Marcincin, Progress in Polymer Science 2002, 27, 853.

[96] S.S. Ray, M. Okamoto, Progress in Polymer Science 2003, 28, 1539.

[97] S.S. Sternstein, Zhu, A. J. Macromolecules 2002, 35, 7262.

[98] D.N. Bikiaris, G.Z. Papageorgiou, E. Pavlidou, Journal of Applied Polymer Science 2006, 100, 2684.

[99] S. Ran, C. Burger, I. Sics, K. Yoon, D. Fang, K. Kim, Colloid Polymer Science 2004, 282, 802

[100] J.K.W. Sandler, S. Pegel, M. Cadekc, F. Gojny, Polymer 2004, 45, 2001.

[101] X. Zhang, M. Yang, Y. Zhao, S. Zhang, X. Dong, X. Liu, J Appl Polym Sci 2004, 92, 552.

[102] G.H. Guan, C.C. Li, D. Zhang, J Appl Polym Sci 2005, 95, 1443.

[103] A. Boudenne, L. Ibos, M. Fois, E. Gehin, J.C. Majeste, Journal of Polymer Science Part B: Polymer Physics 2004, 42, 722.

[104] J. Chen, C. Carrot, Y. Chalamet, J.C. Majeste, Journal of Applied Polymer Science 2003, 88, 1376.

[105] F. Bauer, H. Ernst, U. Decker, M. Findeisen, H.J. Glaesel, H. Langguth, Macromolecular Chemistry and Physics 2000, 201, 2654.

[106] H.J. Glaesel, F. Bauer, H. Ernst, M. Findeisen, E. Hartmann, Macromolecular Chemistry and Physics 2000, 201, 2765.

[107] H. Mahfuz, M. Hasan, V. Dhanak, Nanotechnology 19 (2008) 445702 (7pp)

[108] F. Luis, E. Mauricio, L.L. Betty, Macromol. Symp. 2007, 258, 119–128

[109] B. Salima, B. Elodie, Z. Nathalie, Macromol. Rapid Commun. 2005, 26, 1860–1865,

[110] M.Hosokawa, K.Nogi ,Nanoparticle Technology Handbook, page 5

[111] M.Hosokawa, K.Nogi ,Nanoparticle Technology Handbook, page 10

[112] H. Hommel, A. Touhami, A.P. Legrand, Makromol. Chem. 1993, 194 879

[113] R.K. Iler The chemistry of silica. New York: Wiley, 1979.

[114] R.P.W. Scott, Silica gel and bonded phases. New York: Wiley, 1993.

[115] Bergna. The colloid chemistry of silica, vol. 1. Washington,DC:American Chemical Society, 1994

[116] S. Spange, Prog. Polym. Sci. 25 (2000) 781–849

[117] Lynn Townsend White, Jr. (1961). "Eilmer of Malmesbury, an Eleventh Century Aviator: A Case Study of Technological Innovation, Its Context and Tradition". Technology and Culture (Society for the History of Technology) 2 (2): 97–111. doi:10.2307/3101411.

[118] A.F. Holleman, E. Wiberg, Inorganic Chemistry, San Diego: Academic Press, (2001)

[119] L. Sunggyu, Encyclopedia of chemical processing. CRC Press. (2006)

[120] R. Doering, Y. Nishi (2007). Handbook of Semiconductor Manufacturing Technolog, Marcel Dekker, New York

[121] A.B.D. Nandiyanto; S.-G Kim; F. Iskandar; and K. Okuyama (2009), Microporous and Mesoporous Materials 120 (3): 447–453

[122] N. Greenwood, A. Earnshaw, (1984), Chemistry of the Elements, Oxford: Pergamon, pp. 393–99

[123] W. Stöber, A. Fink, E.J. Bohn, J. Colloid Interface Sci. 1968, 26, 62.

[124] Marie-Alexandra Neouze, Ulrich Schubert , Monatsh Chem 139, 183–195 (2008)

[125] E. Ruckenstein, Li ZF (2005) Adv Colloid Interface Sci 113: 43

[126] B. Pukanszky, E. Fekete, (1999) Adv Polym Sci 139: 109

[127] SG. Grancharov, H. Zeng, S. Sun, S.X. Wang, (2005) J Phys Chem B 109: 13030

[128] RC. Doty, T.R.shikhudo, M. Brust, DG. Fernig, (2005) Chem Mater 17: 4630

[129] J.H. Moon, Y.G. Shul, Hong SY, Choi YS, Kim HT (2005) Inter J Adhes Adhes 25: 534

[130] F. Liu, Quan B, Liu Z, Chen L (2005) Mater Chem Phys 93: 301

[131] F. Hua, Swihart MT, Ruckenstein E (2005) Langmuir 21: 6054

[132] T. Kikukawa, Kuraoka K, Kawabe K, Yamashita M, Fukumi K, Hirao K, Yazawa T (2005) J Membr Sci 259: 161

[133] E. Pere, H.Cardy, Latour V, Lacombe S (2005) J Colloid Interface Sci 281: 410

[134] S. Reculusa, C. Poncet-Legrand, A. Perro, E. Duguet, E. Bourgeat-Lami, C. Mingotaud, S. Ravaine, (2005) Chem Mater 17: 3338

[135] Y.P. Wang, X.W. Pei, K. Yuan, (2004) Mater Lett 59: 520

[136] C.G. Wu , Tzeng L-F, Kuo Y-T, Shu CH (2002) Appl Catal A 226: 199

[137] Rajesh Ranjan, May, 2008, PhD thesis

[138] R. David Green. Part of PhD thesis CARBON DIOXIDE REDUCTION ON GADOLINIA-DOPED CERIA CA THODES.

[139] Katz, Harry Charles, Handbook of fillers for plastics, Springer 1987

[140] Technical Bulletin Fine Particles, No. 11, Basic Characteristics of AEROSILR fumed silica, 6th edition 2003, Degussa AG, D-40402 Dusseldorf,Germany

[141] German patent No. 762,732.1942, Degussa.

[142] M.I. Kohan, Polyamide plastics handbook, carl Hanser verlag, munich 1995

[143] J. C. Ho, K.H. Wei, Macromolecules 2000, 33, 5181-5186

[144] D.R. Holmes, Bunn, C. W.; Smith, D. J. J. Polym. Sci. 1955, 17, 159.

[145] C. Donald, Vogelsong, D. C. J. Polym. Sci., Part A 1963, 1, 1055.

[146] H.J. Arimoto, Polym. Sci., Part A 1964, 2, 2283.

[147] H. Arimoto, M. Ishibashi, M. Hirai, J. Polym. Sci., Part A 1965, 3, 317.

[148] A. Ziabicki, Kolloid-Z. 1959, 167, 132

[149] N. Murthy, S. Curran, S.M. Aharoni, H. Minor, Macromolecules 1991, 24, 3215.

[150] G. Gurato, A. Fichera, Grandi, Makromol. Chem. 1974, 175, 953.

[151] Y. Kinoshita, Makromol. Chem. 1959, 33, 1.

[152] M. Ito, K. Mizuochi, T. Kanamoto, Polymer 1998, 39, 4593.

[153] C.W. Bunn, E.V. Garner, proceeding of the royal society, 1974, 189A, 39

[154] Y. Kinoshita, makromolekulare chemie 1959, 33,1

[155] H. Arimoto,M. Ishibashi, M. Hirai, Y. Chatani, Journal of polymer science A 1965, 3, 317

[156] S. Dasgupta, Hammond, W. B.; Goddard, W. A. III. J. Am. Chem. Soc. 1996, 118, 12291.

[157] N. Hiramatsu, K. Haraguchi, Japanese journal of applied physic, 1983, 22, 335.

[158] Y. Kojima, T. Matsuoka, H. Takahashi, J Material Science Letter 1993, 12, 1714.

[159] X. Liu, Wu, Q. European Polymer Material 2002, 38, 1383.

[160] L.J. Mathias, Davis, R. D.; Jarrett, W. L. Macromolecules 1999, 32, 7958.

[161] T.D. Fornes, D.R. Paul, Polymer 2003, 44, 3945.

[162] T.M. Wu, Chen, E. C.; Liao, C. S. Polymer Engineering Science 2002, 42, 1141.

[163] P. Maiti, M. Okamoto, Macromolecule Materials and Engineering 2003, 288, 440.

[164] D. Lincoln, R. Vaia, Z. Wang, Hsiao, B. S.; Krishnamoorti, R. Polymer 2001, 42, 9975.

[165] L.M. Liu, Z.N. Qi, X.G. Zhu, J Applied Polymer Science 1999, 71, 1133.

[166] L.J. Mathias, R.D. Davis, W.L. Jarrett, Macromolecules 1999, 32, 7958.

[167] T.M. Wu, C.S. Liao, Macromolecule Chemistry Physics 2000, 201, 2820.

[168] K. Varlot, E. Reynaud, M.H. Kloppfer, G. Vigier,J. Varlet, J Polymer Science Part B: Polymer Physics 2001, 39, 1360.

[169] P.C. LeBaron, Z. Wang, T.J. Pinnavaia, Applied Clay Science 1999, 15,11

[170] R.A. Vaia, G. Price, P.N. Ruth, H.T. Nguyen, J.J. Lichtenhan, Applied Clay Science 1999, 15, 67.

[171] A. Okada, Y. Fukushima, M. Kawasumi, S. Inagaki, A. Usuki, S. Sugiyami, T. Kurauchi, O. Kamigaito, U.S. Pat. 4,739,007, (1998).

[172] M. Kata, A. Usuki, In Polymeric-Clay Nanocomposites; Pinnavaia, T. J., Ed.; JWS: England, 2000.

[173] S.M: Aharoni, n-Polyamides, their synthesis, structure, and properties. Chichester; New York: Wiley; 1997.

[174] Arimoto H, Ishibashi M, Hirai M, Chatani Y. Journal of Polymer Science Partt A 1965; 3(1):317–26.

[175] D.R. Holmes, C.W. Bunn, D.J. Smith, Journal of Polymer Science 1955;17:159–77.

[176] N. Murthy, Polymer Communications 1991;32(10):301–5.

[177] F. Rybnikar, Burda J. Faserforsch u Textiltech 1961;12:324–31.

[178] L.G. Roldan, H.S. Kaufman, Polymer Letter 1960;1:603–8.

[179] T. Itoh, H. Miyaji, K. Asai, Japanese Journal of Applied Physics 1975;14(2):206–15.

[180] A. Reichle, A. Prietzschk, Angew Chem 1962;74:562–9.

[181] L.G. Wallner, Monatsh 1948;79:279–95.

[182] K.H. Illers, H. Haberkorn, P. Simak, Makromolekulare Chemie1972;158: 285–311.

[183] K.H. Illers, Makromolekulare Chemie 1978;179(2):497–507.

[184] K.H. Illers, H. Haberkorn, Makromolekulare Chemie 1971;142:31–67.

[185] S. Gogolewski, M. Gasiorek, K. Czerniawska, A. Pennings. Colloid and Polymer Science 1982; 260(9):859–63.

[186] D.C. Vogelsong, J Polymer Science 1963; 1(Pt. A):1055–68.

[187] P. Marx, C. Smith, A. Worthington, M. Dole, Journal of Physical Chemistry; 59: 1015–9.

[188] M. Dole, B. Wunderlich, Makromolekulare Chemie 1959;34:29–49.

[189] M. Inoue, J Polymer Science Part A 1963; 1:2013–20.

[190] J.R. Starkweather, P. Zoller, G.A. Jones, J Polymer Science, Polymer Physics Edition 1984; 22(9):1615–21.

[191] B. Wunderlich, Macromolecular physics, vol. 3. New York: Academic Press; 1973.

[192] G. Gurato, A. Fichera, F.Z. Grandi, R. Zannetti, P. Canal, Makromolekulare Chemie 1974;175(3):953–75.

[193] M. Kyotani, S. Mitsuhashi, J Polymer Science, Part A-2 1972; 10(8): 1497–508.

[194] R.J. Brill für Praktische Chemie 1942;161:49–64.

[195] N. Murthy, S.M. Aharoni, A. Szollosi, J Polymer Science, Polymer Physics Edition 1985; 23(12):2549–65.

[196] N.Murthy, S.A. Curran, S.M. Aharoni, H. Minor, Macromolecules 1991; 24(11):3215–20.

[197] C. Ramesh, E.B. Gowd, Macromolecules 2001; 34(10):3308–13.

[198] D.M. Lincoln, R.A. Vaia, Z.G. Wang, B.S. Hsiao, R. Krishnamoorti, Polymer 2001; 42(25):09975–85.

[199] D.R. Salem, R. Moore, H. Weigmann, J. Polymer Science, Part B: Polymer Physics 1987; 25(3):567–89.

[200] I. Campoy, M.A. Gomez, C. Marco, Polymer 1998; 39(25):6279–88.

[201] A. Okada, M. Kawasumi, I. Tajima, J Applied Polymer Science 1989;37(5):1363–71.

[202] J.H. Magill, Polymer 1962; 3:655–64.

[203] Y. Kojima, A. Usuki, M. Kawasumi, A. Okada, J Material Research 1993; 8(5):1185–9.

[204] Q. Wu, X. Liu, L. Berglund, Macromolecular Rapid Communications 2001;22(17): 1438–40.

[205] X.Liu, Q. Wu, European Polymer Journal 2002;38(7):1383–9.

[206] Q. Wu, X. Liu, Berglund LA. Polymer 2002;43(8):2445–9.

[207] X. Liu, Q. Wu, Polymer 2002;43(6):1933–6.

[208] T.M. Wu, C.S. Liao, Macromolecular Chemistry and Physics 2000;201(18):2820–5.

[209] T.M. Wu, E.C. Chen, C.S. Liao, Polymer Engineering Science 2002;42(6):1141–50.

[210] E.Giza, H.Ito, T. Kikutani, Journal of Macromolecular Science Part B: Physics, B39(4), 545–559 (2000)

[211] D. C. Vogelsong, J. Polym. Sci., Part A: Polym. Chem., 1, 1055 (1963).

[212] H. M. Heuvel and R. Huisman, J. Polym. Sci., Polym. Phys., 19, 121 (1981).

[213] M. Ito, K. Mizuochi, and T. Kanamoto, Polymer, 39, 4593 (1998).

[214] D.L. VanderHart, A. Asano, J.W. Gilman, Chemistry of Materials 2001; 13(10): 3796–809.

[215] D.L. VanderHart, A. Asano, J.W. Gilman, Chemistry of Materials 2001; 13(10): 3781–95.

[216] E.M. Bradbury, A. Elliot, Polymer, 1963, 4, 47-59

[217] I. Matsubara, J.H. Magill, Polymer 1966, 1, 199-215

[218] H. Arimoto, Journal of Polymer Science 1964, 2, Part A, 2283-2295

[219] G. Rotter and H. Ishida, 1992, J. Polym. Sci. Part B. Polym. Phys. 30 489

[220] J. Ho and K. Wei Macromolecules 33 (2000), p. 5181

[221] Q. Wu, X. Liu and Lars A. Berglund, Polymer Volume 43, Issue 8, April 2002, Pages 2445-2449

[222] S. Dasgupta, W. Hammond and W.A. Goddard J Am Chem Soc 118 (1996), p. 12291

[223] Y. Kinoshita Makromol Chem 33 (1959), p. 1

[224] Y. Kojima, A. Usuki, M. Kawasumi, A. Okada, T. Kurauchi, O. Kamigaito and K. Kaji J Polym Sci: Polym Phys 32 (1994), p. 625

[225] Y. Kojima, A. Usuki, M. Kawasumi, A. Okada, T. Kurauchi, O. Kamigaito and K. Kaji J Polym Sci: Polym Phys 33 (1995), p. 1039

[226] L. Mathias, R. Davis and W. Jarrett Macromolecules 32 (1999), p. 7958

[227] L. Liu, Z. Qi and X. Zhu J Appl Polym Sci 71 (1999), p. 1133

[228] Y. Kojima, T. Matsuoka, H. Takahashi and T. Kurauchi J Appl Polym Sci 51 (1994), p. 683

[229] Q. Wu, X. Liu and L.A. Berglund Macromol Rapid Commun 22 (2001), p. 1438

[230] D.M. Lincoln, R.A. Vaia, Z.G. Wang and B.S. Hsiao, Polymer 42 (2001), p. 1621.

[231] N. VASANTHAN, D. R. SALEM, Journal of Polymer Science: Part B: Polymer Physics, Vol. 39, 536–547 (2001)

[232] L.H., Sperling, Introduction to physical polymer science, 2006 by John Wiley & Sons, Inc.

[233] L.E. Alexander, X-ray diffraction methods in polymer science,Wiley, New York ,1969

[234] K.Kakudo, N.Kasai, X-ray Diffraction by polymers, Elsevier 1972

[235] B.D. Culliy, Elements of X-ray Diffraction, Addison- Wesley, Reading MA. 1976

[236] Williams, David Bernard, Transmission electron microscopy : a textbook for materials science. Plenum Pr., 1996

[237] Brent Fultz; James Howem ,Transmission electron microscopy and diffractometry of materials ,Springer, 2004

[238] K.-H. Henning; M. Störr ,Electron micrographs (TEM, SEM) of clays and clay minerals , Berlin : Akad.-Verl., 1986

[239] V.B. Gupta, V.K. Kothari, Manufactured Fiber Technology, Chapmann and Hall 1997

[240] Ning, Yong-Cheng, Structural identification of organic compounds with spectroscopic techniques: Wiley-VCH, Weinheim, 2005

[241] Martin, Derek H., Spectroscopic techniques for far infra-red, submillimetre and millimetre waves - Amsterdam : North-Holland, 1967

[242] A. Turi, Thermal characterization of polymeric materials / ed. by Edith 2 London : Academic Press, 1997

[243] Höhne, Günther, Differential scanning calorimetry : with 19 tables., Berlin : Springer, 2003

[244] E. A. Turi, thermal analysis of polymers, Academic press, New York1982

[245] Collins, Edward A., Experiments in polymer science, Wiley, c 1973

[246] Billmeyer, Fred W., Textbook of polymer science,- 3. Ed, Wiley, 1984

[247] Harry. R. Allcock, F.W. Lampe, Contemporary Polymer Chemistry, Prentice-Hall 1981

[248] Kulicke, Werner-Michael. , Analysis of polymers : molar mass and molar mass distribution of polymers, polyelectrolytes and latices;, Basel : Hüthig & Wepf, 1992

[249] J. Knott and V. Rossbach, Makromolekulare Chemie 86 (1980) 203-213

[250] S.F. Sun, Physical chemistry of macromolecules: basic principles and issues, 2nd edition - Hoboken, NJ : Wiley, 2004

[251] H. Mahfuz, M. M. Hasan, Macromol. Mater. Eng. 2007, 292, 437–444, and references therein.

[252] W. D. Zhang, Macromol. Rapid Commun. 2004, 25, 1860.

[253] L.S. Schadler, In Nanocomposite Science and Technology; Ajayan, P. M.; Schadler, L. S.; Braun, P.V., Eds., Wiley-VCH: Weinheim, 2003, Chapter 2, pp 77–144.

[254] J. Rottstegge, X. Zhang, Y. Zhou, D. Xu, J Appl Polym Sci 2007, 103, 218.

[255] G. Qian, T. Lan, In Handbook of Polypropylene and Polypropylene Composites; Harutun, G. K., Ed., Marcel Dekker: New York, Basel, 2003; Chapter 20, pp 707–728.

[256] J.W. Cho, D.R. Paul, Polymer 42 (2001) 1083-1094

[257] S. H. Kim, S. H. Ahn, and T. Hirai, Polymer, 44, 5625 (2003).

[258] S. Buchner, D. Wiswe, and H. G. Zachmann, Polymer, 30, 480 (1989).

[259] S. S. Im, S. C. Chung, W. G. Hahm, and S. G. Oh, Macromol. Res., 10, 221 (2002).

[260] ASTMD-3822–07 (Standard test method for tensile properties of single textile fibers), ASTM International: West Conshohocken, PA. Available at www.astm.org.

[261] S. Z. D. Cheng, Z. Q. Wu, and B. Wunderlich, Macromolecules, 20, 2802 (1987).

[262] H. G. Kim and R. E. Robertson, J. Polym. Sci. Polym. Phys.Ed., 36, 1757 (1998).

[263] D. J. Blundell, Polymer, 37, 1167 (1987).

[264] F. J. Medellin-Rodriguez, P. J. Phillips, and J. S. Lin, Macromolecules,29, 7491 (1996).

[265] J. Y. Kim, E. S. Seo, S. H. Kim, and T. Kikutani, Macromol.Res., 11, 62 (2003).

[266] T. Sabu, G.E Zaikov, Polymer nanocomposite research advance , Nova science publisher, New York 2008

[267] D.P.N. Vlasveld, J. Groenewold, H.E.N. Bersee, E. Mendes, S.J. Picken , Polymer 46 (2005) 6102–6113

[268] Y. Kojima, A. Usuki, M. Kawasumi,T. Kurauchi, et al., J Mater Res 1993;8(5):1185–9.

[269] J.S. Shelley, P.T. Mather, K.L. DeVries, Polymer 2001; 42(13):5849–58.

[270] E.P. Giannelis, Adv Mater 1996; 8(1):29.

[271] A. Usuki, A. Koiwai, Y. Kojima, Kurauchi T, et al. J Appl Polym Sci 1995;55(1):119–23.

[272] T.D. Fornes, D.R. Paul, Polymer 2003; 44(17):4993–5013.

[273] N. Hasegawa, H. Okamoto, M. Kato, A. Usuki, N. Sato, Polymer 2003; 44(10):2933–7.

[274] M. Maiti, A.K.Bhowmick, Journal of Applied Polymer Science, Vol. 101, 2407–2411 (2006)

[275] Y. Kojima, A. Usuki, M. Kawasumi, Y. Fukushima, Journal of Material Research 1993, 8, 1185.

[276] G. Chen, S. Liu, S. Chen, Z. Qi, Macromolecule Chemistry Physics 2001, 202, 1189.

[277] X. Li, T.K. Kang, W.J. Cho, Macromolecule Rapid Communication 2001, 22, 1306.

[278] P.B. Messermith, E.P. Giannelis, Chemistry Material 1994, 6, 1719.

[279] S. Sadhu, A.Bhowmick, Journal of Polymer Science Part B: Polymer Phys 2004,42, 1573.

[280] M. Maiti, S. Sadhu, A. Bhowmick, Journal of Polymer Science Part B: Polymer Phys 2004, 42, 4489.

[281] T. Lan, T. Pinnavaia, Journal of Chemistry Material 1999, 6, 2216.

[282] Zh. Shen, G.P. Simon, Polymer 43 (2002) 4251-4260

[283] Y. Li, H. Ishida, Polymer 44 (2003) 6571–6577

[284] E. Ruiz-Hitzky, Advanced Material 1993; 5:334.

[285] H.G. Jeon, H. Jung, S. Lee, S.Hudson, Polymer Bulletin 1998; 41:107.

[286] F.Yang, Y. Ou, Zh. Yu, JournalJournal of applied polymer science, vol.69, 355-361 (1998)

[287] L.Liu,Z.QI,X.ZHU, J.of applied polymer science, Vol.71, pp. 1133-1138(1999)

[288] H.Yang, C.Huang , ANTEC 2006 pp. 526-531

[289] T.D.Fornes,D.R.Paul, Polymer 44 (2003) pp. 3945-3961

[290] M.Yuan, L.S.Turng, S.Gong, J.of CELLULAR PLASTIC Vol.40 Sep2004

[291] Huimin Lu et al. Bull.Mater.Sci.,Vol. 29 , Nov 5 , October 2006 pp 485-490

[292] Seong Hun Kim et al. , Macromolecular Research, Vol. 14,No. 2, pp.146-154(2006)

[293] L. Shen, Q. Du, H. Wang, W. Zhong and Y. Yang, 2004, Polym.Int. 53 1153

[294] G. Rusu, E. Rusu, high performance polymer, 18: 355-375, 2006

[295] G. Rusu and E. Rusu, 2004, high performance polymer 16 569

[296] S.Z. Petrovic, I. Javni, A.Waddon and G. Banhegyi, 2000, J.Appl.Polym.Sci. 76 133

[297] P. C. Powell, A. J. I. Housz, ‘‘Engineering with Polymers’’, 2nd edition, Stanley Thornes Publishers, Ltd., Cheltenham, UK 1998.

[298] P.B. Messersmith and E. Giannelis,1995, J. Polym. Sci. Part A. Polym Chem. 33 1047

[299] A. Usuki, Y. Kojim, M. Kawasumi, A. Okada, Y. Fukushima, 1993 J. Mater.Res. 8 1179

[300] K.A. Carrado and L. Xu, 1998, Chem. Mater. 10 1440

[301] J.W. Cho and D.R. Paul, 2001, Polymer 42 1083

[302] H. Dennis, D. Hunter, D. Chang ,S. Kim, J. White, J. Cho, D. Paul, 2001 Polymer 42 9513

[303] T.D. Fornes, P.J. Yoon, H. Keskkula and D.R. Paul, 2002, Polymer 43 2121

[304] W.E. van Zyl, M. Garcia, B. Schrauwen, B. Kooi, 2002, Macromol. Mater. Eng. 287 106

[305] W. Helbert, J.Y. Cavaille and Dufresne A, 1996, Polym. Comp. 17 604

[306] M. Rong, M. Zhang, W. Ruan, Materials Science and Technology, 22, 787–796 (2006).

[307] T.F. Tadros, Advances in Colloid and Interface Science, 46, 1–47 (1993).

[308] R.O. James, American Ceramic Society, Westerville, 349–410 (1987).

[309] G.R. Joung, W. Sang, H. Kim, J. Lee, Materials Science Engineering: C, 24, 285–288 (2003).

[310] L. F. Cai1, Z. Y. Lin2, H. Qian,Polymer Letters Vol.4, No.7 (2010) 397–403

[311] LI. YING, YU. JIAN, Journal of Applied Polymer Science, Vol. 84, 827–834 (2002) ,

[312] X. Liu, Q. Wu, L.A. Berglund and Qi Z, 2002, Macromol. Mater. Eng. 287 515

[313] L. LIMIN, Q. ZONGNENG, ZHU. XIAOGUANG , Journal of Applied Polymer Science, Vol. 71, 1133–1138 (1999)

[314] T.Wu, C.S. Mand Liao, 2000, Macromol. Chem. Phys. 201 2820

[315] T.X. Liu, Z.H. Liu, K.X. Ma K, L. Shen, 2003 Composit. Sci. Technol. 63 331

[316] L. Shen, Q. Du, H. Wang, W. Zhong and Yang Y 2004 Polym. Int. 53 1153
[317] J. Kondelkova, Z.Tuzar, J. Kraliceck, Angew, Macromol. Chem. 64 123, 1977
[318] J.G. de la Campa, E. Guijarro, F.J. Serna and J. de Abajo, Eur. Polym. J. 21 1013, 1985
[319] J.K. Kap, S.L. Jong, A.P. Arun, H.K. Taek, POLYMER COMPOSITES 30, 265(2009)
[320] Y.P. Khanna, R. Kumar, A.C. Reimschuessel, Polym Eng Sci 1988; 28(24):1607–11.
[321] Y.P. Khanna, A.C. Reimschuessel, A. Banerjie, Polym Eng Sci 1988; 28(24):1600–6.
[322] Y.P. Khanna, R. Kumar, A.C. Reimschuessel, Polym Eng Sci 1988; 28(24):1612–5.
[323] Y.P. Khanna, A.C. Reimschuessel, J Appl Polym Sci 1988; 35(8): 2259–68.
[324] Y.P. Khanna, Polym Eng Sci 1990; 30(24):1615–9.
[325] N. Avramova, Polym Polym Compos 1993; 1(4):261–74.
[326] JH. Magill, Polymer 1962; 3(No. 1):43–51.
[327] E. Turska, S. Gogolewski, Polymer 1971;12(10):616–28.
[328] E. Turska, S. Goglewski, J Appl Polym Sci 1975;19(3):637–44.
[329] N. Avramova, S. Fakirov, I. Avramov, J Polym Sci, Polym Phys 1984; 22(2):311–3.
[330] N. Avramova, S. Fakirov, J Polym Sci, Polym Phys 1986; 24(4):761–8.
[331] I. A.M. Ibrahim, A.A.F. Zikry, M. A. Sharaf, Journal of American Science, 2010;6(11)

Lebenslauf

Mohammad Reza Sarbandi

Persönliche Daten:

Geburtsdatum:	29.08.1976
Geburtsort:	Tehran - Iran
Staatsangehörigkeit:	Iraner
E-mail:	reza.sarbandi@gmail.com

Schulbildung

1982-1987	Primary School -Tehran-Iran
1987-1990	Guidance School - Tehran- Iran
1990-1994	High School - Tehran- Iran

Studium

1994-1999	Bachelor of Science in Textile chemistry & Fiber Science engineering Polytechnic university - Tehran - Iran
1999-2002	Master of Science in Textile chemistry & Fiber Science engineering Isfahan University of Technology - Isfahan – Iran
Seit Juni 2008	Promotionsstudium in Chemie Institut für Polymerchemie Lehrstuhl für Makromolekulare Stoffe und Fasserchemie An der Universität Stuttgart Bei Herrn Prof.Dr. Dr. h.c. Franz Effenberger